

THE DEVELOPMENT OF SUB-MICRO
FILLER ENHANCED POLYMER
COMPOSITES

YALAN LI

A thesis submitted in partial fulfilment of the requirements
of Nottingham Trent University for the degree of Doctor
of Philosophy

November 2007

Copyright Statement

This work is the intellectual property of the author and may also be owned by Nottingham Trent University. You may copy up to 5% of this work for private study, or personal, non-commercial research. Any re-use of the information contained within this document should be fully referenced, quoting the author, title, university, degree level and pagination. Queries and requests for any other use, or if a more substantial copy is required, should be directed in the first instance to the author.

Abstract

Sub-micro silica flakes and graphite reinforced polymer composites have been developed in this research. The sub-micro polymer composites are designed to overcome problems associated with nanocomposite technology. Apart from the high cost of production, the other major problem in nanocomposites is reduced efficiency in mechanical reinforcement at high filler loadings. The surface area of nano-fillers in high filler loaded composites is too high resulting in insufficient polymer molecules to wet the filler surface and hence increased filler agglomeration occurs. Increasing filler dimension into the sub-micro range can avoid such difficulties. The dimension of fillers in the sub-micro range also has the advantage of utilising modern polymer processing technologies.

In this thesis, sub-micro composite reinforcement has been studied through the identification of suitable fillers, modelling of sub-micro composites and experimental validation of model predictions. The processing methodology, effects of filler loading, aspect ratio and compatibility of filler with matrix are also investigated. In addition, rheology, crystallisation, fracture toughness and the thermodynamic behaviour of sub-micro filler reinforced polymer composites are studied. The investigation was primarily focused on various combinations of single-layered silica flakes and multi-layered graphite sheets reinforced nylon-6 and polypropylene. The predicted Young's modulus and strengths of developed composites are as high as 3.3 GPa and 81 MPa at 5wt% silica flake content as well as 11.75 GPa and 301MPa at 30wt% flake fraction, respectively. Experimental results show that tensile modulus and strengths of the sub-micro composites produced agree well with modelling data at low filler loading. They are, however, much lower than the predictions in the high filler loading range due to the

breakage of silica flakes during composite processing. In spite of filler breakage, the tensile modulus and strength of 5wt% silica flake reinforced N6 improved 68% and 67% respectively, compared to the N6. The tensile strength is also 38% higher than that of 5wt% clay/N6 nanocomposites. The tensile modulus of 30wt% silica flake reinforced N6 improved over 240% which is similar to the achievement of 30wt% glass fibre/N6 composites. In addition, the fracture toughness and thermal deflection temperature of a silica flake/N6 composite improved by 17% at 5wt% and 20.3 °C at 10wt% filler content respectively.

For multi-layered graphite sheet reinforced polypropylene sub-micro composites, mechanical properties are a function of both filler thickness and filler loading. Over 112% improvement in Young's modulus has been achieved with a composite produced via a multi-extrusion method at 20wt% filler loading, compared with the pure polymer. The crystallinities of all sub-micro composites produced are either similar to or lower than those of pure polymers. This implies that the major contribution to the improvement of mechanical properties is from sub-micro fillers. In addition, the crystallisation rate and crystallisation temperature of sub-micro composites are increased when compared with base polymers due to the nucleation effect of fillers. The introduction of sub-micro fillers into nylon-6 and polypropylene did not result in significant change in rheology. This may be associated with flake breakage and relatively poor interfacial bonding at the filler/polymer interface.

In summary, this work demonstrates the potential of sub-micro filler enhanced composites in improving major engineering properties. It also proves that the sub-micro approach can fill the gap between nano and fibre reinforcement.

Acknowledgements

I would like to extend thanks to my supervisors, Dr Fengge Gao and Dr John Hearn for their guidance, advice, and input regarding this research.

I would like to acknowledge Dr Peter Hine of the University of Leeds for providing, guidance and advice on mechanical testing and dynamic mechanical analysis, especially on the adoption of thermal deformation temperature measurement.

I must thank my father Shaojiang, brothers Qifang, Qiang, and Jianfeng as well as my fiancé Dr Roger Tait for their love and encouragement. Especial appreciation to Roger for programming the image processing software used in flake orientation analysis and for helping in language improvement throughout the study.

Acknowledgement is also given to the technical staff of the School of Biomedical and Natural Sciences as well as and the previous material research group for providing and maintaining the instruments used throughout this project. The contributions of Judith Kipling are especially recognised.

Finally, to friends and colleagues who have not been mentioned, thank you for your ideas and informal discussions.

Table of contents

ABSTRACT	I
ACKNOWLEDGEMENTS	III
TABLE OF CONTENTS	IV
LIST OF FIGURES	VII
LIST OF TABLES	X
1 INTRODUCTION	1
1.1 BACKGROUND OF THIS RESEARCH	1
1.2 AIMS OF THIS PROJECT	3
2 LITERATURE SURVEY	4
2.1 THE ADVANTAGES AND DISADVANTAGES OF POLYMERS IN DOMESTIC AND ENGINEERING APPLICATIONS	4
2.1.1 <i>The development and importance of polymers</i>	4
2.1.2 <i>Advantages and disadvantages of polymer</i>	6
2.2 THE ENHANCEMENT OF POLYMER MECHANICAL PROPERTIES	7
2.2.1 <i>Historic development of polymer reinforcement</i>	7
2.2.2 <i>The reinforcement of polymers</i>	9
2.2.3 <i>Fibre composites</i>	22
2.2.4 <i>Nanocomposites</i>	29
2.3 THE ENHANCEMENT OF OTHER PHYSICAL AND ENGINEERING PROPERTIES	35
2.3.1 <i>Flame retardancy</i>	35
2.3.2 <i>Barrier properties</i>	38
2.3.3 <i>Electrical conductivity</i>	39
2.4 THE ADVANTAGES AND LIMITATIONS OF POLYMER ENHANCEMENT IN DIFFERENT SIZE REGIMES	42
2.4.1 <i>The limitations of polymer reinforcement in micro scale</i>	42
2.4.2 <i>The problems with polymer reinforcement in nanoscale</i>	44
2.4.3 <i>The need for sub-micro technology and development of sub-micro polymer composites</i>	45
3 EXPERIMENTAL METHODS	49
3.1 MATERIALS STUDIED.....	49
3.2 PREPARATION OF EXPANDABLE GRAPHITE	52

3.3 CHARACTERISATION OF SURFACE AREA OF GRAPHITE FLAKES AND EXPANDED GRAPHITE	53
3.4 THE CHARACTERISATION OF SUB-MICRO AND NANO STRUCTURE	53
3.4.1 X-ray diffraction analysis.....	53
3.4.2 Scanning and transmission electron microscopy	54
3.5 THE PREPARATION OF SUB-MICRO FILLER ENHANCED POLYMER COMPOSITES	54
3.5.1 The melt blending method.....	54
3.5.2 The solution method to produce sub-micro graphite/polypropylene conductive composites ...	55
3.6 MECHANICAL PROPERTIES OF POLYMER AND THEIR COMPOSITES	55
3.6.1 Tensile loading test	55
3.6.2 Impact fracture analysis.....	56
3.7 DYNAMIC MECHANICAL ANALYSIS	57
3.8 CHARACTERISATION OF THE DISPERSION STRUCTURE OF REINFORCEMENTS IN COMPOSITES	58
3.9 CHARACTERISATION OF THE CRYSTALLISATION BEHAVIOUR OF THE COMPOSITES	58
3.9.1 Differential scanning calorimetric analysis	58
3.9.2 Polarised microscopy with hot stage.....	59
3.10 THE RHEOLOGICAL CHARACTERISATION OF THE COMPOSITES	60
3.11 ELECTRICAL CONDUCTIVITY MEASUREMENT OF SUB-MICRO GRAPHITE POLYPROPYLENE COMPOSITES	60
4 PREDICTION OF YOUNG’S MODULUS AND STRENGTH OF N6 COMPOSITES REINFORCED BY SUB-MICRO SILICA FLAKES	62
4.1 THEORIES OF COMPOSITE MECHANICAL PROPERTIES PREDICTION	62
4.1.1 Theories of modulus prediction	62
4.1.2 Theories for strength prediction	67
4.2 NUMERICAL ASPECTS	70
4.2.1 Length of flakes	70
4.2.2 Length distribution	71
4.2.3 The orientation of silica flakes in N6 composites.....	73
4.3 MODEL PREDICTION OF THE YOUNG’S MODULUS AND STRENGTH OF 350NM SILICA FLAKE/N6 COMPOSITES	77
5 EXPERIMENTAL RESULTS AND DISCUSSION.....	81
5.1 THE IDENTIFICATION OF FILLERS AS THE CANDIDATES FOR SUB-MICRO COMPOSITE APPLICATION	81
PART I: REINFORCEMENT WITH SINGLE-LAYERED SUB-MICRO FILLERS.....	86
5.2 TENSILE MODULUS AND STRENGTH OF SUB-MICRO SILICA FLAKE/N6 COMPOSITES	86

5.3 A COMPARISON IN MECHANICAL PROPERTIES AMONGST THE SUB-MICRO FILLER REINFORCED COMPOSITES, NANOCOMPOSITES AND SHORT FIBRE COMPOSITES.....	89
5.4 KEY FACTORS OF SUB-MICRO SILICA FLAKE ENHANCEMENT	93
5.4.1 <i>The effect of aspect ratio on tensile modulus and strength of sub-micro silica flake composites</i>	94
5.4.2 <i>Extrusion speed and surface protection of silica flakes</i>	100
5.4.3 <i>Degradation of materials during composite processing</i>	104
5.4.4 <i>The compatibility of silica flakes with polymer</i>	106
5.5 RHEOLOGY OF GLASS FLAKE POLYMER COMPOSITES	109
5.6 CRYSTALLISATION BEHAVIOUR OF GLASS FLAKE POLYMER COMPOSITES	114
5.7 IMPACT FRACTURE AND DYNAMIC THERMAL MECHANICAL ANALYSIS OF SUB-MICO SILICA FLAKE COMPOSITES.....	124
5.7.1 <i>Impact fracture of sub-micro silica flake/N6 composite</i>	124
5.7.2 <i>The dynamic thermal mechanical properties of glass flakes composites</i>	125
PART II: THE ENHANCEMENT WITH MULTI-LAYERED SUB-MICRO FILLERS	129
5.8 DEVELOPING MULTI-LAYERED SUB-MICRO FILLERS	129
5.9 THE DISPERSION OF EXPANDED GRAPHITE AND THE MECHANICAL PROPERTIES OF SUB-MICRO GRAPHITE PP COMPOSITES	134
5.9.1 <i>The dispersion of expanded graphite in polymers</i>	135
5.9.2 <i>The mechanical properties of sub-micro graphite reinforced polypropylene composites</i>	139
5.10 THE RHEOLOGY AND CRYSTALLISATION BEHAVOIR OF SUB-MICRO GRAPHITE COMPOSITES	142
5.10.1 <i>Rheology of sub-micro graphite polypropylene composites</i>	142
5.10.2 <i>Crystallisation of sub-micro graphite composites</i>	145
5.11 CONDUCTIVE SUB-MICRO GRAPHITE COMPOSITES.....	148
6 CONCLUSIONS	152
7 FUTURE WORK	155
REFERENCES.....	157
APPENDIX A : DEFINITION OF TERMINOLOGY.....	172
APPENDIX B : LIST OF SYMBOLS.....	174
APPENDIX C : LIST OF ABBREVIATIONS.....	175

List of figures

Figure 1: A commercial carbon fibre production process	12
Figure 2: Typical models of the carbon fibres	13
Figure 3: The direct melt processing of glass fibres	15
Figure 4 : The structure of clay building blocks	16
Figure 5: The structure of 1:1 and 2:1 clays	17
Figure 6: The crystal structure of graphite	18
Figure 7: Structure models of single walled carbon nanotubes	20
Figure 8: The Marsh-Griffith model of carbonisation/graphitisation process	43
Figure 9: Schematic illustration of volume conductivity measurement.....	61
Figure 10: A schematic illustration of a unidirectional composite.....	63
Figure 11: Schematic illustration of the fibre and matrix used in Shear Lag analysis.....	66
Figure 12: The shapes of silica flakes	70
Figure 13: Length distribution of 350nm SF	72
Figure 14: The scheme of image acquisition pattern	73
Figure 15: Schematic orientation of 350nm silica flakes in N6 composites	75
Figure 16: Orientation efficiency factors of eleven layers at five regions (A-E)	76
Figure 17: Dependence of the predicted longitudinal modulus of 350nm SF/N6 composites on silica flake content based on flake aspect ratio of 475 and average length of 166.2μm	78
Figure 18: Dependence of predicted longitudinal strength of 350nm SF/N6 composites on flake content based on flake aspect ratio of 475 and average length of 166.2μm.....	78
Figure 19: TEM micrograph of carbon nanotube pyrograf III and boehmites	83
Figure 20: SEM micrograph of beomite, silica flakes and sub-micro graphite.....	84
Figure 21: The dependence of tensile modulus of 350nmSF/N6 sub-micro composites on filler contents	88
Figure 22: The dependence of tensile strength of 350nm silica flake/N6 composites on filler contents	88
Figure 23: Tensile modulus comparison of sub-micro, micro and nano composites	90
Figure 24: Tensile strength comparison of sub-micro, micro and nano composites.....	90
Figure 25: XRD patterns of clay/N6 composites	93
Figure 26: Length distributions of silica flakes in 1wt% SF/N6 composites	95
Figure 27: Length distributions of silica flakes in 3wt% SF/N6 composites	95
Figure 28: Length distributions of silica flakes in 5wt% SF/N6 composites	96
Figure 29: Length distributions of silica flakes in 25wt% SF/N6 composites	96

Figure 30: Dependence of elastic modulus of sub-micro SF/N6 composites on the fraction, aspect ratio and orientation of flakes based on Shear Lag models.....	99
Figure 31: Dependence of tensile strength of sub-micro SF/N6 composites on the fraction, aspect ratio and orientation of flakes based on modified Rule of Mixtures	99
Figure 32: The effect of extrusion speed and surface modification on silica flake breakage	102
Figure 33: The effect of different silanes on flake surface protection	103
Figure 34: The effect of extrusion speed on degradation of sub-micro composites	105
Figure 35: Chemical structure of polypropylene and silane coupling agents.....	108
Figure 36: The possible mechanism of chemical bonding between silica flakes and N6 ...	108
Figure 37: Shear viscosity and shear rate of 350nm SF/PP composites with different filler fractions	111
Figure 38: Effect of filler thickness and flake surface treatment on PP sub-micro composites.....	111
Figure 39: Effect of filler content and flake surface treatment on N6 sub-micro composites	113
Figure 40: The effect of flake fraction on sub-micro SF/N6 composite crystallisation.....	118
Figure 41: The effects of flake surface treatment and thickness on sub-micro SF/N6 composite crystallisation	119
Figure 42: The effect of flake fraction on sub-micro SF/PP composite crystallisation.....	120
Figure 43: The effects of flake surface treatment and thickness on sub-micro SF/PP composite crystallisation	121
Figure 44: DSC melt curves of 350nm silica flake/N6 composites.....	122
Figure 45: impact fracture toughness of N6, 350nmSF/N6 and 850nmSF/N6 composites	125
Figure 46: Storage modulus & temperature of sub-micro SF/N6 composites.....	128
Figure 47: Tan δ & temperature of sub-micro SF/N6 composites.....	128
Figure 48: The relationship between expansion volume of expandable graphite and microwave irradiation time	130
Figure 49: Micrograph of the cross-section of the expandable graphites under optical microscopy	131
Figure 50: Dependence of expansion rate on particle thickness of expandable graphite..	132
Figure 51: SEM morphology of graphite before and after expansion	133
Figure 52: Structures of expanded graphite in cyanoacrylate and PP under different processing methods	137
Figure 53: The optical microscopic morphology of expanded graphite dispersions in PP under the two-feeder fed and multi-extrusion methods	138

Figure 54: Individual graphite sheets produced via the sonication and multi-extrusion ..138

Figure 55: The dependence of shear viscosity of sub-micro graphite PP composites on the shear rate and structure of reinforcements143

Figure 56: The dependence of shear viscosity on the shear rate of 20wt% sub-micro graphite PP composites.....143

Figure 57: The structure of expanded graphite in PP composites synthesised via the solution method with and without compatiliser as well as the two-feeder extrusion.150

Figure 58: The conductivity dependence of sub-micro graphite enhanced PP on structures and content of the fillers151

Figure 59: The critical percolation threshold of different structural sub-micro graphite/PP composites151

List of tables

Table 1: Reinforcement fillers in polymer composites	10
Table 2: Dimensions of the reinforcing phase	10
Table 3: The purity and particle size of graphite and nanofibres used	50
Table 4: The composition, particle size and surface area of the boehmites used.....	51
Table 5: The thickness, diameter distribution and surface modification of silica flakes	52
Table 6: The physical parameters of silica flakes and N6 for predicting the Young's modulus and strength of the composites	77
Table 7: Thicknesses and diameters of candidate fillers for sub-micro application.....	82
Table 8: The dependence of residence time on screw speed of the extrusion at 20vol% feeding rate	101
Table 9: Tensile modulus and strength of 30wt% 350nm SF/N6 composite with and without surface modification	106
Table 10: Tensile modulus and strength of 30wt% 350nm SF/PP composite with and without surface modification	107
Table 11: Crystal diameters in sub-micro silica reinforced N6 and PP composites	122
Table 12: Summary results DSC analysis of sub-micro SF composites	123
Table 13: Thermal deflection temperature of sub-micro SF/N6 composites.....	127
Table 14: BET specific surface area of graphite before and after expansion.....	134
Table 15: The sonication time for separating the layers of expanded graphite into individual sheets.....	138
Table 16: Tensile modulus and strength of sub-micro graphite/PP composites	141
Table 17: A comparasion of the mechanical property improvement between 20wt% single and multi-layered sub-micro filler reinforced polypropylene	142
Table 18: the demensions of expended and exfoliated graphite.....	144
Table 19: Summary of DSC results of sub-micro graphite polypropylene composites	147

1 Introduction

Sub-micro filler reinforced composites are designed to address the problems associated with nano polymer reinforcement. The research in this project explores the potential of sub-micro range reinforcement. This is achieved through the development of novel polymer composites reinforced with sub-micro materials.

1.1 Background of this research

In order to meet industrial requests for polymers with better properties, fibre reinforced polymer composites appeared during the 1940s. Due to significantly improved mechanical properties, they were soon used in many applications from the aircraft to vehicle industries [1]. At present, fibre composites are still an important branch in the advanced materials market. There are, however, two weaknesses with fibre reinforcement. One is low strain fracture caused by strain magnification due to differences in stiffness between fibre and matrix. The other is low reinforcement efficiency in the low filler loading range [2]. These problems are addressed by means of nanocomposite reinforcement. Once fillers are dispersed into a polymer at the nanometric level, they are strongly interlinked by polymer molecules. As a consequence, the effect of strain magnification is reduced meanwhile the inherent properties of the fillers can be fully utilised and hence the reinforcement efficiency at low filler loading is increased significantly.

In reality, nanocomposite reinforcement has improved a wide range of the physical and engineering properties of polymers, when compared with traditional fibre reinforced composites at a low filler loading range [2]. The market for fibre composites with a high fibre volume fraction, however, has not been challenged [2]. The mechanical properties

of the best nanocomposite produced so far are much lower than those of conventional fibre reinforced composites with a high fibre volume fraction. The primary reason for this is that reinforcement is a function of filler loading [4], [5] and further mechanical property improvement of nanocomposites should rely on high filler loadings. However, a high nano-filler fraction in nanocomposites results in an extremely high filler surface area. This leads to insufficient numbers of polymer molecules to wet the filler surface resulting in a decrease in the mechanical properties of the composites. It is therefore not possible to produce nanocomposites with high mechanical properties with high filler loading.

In addition to filler loading, it is difficult to produce nanocomposites with thermoset polymers. The engineering properties of thermoset polymers strongly depend on the cross-linking extent of polymer. Current nanotechnology works in a size range which is very close to the molecular scale. Intercalation at such a scale would change the functionality of polymer precursors and hence result in changes in the extent of cross-linking. This would be detrimental to the engineering properties of thermoset polymers. In reality, the application of nanocomposite technology to highly cross-linked thermoset polymer systems has proved to be difficult [2].

In order to overcome these problems, investigations into a new area of polymer enhancement is required, that is reinforcement in the sub-micro scale, which fills the gap between nano and micro reinforcement regimes. Sub-micro is defined as a dimensional range between 100nm and 5 μ m. This size range is larger than the dimensions currently investigated in nanotechnology but smaller than micro

dimensions. Thus, sub-micro composites may be capable of overcoming the difficulties faced in current nano and micro technology.

1.2 Aims of this project

The primary aim of this project was to develop a composite technology which produces polymer with enhanced properties by utilising single and multi-layered sub-micro fillers. In the study, modelling of sub-micro composites was conducted in order to predict the potential of sub-micro filler enhanced composites. Preliminary experimental studies, using both single layered silica flakes and multi-layered graphite, were also carried out towards developing the right solution to fill the gaps between nano and sub-micro reinforcement technology. The experimentations include an investigation of the fillers suitable for sub-micro reinforcement, the development of processing technology and the study of the relationships between structure, properties and processing techniques. All the work is covered in this thesis. The thesis is divided into seven chapters. The literature review will follow this introduction and Chapter 3 describes the experimental methods used in this study. Chapter 4 predicts the potential of sub-micro reinforcement in Young's modulus and strength. Chapter 5 presents the experimental results and the discussions. Chapter 6 provides overall conclusions and Chapter 7 suggests areas for future work.

2 Literature survey

Relevant fundamental knowledge and progress in composite science is reviewed in this chapter. This includes the advantages and disadvantages of polymers, the historic development of composites, property improvements of micro and nano composites as well as the advantages and limitations associated with composite reinforcement in different size ranges. Section 2.1 examines the advantages and disadvantages of polymers in their applications. In Section 2.2 the historic development of composites, detailed descriptions of selected common reinforcing materials as well as mechanical properties of fibre and nano composites are reviewed. Section 2.3 widens the review into the enhancement of other physical and engineering properties of composites such as fire retardancy, solvent/gas barrier and electrical conductive properties. Under the heading of advantages and limitations of polymer composite enhancement, Section 2.4 discusses the benefits and problems of both micro and nano composite reinforcement. The current research in sub-micro and sub-micro composites is also reviewed.

2.1 The advantages and disadvantages of polymers in domestic and engineering applications

2.1.1 The development and importance of polymers

Development and research into polymers began in the 1840s when the first semi-synthetic polymer, cellulose nitrate, was produced [6]. The concept of macromolecule and long chain structure of polymer, however, was not developed until the work by Hermann Staudinger, Wallace Carothers and Herman Mark in 1935 [7]. Before that, polymers were thought of as aggregations of small molecules or micellar. After

macromolecular theory was developed, knowledge of chemistry and manufacturing technology of polymers rapidly expanded. This led to an enormous growth in the synthetic polymer industry between the 1950s and the 1970s. The worldwide production of plastics increased sixteen-fold to approximate 9×10^6 tons in 1970. Natural rubber and fibres increased two-fold during the same 20-year period [8]. This tendency has continued since then and by 1995, the annual production of plastics had climbed to 114×10^6 tons. In the subsequent five years, the amount reached to 154×10^6 tons [9].

The emergence of polymers, especially synthetic polymers, has made a great difference in industrial fields and to human lifestyles. For example, the discovery of celluloid stimulated the development of the film industry and brought about revolutionary changes in the toy industry [6]. Bakelite, polyolefin and epoxy resins were essential to the electronics industry as insulators [10]. Polyaniline, polypyrrole, polythiophenes were used as plastic batteries, capacitors, and conductive adhesives. The products made with these polymers possess higher voltage, higher capacity, longer life and better shape design compared with their traditional counterparts [11]. Butadiene-styrene copolymer and butadiene-acrylonitrile copolymer contributed to the development of the automotive industry [7]. Poly (methylmeth) acrylate, polystyrene, polycarbonate and fluorinated polymers have been applied as optical fibres which reduced the installation and maintenance costs of computer and telecommunications networks. As a result, total system costs drop leading to the use of such technologies domestically [12], [13]. Polysaccharides and silicones have been used extensively as biomedical materials in drug delivery control and orthopaedic surgery [14], [15]. Today polymers are an integral part of our lives. Without polymers, it would be impossible to maintain our current lifestyles.

2.1.2 Advantages and disadvantages of polymer

Compared to steel and other metals, polymers are much lighter. This is beneficial as it reduces the weight of final products and the cost of transportation. Installation and maintenance expenditure are also kept to a minimum. For example, by replacing metal containers with ones made of polymers, transportation costs can be decreased dramatically due to the reduction in weight [16].

Most polymers have outstanding corrosion resistance. They are inert to most solvents and a wide range of chemicals. These properties make polymers suitable for application in harsh environments where metals are not a practical option. The excellent corrosion resistance in high humidity environment allows polymers to be used as instant dams and artificial seaweeds [17]. The electrical resistance of polymers makes them suitable insulators in both household and industrial electrical components. With the advantage of easy processing, they are ideal materials for the production of ergonomically and irregular designed shapes.

Nevertheless, polymers are not as strong in yielding strength as metals. They are also sensitive to heat resulting in low service temperature and ease of burning. They degrade into smaller molecules when exposed to excessive heat. In addition, polymers are also known to possess poor barrier properties.

While polymers have a number of advantages over metal, industry has a need for mechanically strong, electrical conductive, flame resistant and solvent/gas barring materials. Polymer properties have to be enhanced to give them the required properties.

2.2 The enhancement of polymer mechanical properties

2.2.1 Historic development of polymer reinforcement

Historically, there are two methods of making polymers stronger. The first is to make a polymer into fibres. The second method is the production of polymer composites. Polymer fibres are usually called organic fibres. Nylon 6, 6 was the first total man-made organic fibre synthesised by Wallace Carothers in 1935 [18].

Reinforcement using the fibre method results in the preferred orientation of molecular chains and a subsequent reduction in flaws and voids during processing. A polymer fibre thus becomes much stronger than its bulk form. High density polyethylene (HDPE) is a typical example. The tensile modulus and strength of monolithic HDPE are typically 0.4 GPa and 20-30 MPa respectively. In contrast, the modulus and strength of high drawn HDPE fibres can reach 117 GPa and 2.5 GPa respectively [19].

However, fibres have limited applications. Although the mechanical properties of a polymer increase after being drawn and stretched into fibre, fibres are easily damaged during subsequent processes when their diameter becomes smaller. This occurs because the fibre form cannot completely remove all voids from its structure, especially on its surface. Surface voids often lead to cracks when an extra force is applied. In order to overcome this, polymer fibres are usually produced as bunches, mats and yarns. An alternative solution is to bind fibres with other materials to form a composite. Composites are an important development in advanced materials. The application of this concept and technology has overcome many disadvantages of polymers and has

extended their use into a wide range of applications where polymers alone could not previously be employed.

The development and commercial application of polymer composites commenced in the 20th century. In 1913, laminated paper reinforced phenol formaldehyde resins were produced and used as electrical insulators [6]. Two decade later, a high tensile strength composite of silk/flax phenolic resin was reported by De Bruyne [20]. Two years later in 1939, high strength plywood with weather resistance was produced by hot-compressing phenolic resin pre-impregnated paper veneers. These products were used in the construction of Mosquito aircraft and motor torpedo boats, during World War II. After 1942, the research and market for reinforced polymers was gradually overtaken by carbon and glass fibre composites aimed at the aircraft and boat industry. These products include aircraft nose cones, airborne and ground radomes as well as structural parts of personal carrier boats [20]. Expansion into many other applications soon occurred. Today, polymer composites are widely utilised in buildings, bridges, tunnel construction, sporting equipment, vehicle and aircraft components [21]-[23].

Due to high specific modulus and strength, fibre composites are much stiffer and stronger per unit weight than metals. When achieving similar mechanical performance, the products of composites are much lighter than metals. This is especially an advantage of fibre composites where both mass and mechanical performance of components are of critical importance. For example, in aeronautical industry, the replacement of aluminium wings with polymer composites in Airbus A340-500/600 achieved a 20% weight reduction when compared to its predecessor the A340-200/300. Such weight reduction using polymeric components results in lower energy consumption [24].

Additionally, in the recent ‘Green Automobile Industry’ campaign, high performance long-fibre composites were considered by car manufacturers as a viable method to reduce the weight of vehicles. Understandably, the reduction of weight was designed to improve fuel efficiency and reduce carbon dioxide emissions [25].

A new generation of polymer composites, nanocomposites, appears in the late 1980s. The first real nanocomposite was developed by Toyota, via exfoliation of clay in N6 [2]. Since then, nanocomposites have attracted a lot of attention. At present, such products have become a competitor of carbon/glass fibre composites. Clay nanocomposites are the most successful commercially developed nanocomposites. They have been extensively used as engineering construction materials [26], [27], flame retardant [28] and barrier materials [29] in many industrial applications. Carbon nanotube composites are also an important branch of nanocomposites and have many outstanding properties such as high stiffness, outstanding electric and thermal conductivity [30]. Current research in this area is focused upon solutions for the filler agglomeration problem and the high production costs of nanotubes [31], [32].

2.2.2 The reinforcement of polymers

In general, composites consist of two or more constituents and possess superior properties to any individual component. One of the components is called the matrix. The matrix can be a polymer, a metal or a ceramic. When the matrix is a polymer, the material is known as a polymer composite.

The other component of a composite is the reinforcing phase which is usually strong and stiff and known as reinforcements. The reinforcing phase can be fibres, layer-

structured or particulate materials, which is embedded in the matrix. In the classification of reinforcing components according to material geometry, fibres are one-dimensional reinforcement, layered-structural reinforcing components are two-dimensional and spherical particles are zero-dimensional reinforcement. Several examples for each type of reinforcement material are illustrated in Table 1.

Table 1: Reinforcement fillers in polymer composites

Spherical particles 0-D reinforcement	Fibres 1-D reinforcement	Layered-structure fillers 2-D reinforcement
CaCO ₃ , Al(OH) ₃ Silicas Carbon black Glass beads Nano-particles	Carbon fibre Glass fibre Organic fibre Boron, Silica fibre Carbon nano tube/fibres	Smectite Clay Silica/glass flakes Bhomites Graphite

Understandably, the production of composites using reinforcements in different size ranges results in products with different properties. Consequently, polymer composites are also categorised by filler size as micro, nano and sub-micro composites. The dimensional range of each regime is shown in Table 2.

Table 2: Dimensions of the reinforcing phase

Molecular	Nanoscale	Sub-micro	Micro
< 0.1nm	~1nm—100nm	100nm—5µm	5—30µm

Carbon fibre and glass fibre are the most popular reinforcements used in fibre microcomposites. Clay, graphite, CaCO₃, Al(OH)₃ and silicas can be used as either micro or nano fillers dependent on their size in the micro or nano range. Carbon nano

tubes/fibres are important for the production of carbon nanocomposites. Several individual fillers are discussed in this section including carbon fibres, glass fibres, clays, graphite flakes, carbon nanotube/fibres and glass flakes.

2.2.2.1 Carbon fibres

Carbon fibres are essentially produced from organic materials such as rayon, pitch, polymers which already contain or readily form aromatic structures when undergoing graphitisation/carbonisation heat treatment. The manufacture of carbon fibre is energy intensive and hence expensive. The production process comprises of melt spinning, stabilisation, carbonisation/graphitisation, surface treatment and sizing. A commercial carbon fibre production process for pitch and polyacrylonitrile (PAN) is shown in Figure 1 [33].

The properties and structures of carbon fibres are affected by heat treatment temperature and the ability of graphitization of the carbon fibre precursor. High strength fibres are produced at temperature between 1200-1600 °C while high modulus carbon fibre are produced at temperatures over 1800 °C. At present, a high stiffness carbon fibre with an axial tensile modulus of 895 GPa and a high strength carbon fibre with an axial tensile strength of 4.7 GPa are commercially available [34].

Pitch-based carbon fibres have sheet-like structures, while PAN-based carbon fibres have a turbostratic texture. These structures are shown schematically in Figure 2 [33].

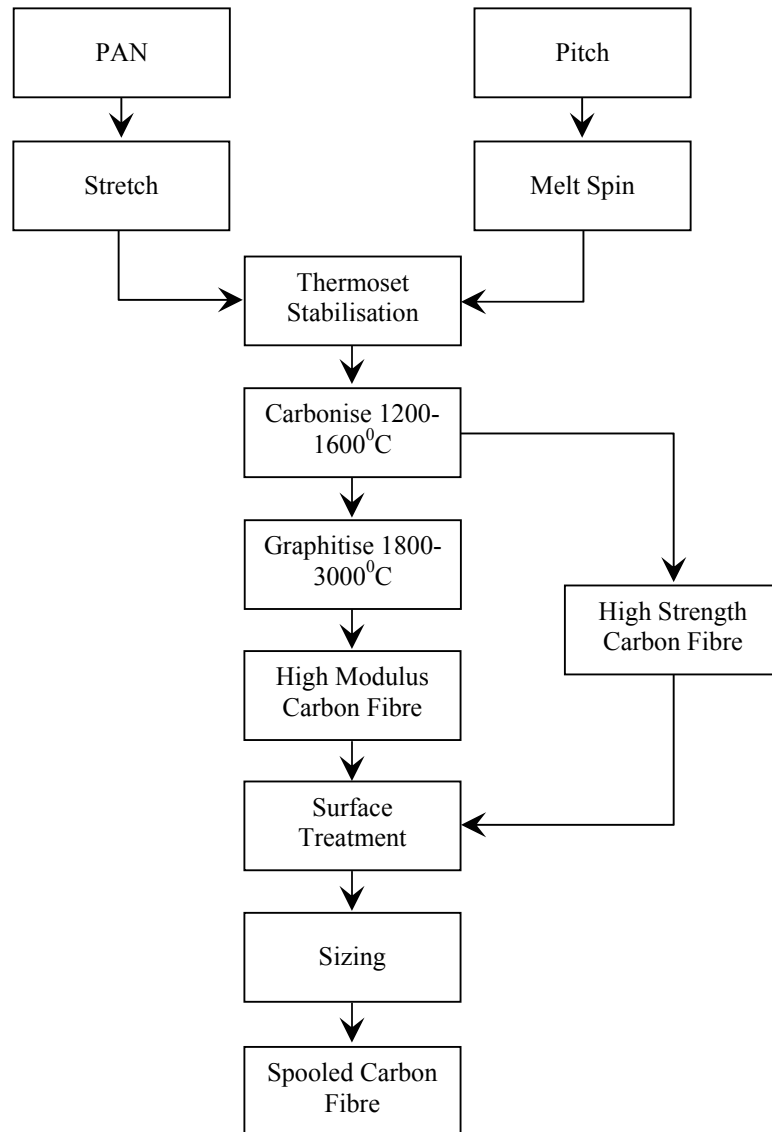


Figure 1: A commercial carbon fibre production process [33]

are formed. After high speed winding, glass fibres are twisted, roved, woven or chopped into short fibres ready for use. With this process, glass beads and micro-sized glass flakes can also be obtained. Figure 3 shows a direct melt processing of glass fibres [36].

Different types of glass fibres can be produced using different compositions of raw materials. The different types have different properties and application domains. Depending on the properties of resulting products, glass fibres are classified as electrical insulation, high strength, and chemical resistance fibres. These are correspondingly referred to E-glass, S-glass, and C or A-glass [36] respectively. The tensile yielding strength of commercial S and C glass fibres can reach up to 3.1-3.8 GPa and 2.7-3.03 GPa while the tensile modulus is 76-81GPa and 63-69 GPa respectively [37].

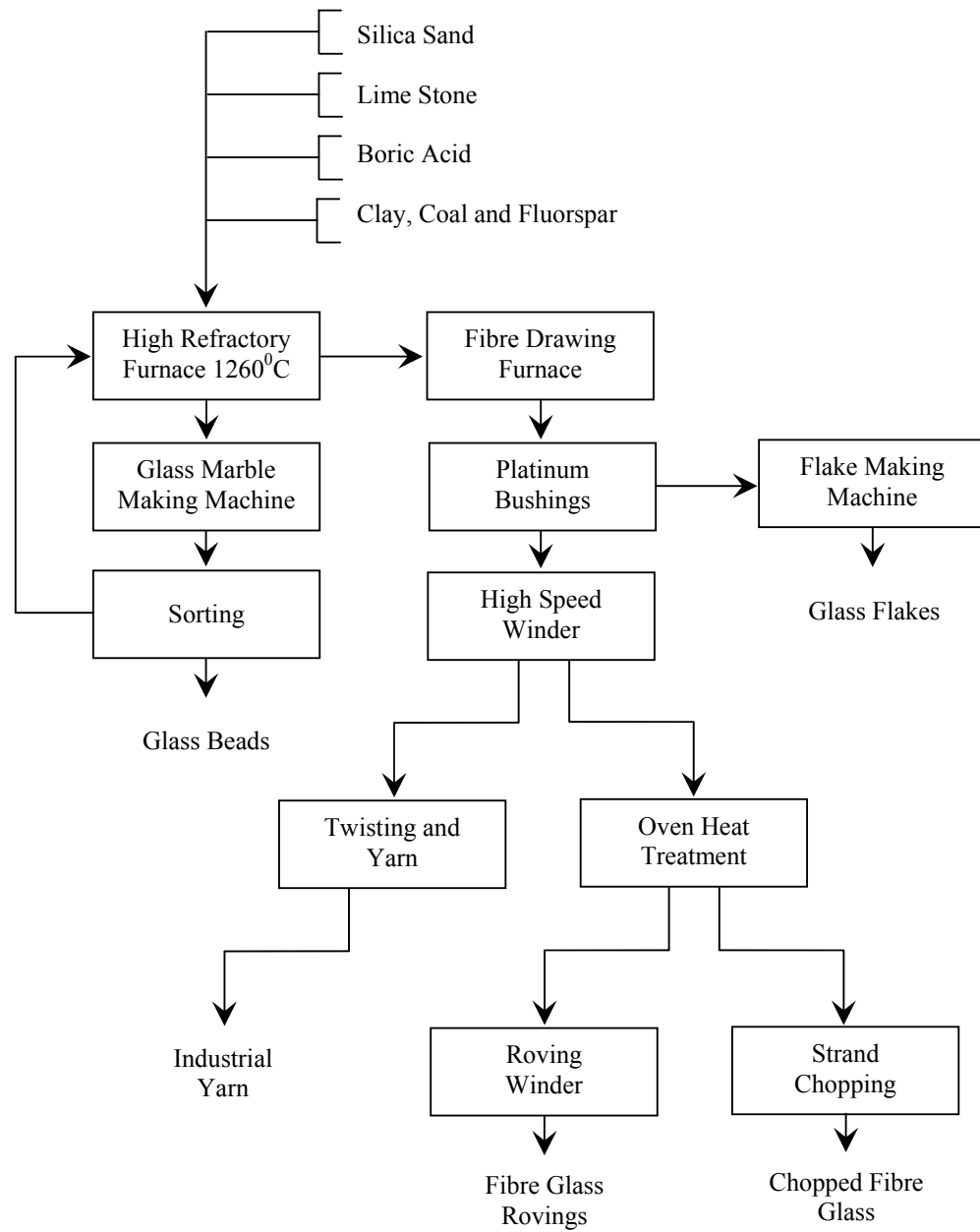


Figure 3: The direct melt processing of glass fibres [36]

2.2.2.3 Clay

The popular clays used for composite application are kaolin and smectite groups. The smectite group is particularly useful for nanocomposite application. The structure of kaolin and smectite clays consist of two basic building blocks, tetrahedral silica ($\text{Si}_2\text{O}_5^{-2}$) and octahedral alumina ($\text{Al}(\text{OH})_6^{-3}$) as shown in Figure 4 [38]. In the tetrahedral silica, one silicon atom bonds with four oxygen atoms. The tetrahedrons share three out of every four oxygen atoms and are arranged in a hexagonal pattern where the basal oxygen atoms link together and apical oxygen atoms point up or down. In the octahedral alumina, one aluminium atom bonds with six oxygen atoms. These octahedrons join together at their edges and are arranged in a hexagonal pattern.

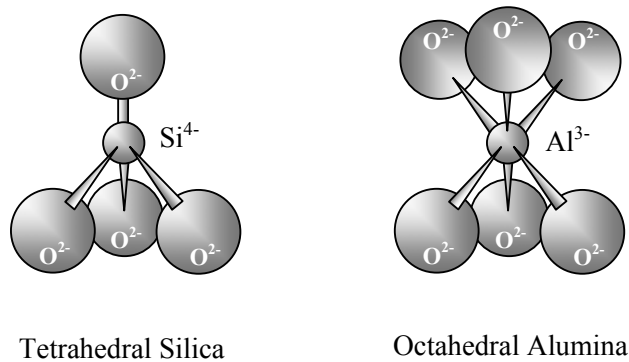


Figure 4 : The structure of clay building blocks [38]

Kaolinite is from the kaolins group and has the structural formulae $\text{Al}_4\text{Si}_4\text{O}_{10}(\text{OH})_8$. The kaolinite lattice consists of one sheet of silicon tetrahedron and one sheet of aluminium octahedron and hence a 1:1 or a two-layer structure clay. Two layers join together by the apical oxygen ions, of the silicon tetrahedron layer, as shown in Figure 5. Kaolinite

has a basal spacing of 0.71 nm across the (001) plane. It is a non-expanding clay mineral and has a low cation exchange capacity of 0.03-0.15 meq/g [39]-[41].

Smectites have a 2:1 or triple layer sandwich structure that comprises of an octahedral alumina sheet at the centre, bonded to two tetrahedral silica sheets by oxygen ions. The oxygen ions belong to both the octahedral alumina sheet and tetrahedral silica sheet after the bonding [40]. Aluminium in octahedral sheets can be substituted by magnesium and iron. The replacement of Al by Mg or Fe with less numbers of valence electrons gives the clay layers an overall negative charge. The charge is often balanced by the presence of calcium, potassium and sodium cations absorbed between the three layers. These cations, however, are held relatively loose and are readily exchanged by other cations with either long or short chains [41]. The triple sheet layer is 0.22 nm thick [39] and its basic structures are illustrated in Figure 5.

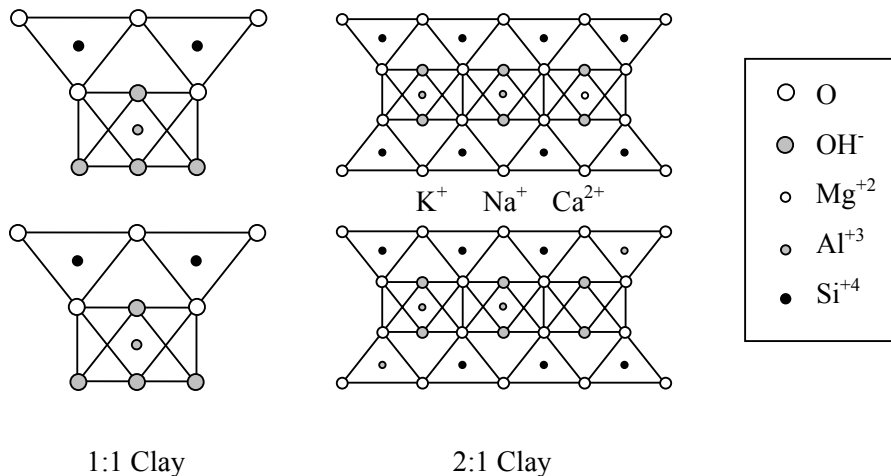


Figure 5: The structure of 1:1 and 2:1 clays [40], [41]

The triple sheet layers form stacks with the interlaminar gallery between them. Montmorillinite is the most common smectite with a general structural formulae of $(\frac{1}{2}\text{Ca,Na})(\text{Al,Mg,Fe})_4(\text{Si,Al})_8\text{O}_{20}(\text{OH})_4 \cdot n\text{H}_2\text{O}$ and typical basal spacing of 1.2-1.4 nm. Montmorillinite is an expandable clay mineral and has a high cation exchange capacity of 0.8 to 1.2 meq/g [41]. The expandable inter-layer space and high cation exchange capacity allow polymer monomers or chains intercalating into the clay structure resulting in the formation of nano polymer composites. This characteristic permits smectite clays to play an important role in polymer nanocomposite reinforcement.

2.2.2.4 Graphite

Graphite flakes are made from natural graphite. The degree of graphitization can be as high as 99.9%. They possess the lowest level of crystal defect amongst graphite products [42]. A graphite crystal is comprised of parallel planes, stacked in a regular ABAB... sequence or ABCABC... The ABCABC... sequence is, however, not dominant. The structure of ABAB... sequence is shown in Figure 6.

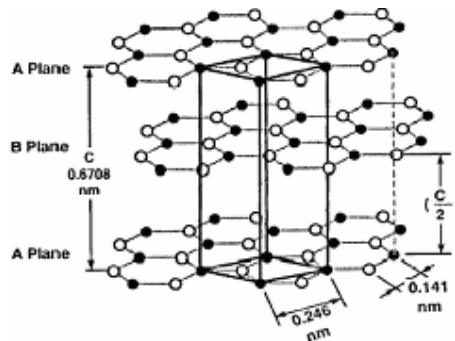


Figure 6: The crystal structure of graphite [42]

Within a single plane, each carbon atom is bonded to three others by strong covalent bonds forming continuous hexagons. This structure can be considered as a two dimensional infinitely large molecule with adjacent planes being held by much weaker van de Waals bonds [42]. As a result of such structure, the Young's moduli in the layer direction can be as high as 1000 GPa [32] with theoretical axial tensile strength of about 100 GPa [3]. The Young's modulus in the direction perpendicular to the planes is 35 GPa [5]. Providing graphite flakes are exfoliated into individual layers in polymer matrices, the outstanding mechanical properties of graphite layers would be fully utilised. Therefore, graphite has great potential for enhancing the mechanical properties of polymers.

2.2.2.5 Carbon nano tubes/fibres

Only a few reports on carbon nanofibres were produced between 1950s-1970s [43], [44]. Little attention was paid to them due to their imperfect structures and high production cost. However, the discovery of tubular structured fullerenes, i.e., multi-walled carbon nanotubes (MWCNTs) in 1991, brought carbon nano-fillers back into research. Shortly afterwards, single-walled carbon nanotubes (SWCNTs) were discovered by Iijima *et al.* in 1993 [45], [46]. At present, thousands of papers on carbon nanotubes are published every year [30], [47]-[50].

The structure of carbon nanotubes consist of long and thin tubes rolled from a graphite sheet with an armchair, zigzag or chiral orientations depended on the rolling angle, as shown in Figure 7 [30]. The edges of tubes have a closed structure apart from Herringbone multi-walled nanotubes which have an open truncated-cone-like structure.

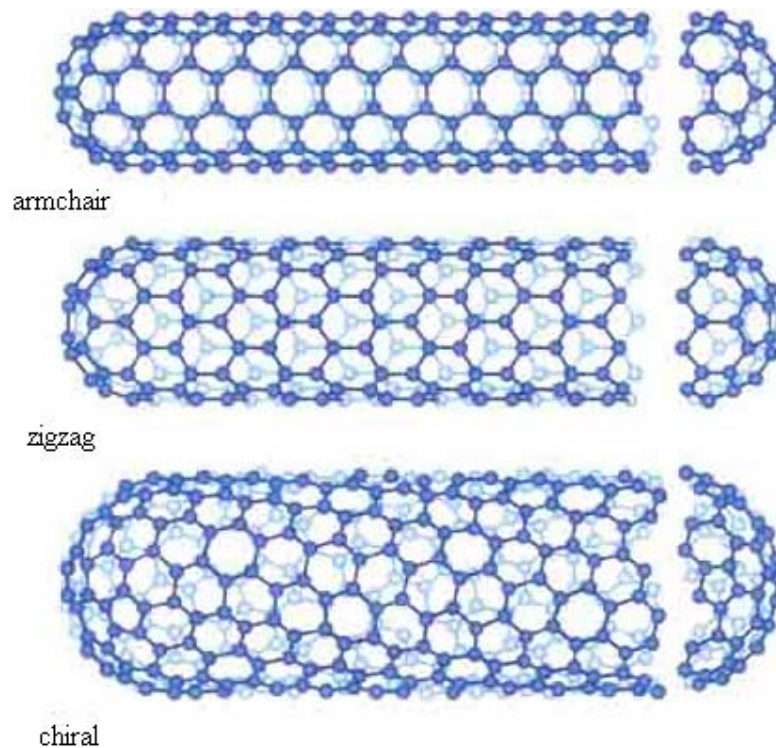


Figure 7: Structure models of single walled carbon nanotubes [30]

Carbon nanotubes possess some outstanding properties due to their exclusive shape and structures. The Young's modulus of SWCNTs can reach 1000 GPa while tensile strength is close to 30 GPa [30]. These properties are theoretical in-plane stiffness and transverse strength of the graphite crystal and are much higher than steel. Carbon nanotubes have extraordinary electronic properties. They offer semi or metallic conductivity depends on their structure. When a nanotube is made by rolling a graphite sheet at a specific angle, its conductivity can be in the metal range. The calculated conductivity of ropes of SWCNTs can be high as 10^4 S/cm [51]. In addition, carbon nanotubes have a remarkable tolerance to high density currents [52].

Commercial applications of carbon nanotubes, however, have been impeded by high production costs and low yields of high quality product. So far, arc-evaporation, laser ablation and chemical vapour deposition have been used to syntheses carbon nanotubes. The first two methods produce high quality carbon nanotubes but involve high temperature, high energy consumption and low productivities. The chemical vapour deposition method, in contrast, has difficulty in producing high quality nanotubes; even though it allows production on a larger scale which results in relative low priced nanotube products.

Due to their excellent mechanical and electrical conductive properties, carbon nanotubes have great potential in polymer enhancement applications. Recent research into carbon nanotube composites has concentrated on the improvement of dispersion extent of nanotubes in polymers and nano-sizing techniques, in order to increase the reinforcement efficiency of carbon nanotubes [32], [52]-[54].

2.2.2.6 Glass flakes

Glass flakes can be used as a replacement for glass fibres to enhance the polymers. Compared to glass fibres, the production costs of micro-sized glass flakes is lower due to their simpler processing procedure as shown in Figure 3 [37].

Ultra-thin flakes, however, are difficult to produce using common melt processing techniques. A sol-gel method has been developed to manufacture glass flakes with thicknesses less than 1 μm by Nippon Sheet Glass Co [55]. Ethane, isopropanol, silane and nitric acid were used to prepare a silica sol solution. The sol was coated on a stainless sheet substrate at low temperature after the required viscosity of solution was

reached. During the drying process, the sol turned into a gel film. By peeling the film off the gel films from the substrate, thin gel flakes were obtained and converted into glass after treatment at 900 to 1200 °C.

Using the sol-gel method, a very narrow thickness distribution of glass flakes can be achieved. The standard deviation of flakes with thickness 0.588 μm can be as low as 0.081 μm according to Takemura [55]. It is not possible to achieve such narrow distributions with conventional methods or naturally formed flakes.

In 1998 ultra-thin glass flakes were developed by Glassflake Ltd. and applied to polymer enhancement in 2000. Today, 750, 350 and 100nm thick products are available but not produced on a commercial scale [56]-[58]. Even now reports on their performance in polymer enhancement are limited.

2.2.3 Fibre composites

Fibre/polymer composites are an important development in advanced materials. This technology has been used to overcome the many disadvantages of polymers and allowed them to be used in a wide range of applications where polymers were previously unsuitable due to their lack of required mechanical properties.

The diameters of fibres used for polymer reinforcement are normally 5 to 30 microns and usually over a hundred microns in length. Classified by the smallest dimension of reinforcement, the enhancement of fibre composites is therefore in the micro range. Carbon and glass fibre composites are the main types of fibre composites and have dominated the market of reinforced polymers since they were developed. Organic,

boron, silica carbide fibre composites are also newly developed for specific applications, such as high temperature resistance [16], [59].

In general, all fibre composites are enhanced by either long or short fibres. Long fibre reinforcement, also called continuous reinforcement, is where fibres are bundled, roved, matted, woven or knitted in aligned and laminated form. Such reinforcement thus has a preferred orientation. Short fibre reinforced composites, in contrast, are less uniform in alignment and have an orientation efficiency factor of 0.6-0.7 in general [60]. In this section, the fabrication of long fibre reinforced thermoset and short fibre reinforced thermoplastic composites as well as mechanical properties of carbon and glass fibre reinforced plastics are discussed.

2.2.3.1 The fabrication of fibre composites

The processing method of long fibre reinforced thermoset composites generally comprises of autoclave moulding, resin transfer moulding, pultrusion and filament winding. Pultrusion and filament winding can also be used for thermoplastic composites [1], [5], [61]-[65].

Prior to autoclave processing, fibre layers are impregnated, hand/automated lay-up and bagged. Autoclave consists of two stages. During the first stage, pressurisation up to 1 MPa coupled with medium temperature and full vacuum underneath the bag are applied in order to get rid of volatiles and allow resin flow. The second stage is resin curing in which the autoclave pressure and temperature is further increased [61]. This process can be used for large component manufacture.

As its name suggests, with resin transfer moulding fibres are arranged in a mould into which resin and cure agent are injected. This method is usually applied to low viscosity resins and can produce relatively large mouldings [5], [65].

Pultrusion and filament winding processes both involve fibre tows being pulled through a resin bath. The impregnated fibres are then fed into a heated and tubular die for consolidation and curing. Pultrusion and filament winding are methods used in the production of continuous length fibre reinforced parts. When compared with autoclave, they are economical and uncomplicated [62]-[64]. However, in the case of high viscosity plastics, with these techniques, it is difficult to achieve uniform impregnation especially at the centre of tows [1], [5].

Short fibre reinforced thermoplastic composites can be produced using universal processes that are commonly in neat thermoplastic production. Injection moulding and extrusion are two such examples [1], [66]-[68]. The injection moulding process is very straightforward. Pre-blended polymer and fibres are fed directly into a heated barrel where the polymer becomes molten. The mixtures are then forced into a relatively cool mould cavity by means of high pressure. Fabricated parts are ejected once the mouldings have solidified. This process can produce complex shaped components with considerable speed and precision. It is, however, difficult to apply this process to high viscosity and high fibre loaded composites [67], [68]. With extrusion techniques, fibres can be well dispersed within composites. Unfortunately, the process can cause fibre breakage leading to significant decreases in fibre length and aspect ratio. This in turn results in reduced mechanical properties of composites [68].

The master batch technique is also used to produce short fibre composites, providing high loaded fibre composites are already available. Pre-blended mixtures of the pure polymer and the composite with a high fibre volume fraction are compounded by injection moulding, extrusion. Using master batch good fibre dispersion can be achieved.

2.2.3.2 The mechanical properties of long fibre composites

The mechanical properties of fibre composites are usually evaluated in terms of Young's modulus, strength and toughness in fibre and transverse directions. Additionally, specific modulus and strength are also widely used as the evaluation. The mechanical performance of long fibre composites is a function of fibre and matrix properties, fibre content, interface bonding between fibre and matrix as well as void and moisture content. Generally, mechanical properties improve with fibre loading and improved interfacial bonding but decrease with increasing void and moisture content. In addition, the modulus and strength of a composite in the fibre direction are usually much higher than those in the transverse direction. For example, with 45% fibre volume content, the stiffness and strength of a carbon fibre unidirectional epoxy composite can be as high as 120-160 GPa and 700 MPa in the fibre direction while the transverse modulus is only 5 to 8 GPa [59], [69]. At the same fibre fraction of 45%, glass fibre reinforced epoxy composites have a lower longitudinal modulus of 20 to 40 GPa and strength of 400-500 MPa [69], [70]. This is a result of the lower mechanical properties of glass fibre.

Fibre volume fraction has a significant effect on the mechanical performance of composites. In results reported by Botelho *et al.* [71], Nylon 6, 6 with 40vol% carbon

fibre had a Young's modulus of 35.4 GPa, a tensile strength of 408 MPa and a compression strength of 290 MPa in the fibre aligned direction. When fibre loading was increased from 40 to 60vol%, the mechanical properties of the composite were improved 44.4% in Young's modulus, 25.5% in tensile strength and 34.8% in compression strength.

The interface bonding between fibre and matrix is also important for the mechanical properties of composites, especially for transverse strength. With a 60% volume fibre glass reinforced unidirectional laminar polypropylene composite, flexural strength and flexural modulus were 774MPa and 38.5 GPa while transverse flexural strength and flexural modulus were 8.6MPa and 4.9GPa respectively. A maleic anhydride grafted polypropylene was added to the matrix to improve the interface bonding of fibre and polypropylene. In doing this, increases of 34% in longitudinal strength, 139.5% in transverse strength and 38.8% in transverse modulus were achieved. The longitudinal modulus, however, reduced by 15.8% while longitudinal elongation to failure remained unchanged at 2-2.6% according to Rijdsdijk *et al.* [72].

Void and moisture have negative effects on the mechanical performance of a composite. The research of Bureau *et al.* [73] shows that the flexural strength and flexural modulus of a unidirectional polypropylene composite reinforced with 60wt% glass fibre was 250MPa and 12.1GPa respectively. The properties, however, decreased to 123MPa and 8.7GPa (i.e. dropped by 54.8% and 28% respectively), when void content of the composites increased from 1-6 to 8-10%. In the case that water interacts with matrix or the surface of fibres, through hydrogen bonding, moisture absorption occurs. This leads

to a reduction of glass transition temperature and deterioration in the dynamic mechanical properties of composites [74].

2.2.3.3 The mechanical properties of short fibre composites

Except for matrix and fibre properties as well as fibre content and interfacial bonding, the mechanical performance of short fibre reinforced composites is also strongly affected by fibre length/aspect ratio and fibre orientation.

Similar to long fibre composites, the mechanical performance of short fibre reinforced composites increases with fibre volume fraction and improvements in the interfacial bonding between fibres and matrices [68], [75]-[82]. For example, when glass fibre fraction is increased from 10 to 30wt%, the mechanical properties of a polyethylene terephthalate composite improve 64.7% in tensile strength and 114% in Young's modulus [75]. According to Ozkoc [76], the addition of N6 into short glass fibre reinforced acrylonitrile-butadiene-styrene (ABS) composites resulted in improved interfacial adhesion between the fibre and ABS. Consequently, the properties of a 30wt% glass fibre/ABS composite, blended with 20wt% N6, increased 17% in tensile strength, 24% in elastic modulus and 300% in unnotched impact strength, when compared with the corresponding glass fibre/ABS composite.

Large fibre length and aspect ratio are the preferred properties for short fibre reinforced composites. Only if fibre length/aspect ratio is superior to critical length/aspect ratio, can the strain in the fibre build up to the matrix value leading to efficient improvements in mechanical properties of composites [5]. Fibre length and aspect ratio in composites, however, can be reduced significantly due to fibre breakage during extrusion and

injection moulding processes. Such breakages result in the decreased mechanical performance of composites. The effect of fibre breakage on the mechanical properties of composites depends on the processing method employed, processing conditions and viscosity of polymers [68], [76], [79]-[83]. It has been reported [68] that when screw speed was increased from 25 to 200 rpm during the injection moulding process, fibre length reduced to 310 μm from 450 μm . Correspondingly, the tensile strength of short glass fibre reinforced polypropylene dropped by 25% from 60 to 45 MPa.

Sui *et al.* [79] used a one-step injection moulding process to avoid thermal mechanical degradation in glass fibre length. They found that by applying the one-step injection process, average fibre length in glass fibre/EPDM-toughened Nylon 6,6 composites are longer than those in the composites produced using an extruding pre-compounding method. Consequently, the tensile strength and modulus of composites, produced using the one-step injection process, were 20-30% and 42.5% higher than the pre-compounded composites. Similar results have also been obtained by Moriwaki [83] with short glass fibre enhanced nylon 6I/6T blended N6 composites.

Ozkoc *et al.* [76] investigated the effects of polymer viscosity on length distributions in short glass fibre composites. By adding N6 into a 30wt% glass fibre/ABS system, the viscosity of composites decreased significantly. Melt flow index was observed to increase to 13.7 g/min from 3.2 g/10 min as did average fibre length, 482 μm from 427 μm , when N6 content increased from 0 to 30wt%. The number of long fibres also significantly increased after the addition of N6.

During the injection moulding process, fibre orientation behaviour is complex and a skin/core/skin structure is generally developed. In the skin region, fibres are usually well aligned along the melt flow direction while random orientation occurs in the core of the moulding. Because only those fibres aligned in the load direction fully contribute to mechanical performance of a composite, the fibre orientation distribution/factor must be taken into account when evaluating the mechanical properties of short fibre reinforced composites. Fibre orientation is also affected by injection speed, melt and mould temperature. With low injection speeds, high melt and mould temperature, fibres tend to align in the flow direction [68], [75], [84].

2.2.4 Nanocomposites

When reinforcing fillers are dispersed into a matrix in the nanoscale, which is defined as less than 100nm in at least one direction, a nanocomposite is formed. The fillers in a nanocomposite can be in the form of particles, fibres or layered-structural sheets. For example, metal nanoparticles, carbon nanotubes and clays [85]-[90]. Boehmite (γ - Al_2O_3) based composites have also recently been reported [91], [92].

At present, nano reinforcing techniques have been applied to a wide range of polymers such as polyamide [27], [92]-[96], polypropylene [95]-[102], polyethylene [90], [103], polystyrene [104], polyimide [106], epoxy [95], [98]-[108], polyurethane [109] and ethylene vinyl acetate copolymer [95], [110]. The extensive research conducted has shown that the properties of polymers can be improved significantly at low filler loadings. These improvements include mechanical properties [93]-[96], [101]-[110], thermal resistance [93], [99]-[109], [111], solvent/gas permeation [27], [112] and flame

retardance [110], [113]. Details on synthesis methods, characterisation and mechanical property improvements of nanocomposites are reviewed in the following section.

2.2.4.1 The synthesis and characterisation of nanocomposites

Nanocomposites can be prepared by means of in-situ polymerisation [114]-[115], solution blending [116], direct melt [117]-[119] and sol-gel methods [91].

The in-situ polymerisation method requires fillers to be completely wetted with polymer precursors. This allows dispersion of fillers and polymerisation to occur simultaneously. This technology is commonly employed in the polymer synthesis industry. It is also useful in the production of thermoset nanocomposites.

Direct solution blending is carried out using solvents to swell and disperse fillers into a polymer solution. The method is limited due to the high cost of solvents as well as health and safety issues associated with the disposal of solvent used [2]. It is, however, advantageous if water can be used as a replacement for solvents in processing [116], [120].

In the direct melt blending technique, fillers are dispersed into a polymer during melt processing. For most polymer systems, the dispersion of fillers in this way is not as efficient as using the in-situ polymerisation method. However, direct melt blending method does play an important role in nanocomposite manufacture since traditional polymer processing techniques, such as extrusion and injection moulding, can be applied directly [2].

The sol-gel method involves the preparation of a sol solution containing inorganic/organic precursors, fillers and monomers/polymers, the gelation of sol and drying of the gel [121]. This process is mainly applied in the synthesis of metal or colloidal particle enhanced nanocomposites and is also popularly used in combination with in-situ polymerisation or direct solution methods [122].

The characterisation of nanocomposites depends on the structure of fillers and properties of nanocomposites. For nanoparticles, carbon nanotubes and single-layered fillers enhanced nanocomposites, the most important issue is the extent of dispersion of fillers within polymers. This can be characterised using scanning and transmission electron microscope imaging analysis [85], [112], [123]. For layer structured fillers, such as clays, the important issues are not only the level of filler dispersion but also layer exfoliation. The basal spacing of clay crystals expands after exfoliation resulting in a shift of X-ray pattern characteristic peaks. X-ray diffraction analysis can therefore be employed to determine the exfoliation level of clay in nanocomposites [112], [124]. In addition, the thermal properties and flame retardancy of nanocomposites can be evaluated by means of differential scanning calorimeter, thermogravimeter and cone calorimeter instruments [85], [123].

2.2.4.2 The enhancement in mechanical properties of nanocomposites

With nanocomposite technology, the mechanical properties in elastic modulus, strength and toughness of polymers can be improved significantly at low filler content [27], [92]-[105]. The degree of mechanical property improvement in nanocomposites is strongly depended on the extent of dispersion of fillers in composites, the compatibility

of filler with matrix as well as matrix properties. In general, the better the reinforcement dispersion the better the mechanical property improvement achieved.

The degree of dispersion of fillers in nanocomposites can be fundamentally determined by the synthesis method. In general, in-situ polymerisation results in better dispersion than the directly melt blending method and leads to better mechanical performance in nanocomposites. For example, N6 nanocomposites synthesised using in-situ polymerisation can achieve improvements in tensile modulus ranging from 68.5 to 165% and increases in tensile strength between 40% and 67.1%. The enhancement of melt compounding products in tensile modulus and strength are lower and in the range of 36-61.65% and 20-34% respectively [27], [92]-[96]. Similar results were also observed in carbon nanotube composites. It was found that the elastic modulus of multi-walled nanotube/polyamide 1010 composites, synthesised using in-situ polymerisation with tube content ranging from 5 to 30wt%, increased by 41.9-87.2% when compared with the pure polymer. For composites prepared using the melt mixing technique, in contrast, the degree of elastic modulus improvement were between 20% and 67.3% when compared with the pure polymer [97].

Also, for clay nanocomposites depending on the property desired, different types of dispersion are required. Wang [98] reviewed the effects of clay exfoliation level on the property improvement of nanocomposites. It was concluded that increased stiffness benefited from the exfoliation of clay whereas improved toughness was due to intercalated clay layers. With 2wt% filler content, fracture toughness of an intercalated clay/epoxy nanocomposite was improved by 77% from 0.62 to 0.97 MPa·m^{1/2} [99].

The compatibility between filler and matrix is crucial in the production of high performance nanocomposites. This issue especially exists within systems where low/non-polar polymers are used as matrix, for example, polypropylene and polyethylene or carbon nanotubes used as reinforcement. When inorganoclays are utilised to prepare polypropylene composites, the tensile properties of resulting products remain unchanged or decrease, when compared with the pure polymer [100]-[102]. When an organoclay, a compatiliser or both were applied, on the contrary, an improvement in the range of 14-42.6% in tensile strength [96], [101], 40-45% in Young's modulus [100], [101] and 70% in notched Izod impact strength was achieved [101]. Jin [105] investigated the effects of modified multiwalled carbon nanotubes using different surfactants on the mechanical properties of PET in-situ polymerised composites. The results obtained showed that with non-modified tubes at a loading of 0.5 to 2wt%, tensile strength and tensile modulus of all composites was reduced when compared to the pure polymer. With a 1,10-diaminodecan modified carbon nanotube composite, a significant increase of 236% in tensile strength and 92.8% in tensile modulus was achieved at 0.5wt% filler content when compared with the PET. An increase of 81% in tensile strength and 178% in tensile modulus was also achieved at 2wt% nanotube content. For the acid modified nanotube composites, strength and modulus reached a maximum at 1.0wt% filler content. Over 2.0wt%, however, a dramatic decrease was demonstrated due to the interface weakening caused by the agglomeration of nanotubes.

The degree of mechanical property improvement of nanocomposites is directly related to the type of matrix material employed. With an elastomeric epoxy nanocomposite in-situ polymerised from octadecyl ammonium ion modified clay, at 20wt% filler loading,

tensile strength and tensile modulus increased 9.5 fold and 8.5 fold when compared with the base polymer. Glassy epoxy clay nanocomposites, in contrast, improved only 15-42.8% in tensile modulus and 19.7-28.9% in tensile strength [98]-[107].

2.2.4.3 The combination of nano and micro reinforcement

Recently, nano reinforcing materials have been introduced into micro reinforcement to improve the interface shear strength between fibre and matrix. Improvements in interface shear strength in turn increase the toughness, transverse and compression properties of fibre composites. Nano-fillers employed in such applications include carbon nanotubes, carbon nanofibres and synthetic mica. For example, carbon nanofibres were used to toughen polyester/glass fibre composites by Sadeghian *et al.* [125]. With 1wt% nanofiller, the toughness of fibre composite was improved nearly 100% based on model-I delamination tests. Zhu *et al.* [126] used glass fibres coated with 0.1wt% single-walled carbon nanotubes to reinforce polyester. The short beam shear strength of the resulting composite, at 70vol% fibre content, was increased by 44.4% when compared with the corresponding composite without carbon nanotube coating. In work carried out by Vlasveld *et al.* [127], by adding 10wt% synthetic nanomica, the compression property of a fibre composite increased approximately 40% at 120 °C. There was, however, no obvious change below 40 °C. Meanwhile, the flexural strength of the same sample was increased by 17% at room temperature and 40% at 120 °C.

These results indicate that fibre composites combined with nano-reinforcement have the potential to produce materials with enhanced mechanical properties. More work, however, is required in order to achieve further improvements in mechanical properties.

2.3 The enhancement of other physical and engineering properties

In addition to mechanical properties, nanocomposite technology can be used to enhance other engineering properties. In this section, nano-enhancement in flame retardancy, barrier and electrical conductive properties of polymers are reviewed. Electrically conductive carbon fibre composites are also briefly outlined.

2.3.1 Flame retardancy

The flame retardant properties of polymers can be improved by clay/polymer nanotechnology. The most attractive achievements in flame retardancy with clay nanocomposites are significant reductions in peak heat release rate (PHRR), mass loss rate (MLR), smoke density and the amount of carbon monoxide (CO) produced during material combustion. According to Gilman [128], with 5wt% clay, the PHRR and MLR of a clay/N6 nanocomposite decreased by 63% and 67% respectively while there was no increase in the release of soot and CO when comparing with the pure N6.

Bourbigot *et al.* [113] studied multi-filament yarns of N6/clay nanocomposites produced by direct melt intercalation and melt spinning processing. They found that the peak heat release rate of their knitted fabrics decreased by 40% with corresponding reduction in smoke density and maximum amount of carbon monoxide produced, compared with pure N6. Zhu *et al.* [114] investigated clay/polystyrene nanocomposites produced using an in-situ polymerisation method. Their results showed that the nanocomposites produced have a much lower peak heat release rate and smoke density than pure polystyrene. Interestingly, the reduction in smoke density was independent of the clay content in composites. Zanetti *et al.* [117] introduced poly ethylene-co-

vinylacetate (EVA) into clay polyethylene (PE) composites in order to improve compatibility between PE and clay and hence achieved better clay dispersion. The maximum MLR of PE/EVA/clay nanocomposite was found to be $0.76\% \text{ sec}^{-1}$ which is half that of the PE/EVA blends.

In addition to clay/polymer nanocomposite itself, synergy between clay nanocomposites and other fire retardants has been reported. The synergy between three universal phosphorus fire retardants and organic clay was investigated by Chigwada *et al.* [129]. The polystyrene nanocomposite, with 30% resorcinol diphosphate and 5% clay, exhibited a reduction in PHRR of up to 92% and a decrease of 60.7% in total heat release from 109.7 to 43.1 MJ/m² when compared with the pure polymer. In the system without clay, the PHRR reduced by 64% only. This approach, however, resulted in the reduction of corresponding mechanical properties due to the high filler content of fire retardants used.

Carbon nanotubes and graphite oxide are also used to enhance the fire retardancy of polymers. Using a Brabender internal mixer, Peeterbroeck *et al.* [110] prepared an EVA nanocomposite with 4.8wt% MWNTs. Results obtained showed that the PHRR of the nanocomposite reduced by 30% while a clay/EVA nanocomposite containing the same filler content decreased by 18.96% when compared with pure EVA. With a combination of both clay and nanotubes at 4.8% loading in total, the PHRR reduction ratio of the composite increased by 6.2% and 17.24% when compared with clay/EVA and carbon nanotube/EVA composites at 4.8wt% filler loading respectively. The reason for this is reported as the synergistic effect between carbon nanotubes and clay. Zhang *et al.* [130] utilised Graphite oxide to improve the flame resistant property of styrene butyl acrylate

copolymer. By adding 1wt% of graphite oxide to the polymer, a reduction of 45% in peak heat release rate was achieved when compared with pure copolymer. Mass loss rate, total smoke production and smoke release rate were also lower than those of the pure polymer.

Improvements in flame retardancy of polymer nanocomposites are essentially caused by the enhanced performance of combustion chars. Chars act as a barrier for heat transfer and volatile evolution. The less flammable volatiles are therefore produced leading to less flammable gas in the flame region. The efficiency of the char barrier formed depends on both quantity and quality of combustion chars [131].

Kashiwagi *et al.* [88] investigated char yield and char morphology of clay/N6 nanocomposites after cone calorimetric measurements in a nitrogen flow. They found that the order of char yield was 5wt% clay nanocomposite > 2wt% clay nanocomposite > pure polyamide. The 2wt% clay/N6 nanocomposite produced a char yield of 5% which is 2.5 fold that of the pure polymer. The char formed from these nanocomposites was reported as being brittle and containing many cracks. In work by Peeterbroeck *et al.* [110] and Gao *et al.* [132] the quality of char produced by a clay nanocomposite can be improved by adding carbon nanotubes into the composite. The research of both groups is based on ethylene vinyl acetate copolymer. The char morphology produced from clay/MWNTs/EVA composites were compared with those from clay/EVA nanocomposites. Results obtained show that chars formed from clay/MWNTs/EVA nanocomposites contain far fewer cracks than clay/EVA nanocomposites [110], [132]. The combustion chars of clay/MWNTs/EVA nanocomposites also exhibited better oxidation resistance than those formed from clay/EVA nanocomposites [132].

2.3.2 Barrier properties

In general, barrier improvement is a function of aspect ratio of fillers. Larger aspect ratios provide greater barrier performance [29]. Clays are the most successful candidates for polymer barrier applications, due to the high aspect ratio of nano-layers after intercalation and exfoliation.

Jiang *et al.* [112] reported on organic montmorillonite/N6 nanocomposites synthesised via the melt compounding method. Compared to pure N6, the barrier property of nanocomposites was improved by a factor of 3 for toluene and by a factor of 4 for ethanol with an organic montmorillonite content of 0.1-0.2wt% only. Wang *et al.* [98] investigated the water, acid, alkali and solvent resistance of exfoliated organoclay elastomeric epoxy composites, with 9.1wt% organoclay loading. The resistance of the nanocomposite is reported as improving by 36% for distilled water, 6% for sodium hydrate, 56.9% for 30% sulphuric acid, 23.5% for methanol and 28% for toluene.

When considering cost, safety and recycle-ability of food and beverage containers, polyethylene terephthalate (PET) is an ideal material. Improving the gas barrier properties of polyethylene terephthalates is therefore considered an important field of research. There has been extensive work on PET clay nanocomposites. However, none of the nanocomposites produced have been commercially used as food packaging materials because of difficulties in colour, transparency and blow moulding. Tsai [133] and Matayabas *et al.* [29] have conducted a comprehensive review on the gas barrier property improvement of PET clay nanocomposites. In typical PET clay nanocomposites, oxygen and carbon dioxide permeation rates have been reduced by 97.8% and 67% from $0.09 \text{ cm}^3/\text{pack 24h 0.2 atm O}_2$ and $60 \text{ cm}^3/\text{m}^2 \text{ 24h}$ to less than

0.002 cm³/pack 24h 0.2 atm O₂ and 20 cm³/ m² 24h respectively, when compared with the pristine PET [29]. The oxygen permeation index of a monolayer PET bottle fabricated from a clay nanocomposite has been observed to decrease by 70% from 100 to less than 30. With PET/N6 multilayer containers, gas barrier properties have been dramatically improved by the replacement of PET with polyethylene terephthalate clay nanocomposites as well as the substitution of N6 with N6/clay nanocomposites [133].

2.3.3 Electrical conductivity

By adding conductive fillers into polymer, conductive polymer composites can be synthesised. The conductive transition of polymer composites requires primary filler loading, namely critical percolation threshold where the electrical conductivity of a composite starts to significantly increase as a function of filler loading [134]. In addition, the conductivity of polymer composites is strongly affected by matrix and conductive network properties as well as application temperature [135]-[137]. Carbon fibre, carbon nanotube and expanded graphite are amongst the most widely used fillers for electrical conductive enhancement of polymers [29]-[31], [137]-[148].

Feller et al. [137] synthesised short carbon fibre unsaturated polyester and epoxy composites by adding fibres into the resin with an initiator and hardener. Electrical resistance was measured using a four-point probe technique. At 45 °C, the percolation threshold was achieved at carbon fibre content 1vol% for both composites, while resistance reduced to a minimum at 2.51vol% for the polyester composite and at 3.15vol% for the epoxy composite. Below 90 °C, conductivities of the composites were relatively stable. In the range 90 to 160 °C, an increase in electrical resistance of composites with temperature was observed, especially with a 1.88vol% fibre enhanced

epoxy composite. Such conductivity change with temperature makes the composite useful in temperature sensing applications [149].

With carbon nanotube enhancement, a low percolation threshold can be achieved in many polymer matrices. For example, an ultra-low percolation threshold in epoxy was reported by Sanler [150]. The composites were in-situ polymerised using aligned chemical vapour deposition grown carbon nanotubes and a bisphenol-A resin. A 0.0025 wt% percolation threshold was observed and a volume conductivity of 2×10^{-2} S/cm was achieved at 1wt% filler fraction. In addition, a 3wt% percolation threshold in an in-situ polymerised MWCNTs/polyimide composite and 5wt% in an extruded MWCNTs/polycarbonate composite have also been achieved according to So [151] and Chen [152]. Such low percolation thresholds with carbon nanotube enhancement allow electrically conductive carbon nanotube polymer composites to be produced with improved or retained mechanical properties [153]. For example, at 3wt% filler content, the volume conductivity of a MWCNTs/polyimide composite achieved 4×10^{-3} S/cm while the mechanical properties of the composite improved 22.4% in tensile modulus and 2-3% in strength [151].

The layer-interlinked porous structure of expanded graphite (EG) allows an intact graphite network to be retained within polymers and hence leads to composites conductive at low filler fractions [143]-[146]. In addition, because of low production costs, expanded graphites have the potential to compete with carbon nanotubes in conductive property enhancement of polymers. The conductivity of expanded graphite composites is dependent on the polymer matrix, post-treatment of expanded graphite and synthesis method of composites. In general, a relatively high conductive composite

can be produced at low filler content if the matrix is anti-static or slightly conductive. For example, in-situ polymerised EG/polyaniline composites can achieve a volume conductivity of 33.3 S/cm at 1.5wt% EG content [135]. In contrast, an in-situ polymerised polystyrene/EG composite exhibited 10^{-2} S/cm conductivity at 13.4wt% EG fraction [140]. An epoxy composite enhanced with expanded graphite possesses a conductivity two orders of magnification higher than its sonicated EG enhanced counterpart [136]. Using an in-situ polymerisation method, the electrical conductivity of an expanded graphite/poly(methyl methacrylate) composite reached 10^{-3} S/cm at 2vol% EG fraction [141]. When a solution synthesis technique is employed, in contrast, volume conductivity of the composite only reached 10^{-5} S/cm at 2vol% EG fraction [142].

In recent years, extending from the conductive property, smart functions have been developed using carbon nanotubes enhanced polymer composites. Since their electrical conductivity varies with the changes in stress, strain and environmental temperature, carbon nanotubes enhanced polymer composites have been employed as strain, damage and temperature sensors. Such sensors are applied in vibration inspection, damage self-monitoring and temperature control [149], [154]. In addition, as reported in [155], by fabricating a fibre-paper-fibre composite sandwich, continuous carbon fibre epoxy composites were used as capacitors. With a capacity of $1.2 \mu\text{F}/\text{m}^2$ at 2 MHz such composites are valuable as power cell components in lightweight solar devices.

2.4 The advantages and limitations of polymer enhancement in different size regimes

High loaded unidirectional fibre composites possess superior axial mechanical properties but relatively poor transverse properties. Nanocomposites can achieve outstanding mechanical property improvements at low filler loadings. In addition, nanotechnology is capable of providing polymers with enhanced functional properties. Further improvements in the mechanical properties of nanocomposites are, however, obstructed by their limited filler loading and the high cost of nanofillers.

2.4.1 The limitations of polymer reinforcement in micro scale

Currently, the limitations of micro polymer reinforcement are the inadequate utilisation of mechanical properties of raw materials and the complex composite fabrications. The following discussions include the theoretical consideration of both fibres and composites.

2.4.1.1 Theoretical consideration of fibres and fibre composites

As reinforcing materials, fibres are expected to inherit properties derived from the strong chemical bonds within the molecular structure of their raw material. This, nevertheless, is unachievable in some cases. Carbon fibre is one such example. The carbon fibre approach is based on utilising the strong covalent bonds within the aromatic sheet structure of graphite [3]. Carbon fibres, however, only achieve 4-5% of the theoretical strength of aromatic sheets. The weak interconnection between aromatic sheets in the carbon fibre structure inhibits the material achieving high strength. In addition, with current fabrication techniques, high modulus and high strength cannot be simultaneously achieved in one carbon fibre product. Conveniently, this can be

explained according to the Marsh-Griffith model of graphitisation/carbonisation process as shown in Figure 8 [3].

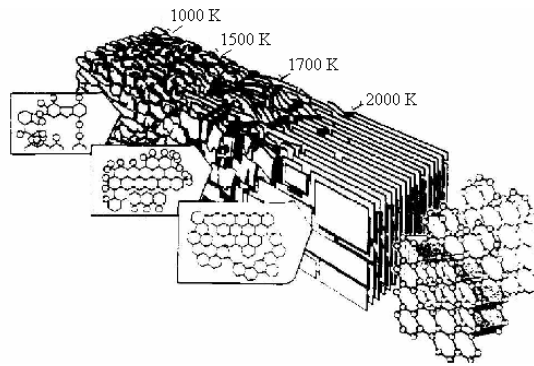


Figure 8: The Marsh-Griffith model of carbonisation/graphitisation process [3]

During fibre processing, aromatic sheets are formed progressively as temperature increases. Over 2000 K, continuous aromatic sheets and 3-D stacked graphitic carbon are formed. A further rise in temperature causes the orientation of aromatic sheets in the fibre direction resulting in carbon fibres with high modulus. Individual aromatic sheets contained within the fibres cannot be considered infinitely large and lack inter-connection. As a consequence, the fibres have a relatively low strength. In order to obtain high strength, a random and cross-linked turbostratic texture is necessary which can only be obtained below 2000 K [31]. Thus a problem arises. Below 2000 K the aromatic sheets are not sufficiently developed or aligned in the fibre direction resulting in a low modulus while above this temperature the structure for high strength disappears. Carbon fibres thus exhibit either high strength or high stiffness but cannot achieve both in the same product. The highest strength reached by carbon fibres is around 4-5 GPa, this is only 4-5% of the theoretical strength of graphite structure. This

is not a problem in nanocomposite technology. Taking clay for an example, when clay is exfoliated into a matrix, the clay nanolayers are connected individually with polymer molecules and hence the inherent properties of the clay layer can be fully utilised.

Furthermore, as a reinforcing component, the fibres are usually much stiffer than the matrix. This difference can cause magnified deformation of the matrix in the local area around the fibres when a transverse stress is applied. This deformation is much larger than the one exerted on the matrix itself. This phenomenon is identified as strain magnification. Such magnification can lead to composite failure at much lower strain than the pure polymer. This problem is unavoidable in fibre composites but can be reduced through the use of reinforcement close to the molecular level, i.e. nano reinforcement [2].

2.4.1.2 Problems associated with other properties and manufacturing difficulties

Difficulty in achieving a high quality surface finish and the failure to utilise conventional polymer processing techniques are additional problems associated with fibre reinforced composites. Apart from these, the viscosity of discontinuous fibre reinforcement composites dramatically increases with the increase of fibre loading. This can cause die blockage, flow difficulties during the manufacturing process when high filler loading composites are produced using injection moulding techniques.

2.4.2 The problems with polymer reinforcement in nanoscale

Although nanocomposites have higher mechanical properties than fibre composites at low loading levels, these properties generally reduce significantly when filler loading

exceeds 10wt%. The reason for this is the agglomeration of nano-fillers at high filler loading.

A key feature of nano reinforcement is the dispersion of fillers into the matrix at the nano level. It is known that once a layer-structured filler is exfoliated in the nano scale their surface area increases greatly. The surface area of a clay particle with thickness of 2-3 μm , for example, can enlarge 4000 to 6000 times when it is exfoliated [156]. As a consequence, at high filler contents there are not enough polymer molecules in the composite to wet the filler surface resulting in the agglomeration of nano-layers. Such agglomeration is detrimental to the interfacial bonding at the filler/matrix and reduces filler aspect ratio in the composites [2], [157]. It is well known that the mechanical properties of a composite are dependent on not only the properties of filler but also filler loading. Therefore, it is difficult to use nanotechnology to achieve very high mechanical properties without sacrifice of the inherent properties of the fillers.

2.4.3 The need for sub-micro technology and development of sub-micro polymer composites

Sub-micro polymer composite techniques have the potential to overcome the difficulties possessed by nano and micro composites mentioned above. The dimension of sub-micro reinforcing phase is larger than the nano scale. Such a scale has advantages over nanocomposites because they avoid the large surface area problems and allow high filler loadings in sub-micro composites to be achieved. This leads to higher mechanical performance when compared with current nanocomposites. The sub-micro dimension, on the other hand, is smaller than the micro scale. Sub-micro fillers therefore possess better bonding capabilities with polymer molecules resulting in better utilisation of

inherent material properties. In addition, the preparation of sub-micro composites is similar to nanocomposites. They are therefore able to make use of the synthetic methods of nanocomposites and can be produced using conventional polymer processing methods.

All of these represent a strong argument for the development of sub-micro polymer composites. The concept of sub-micro has been widely used in metal and ceramic composites. Aluminium, aluminium oxide, titanium oxide, nickel and silica particulates with a size range of 100-700nm are the most utilised sub-micro reinforcement for metals and ceramics [158]-[172]. Sub-micro filler reinforced metal and ceramic composites have demonstrated significant improvement in wear properties, hardness, strength and stiffness of metals and ceramics [165]-[172]. For example, the fracture toughness and bending strength of sub-micro silicon carbide/silicone composites are 107% and 67% higher than those of the pure silicon [170]. Similarly, sub-micro silica carbide reinforced aluminium-lithium alloy results in an increase of 125% in hardness and 47% in ultimate tensile strength, when reinforcement is evenly and finely dispersed in the alloy [171].

Little research has been reported in sub-micro polymer composites [173]-[175]. The research documented is mainly concentrated on the wear property improvement of composites. Xing [173] prepared 120 and 510nm spherical silica particle reinforced epoxy for coating applications. The wear resistance of the resulting composites was improved significantly at low filler loading. For example, a reduction of 275% in wear rate was achieved at 2N normal load with 2wt% 120nm silica filled epoxy. Over 2wt%, wear resistance tends to reduce due to the agglomeration of sub-micro silicon particles

resulting in the poor dispersion of fillers. It was also found that the wear resistance of composites decreases as silica particle size increases. Recently, sub-micro sized titanium oxide and zinc sulphide were applied to short carbon fibre reinforced polyetheretherketone (PEEK) and polyetherimide (PEI) systems to improve the wear resistance of fibre composites [174]. It was reported that the addition of 8% mixture of 300nm titanium oxide and zinc sulphides reduced the wear rate of carbon fibre PEEK composites by 110% and 57-105% as well as frictional coefficient by 75% and 250-280% at 70 and 150 °C, respectively. For carbon fibre PEI composites, the wear rate reduced by 77-150% at 70 °C after the addition of 10% 300nm titanium oxide. The mechanism of such improvements suggested is the change of particle sliding to particle rolling in the presence of sub-micro fillers.

The first report on mechanical reinforcement of sub-micro polymer composites was published in late 2007 and was based on sub-micro pyrogenic silica as reinforcement and epoxy as matrix [175]. The diameter of pyrogenic silica was reported as being 100 to 250nm and formed by the aggregation of primary particles with a size of 5 to 30nm. Thermal mechanical behaviour, tensile modulus, fracture strength and fracture toughness of the composites were investigated using glassy and rubbery epoxy systems. For the glassy epoxy, the addition of 5wt% sub-micro pyrogenic silica led to a 20 °C increase in the temperature of main mechanical relaxation as well as 10%, 41% and 19% improvement in post-relaxation elastic modulus, fracture strength and fracture toughness, respectively. Tensile modulus, however, was not improved due to the low filler fraction. As filler content increased to 10wt% from 5wt%, tensile modulus increased by 8% while fracture strength decreased by 37%. The surface modification of silica using amino-silane did not show any benefits to the mechanical properties

investigated. This was because the agglomeration of filler particles occurred during filler treatment and composite processing. Different from the glassy epoxy system, the rubbery epoxy reinforced with sub-micro pyrogenic silica did not exhibit differences in the temperature of main mechanical relaxation, at any filler content, when compared with pure epoxy. As filler fraction increases, post-relaxation modulus, tensile modulus and tensile maximum strength of the rubbery epoxy were significantly increased up to 4.5, 2.88 and 3.1MPa at 36wt% filler loading. These values represent an improvement of 400%, 460% and 317% respectively, when compared with the matrix. Such improvements are much greater than those achieved by the glassy epoxy system and are due to the contribution of the open fractal structure of silica in its rubbery state. The structure resulted in the better dispersion of silica particles.

Apart from pyrogenic silica in glassy and rubbery epoxy, the mechanical reinforcement of other sub-micro filler and matrix systems has not been reported. As a consequence, research into mechanical enhancement of sub-micro polymer composites is still limited and relatively new. In this research, sub-micro N6 and PP composites are developed based on single and multi-layer structured sub-micro fillers. The mechanical performance, thermal mechanical properties, rheology and crystallisation behaviour of composites produced are investigated systematically. The modelling of 350nm silica flakes/N6 composites is conducted in order to predict the potential of sub-micro composite enhancement. In addition, the relationships between property and structure as well as property and processing are explored in order to produce sub-micro composites with high mechanical performance.

3 Experimental methods

This chapter describes materials used, the methods for composite processing and relevant characterisation techniques used for an investigation of the properties, structure and morphology of both fillers and composites. Section 3.1 provides the details of materials studied. The preparation and surface area characterisation of sub-micro graphite are described in Sections 3.2 and 3.3. Section 3.4 describes the X-ray diffraction, scanning and transmission electron microscopy which were used to investigate the sub-micro and nano structures of composites. Section 3.5 provides a detailed description of the synthesis of sub-micro composites by melt blending and solution methods. The details of tensile modulus, strength, impact fracture and dynamic thermal mechanical analysis are explained in Sections 3.6 and 3.7. Methodologies for the characterisation of filler dispersion, crystallisation behaviour and rheology of composites are in Sections 3.8 to 3.10. Section 3.11 provides electrical conductivity measurement of sub-micro graphite composites.

3.1 Materials studied

In this research, two types of polymer were used as matrices to investigate the structure and properties of sub-micro reinforcement. They are Polypropylene (PP) and Nylon 6 (N6). The PP used is Marlex@ HGN-020-05 homopolymer supplied by Philips. It has a melt flow rate of 2.1g/10min at 230 °C, density of 0.906 g/cm³ and melting range between 180 and 230 °C. The commercial name of the N6 is Ultramid B3 and it was supplied by BASF. N6 has a low zero shear viscosity of 320 Pa·s at 235 °C. Its melting point is 220 °C and density is 1.13 g/cm³.

Maleic anhydride grafted polypropylene, Epolene E43, was used as a compatiliser for the polypropylene application. It was purchased from Eastman and has a melting point of 157 °C. The content of maleic anhydride in E43 is 3.7wt%.

The nano reinforcing materials used for this study are four boehmite products, clay 93a and carbon nanofibres. Two types of sub-micro reinforcements with different structures were evaluated. One of them is single-layered silica flakes with different thickness while the other is multi-layered expanded graphite synthesised from expandable graphite.

Table 3 gives carbon and sulphur content as well as particle size of the graphite flakes, expandable graphite and carbon nanofibres used in this study. The graphite flakes are supplied by Aldrich. ES350, ES120 and ES100 represent different grades of expandable graphite supplied by Branwell. The diameter of the carbon nanofibres (Pyrograf III) is in the range from 50 to 180nm which is partially in the sub-micro scale. Pyrograf III was donated by Wright Patterson AFB, USA.

Table 3: The purity and particle size of graphite and nanofibres used

	Graphite flakes	Nanofibre Pyrograph III	ES350	ES120	ES100
Carbon %	>98.5	>80 Co~0.01%	>88	>85	>85
Sulphur %	–	–	< 0.2	< 1.0	<1.0
Particle size	75%<75mesh	D: 50-180nm	350-900µm	50-380µm	50-300µm

Boehmites are alumina hydrous oxide which contain $\text{AlO}(\text{OH})$ structure. Table 4 shows some physical properties of the boehmites studied, including the content of major components, particle size and surface area. The data were provided by the supplier. As can be seen, MG61HT contains a large fraction of magnesium oxide.

Table 4: The composition, particle size and surface area of the boehmites used

	MG61HT	Dispersal 40	Dispersal 80	Dispersal OS1
Abbreviation	MG61HT	D 40	D 80	D-OS 1
Al_2O_3 %	38.4	82.4	83.7	69.2
MgO %	61.6	–	–	–
Particle size at 50%	5.29 μm	<45 μm	<90 μm	>90 μm
Surface area m^2/g	–	102	96	265
Supplier	Sosal Co. Germany			

The silica flakes are made from E-glass containing SiO_2 of 64-70%, Na_2O of 12-13%, Al_2O_3 of 3-6% as well as minor amount of MgO, CaO, ZnO, K_2O and TiO_2 . The five types of silica flakes studied are abbreviated as SF I-V. The main physical properties of the flakes are shown in Table 5.

SF I and SF II are surface untreated flakes. The flakes have thickness of 850nm and 350nm respectively. SF III, IV and V are 350nm thick with different surface coatings. SF III is surface-coated with 1.43wt% 3-aminopropyl triethoxysilane. SF IV and V are surface-modified by 1.39wt% vinyl trimethoxysilane and 1.67wt% γ -glycid oxypropyl trimethoxysilane, respectively. All five silica flakes have the same diameter distribution of 50 to 150 μm and are supplied by Glass Flake Ltd. UK.

Table 5: The thickness, diameter distribution and surface modification of silica flakes

	SF-I	SF-II	SF-III	SF-IV	SF-V
Thickness nm	850	350	350	350	350
Particle diameter μm	50-150	50-150	50-150	50-150	50-150
Coupling agent	–	–	3-aminopropyl triethoxysilane	vinyl trimeth oxysilane	γ-glycid oxypropyl trimeth oxysilane
Content of the coupling agent, wt%	–	–	1.43	1.39	1.67

Chemicals used were ordered from Aldrich. These included concentrated sulphuric acid (H₂SO₄, 98%) and concentrated nitric acid (HNO₃, 60-63%).

3.2 Preparation of expandable graphite

In order to synthesise expandable graphite, a mixture of concentrated sulphuric and nitric acid was cooled to below 20°C. Different ratios of the acids were used. Ten grams of graphite flakes were added to the acid solution during vigorous stir. Reaction time was varied between 2 and 24 hours and reaction temperatures between 20 and 60 °C to optimise experimental conditions. The resulting product was filtered, washed with water until the pH value of the solution was 5-6 and dried at 90 °C for 16 hours.

3.3 Characterisation of surface area of graphite flakes and expanded graphite

The Brunner-Emmett-Teller (BET) surface area of graphite flakes and expanded graphite were measured using a quantachrome apparatus with nitrogen as the adsorbate gas and helium as the carrier gas. The sample was degassed at 110-120 °C for 30min before being measured.

3.4 The characterisation of sub-micro and nano structure

The techniques used for the characterisation of sub-micro structures included X-ray diffraction, scanning and transmission electron microscopy.

3.4.1 X-ray diffraction analysis

X-ray diffraction analysis was used to characterise the crystal structure of sub-micro fillers and composites. Measurements were carried out using an X'Pert X-Ray diffractometer with a copper radiation source. Operating conditions used during each test were 40 kV volts, 35 mA current and 1° to 90° scanning angle range with a step size of 0.0167.

Prior to XRD testing, flaky or powder samples were compressed into dense plates that fit into the XRD sample holder. For polymer-based samples, a SATRA micro injection-moulding machine was used to produce square plates with dimensions 15mm×15mm×1mm. Polymer pellets were dried in a vacuum oven at 120 °C for 4-6 hours before the injection moulding.

3.4.2 Scanning and transmission electron microscopy

The microstructure and morphology of materials studied were investigated using scanning and transmission electron microscopes (SEM, TEM). Particle size and size distribution of fillers were also measured using these techniques. Before measuring, samples were gold coated for two and half minutes using a vacuum coating apparatus.

3.5 The preparation of sub-micro filler enhanced polymer composites

Melt blending was used to prepare all samples investigated in this research, apart from conductive composites which were synthesised via a solution method.

3.5.1 The melt blending method

The filler and matrix polymer were dried under vacuum at 120°C for 4-6 hours. Dried filler and polymer were pre-blended using a plastic bag before extrusion. The extrusion was carried out using a PRISM EUROLAB 16mm twin screw extruder with two feed ports, nine heating zones and a die. Extruded samples were cooled in a water bath and chopped into 2.5mm pellets using a pelletiser.

The feeding rate and screw speed applied were 15-20% and 300-400 rpm respectively, depending on the material system used. Processing temperature applied was 225°C for PP composites and 235 °C for N6 composites. The temperature in each heating zone of the extruder was identical.

3.5.2 The solution method to produce sub-micro graphite/polypropylene conductive composites

In the solution synthesis of graphite/polypropylene composites, xylene was used as a solvent. Maleic anhydride grafted polypropylene, Epolene E43, was employed as a compatiliser when graphite/E43/PP composites were being produced.

During synthesis, 70ml of xylene was added to a three necked flask containing 10 grams of polypropylene or a mixture of polypropylene and Epolene E43. Expanded graphite, whose quantity was determined by its content in the composite, was soaked in 20ml xylene in a glass beaker. The mixture of solvent and polymer was then heated to 140 °C. After the polymer had completely dissolved, the soaked graphite solution was added. Two hours later, after reducing the temperature to 120 °C, 25ml of acetone were dropped into the flask in order to precipitate the resulting composite. The resulting composite was then filtered and dried for 16 hours under vacuum at room temperature.

3.6 Mechanical properties of polymer and their composites

The mechanical properties of polymers and composites measured in this research include the tensile modulus, tensile strength and impact fracture.

3.6.1 Tensile loading test

Tensile tests were carried out using an RDP Howden servo-mechanical tensile test machine according to ASTM D638. During testing, sample strains were measured by means of a Messphysik video extensometer. Test specimens were dog bone in shape with dimensions 30×10×3mm. The specimens were manufactured using a SATRA

micro injection-moulding machine and were gated from top. The mould was non-heated and 60 seconds to dismantle. During testing, the strain rate applied was 10^{-2} s^{-1} for all samples. Three to five specimens were tested for each sample. Results were averaged and standard deviation was used to express the error of measurement.

3.6.2 Impact fracture analysis

Impact fracture measurements were carried out at room temperature using an Instron Impact instrument according to the standard ISO R180-1991 [176]. A three-point bending technique with 40mm span was used. A crosshead rate of 1 m/s and a crack time in the range of 5-7 ms were applied during testing. The length of crack developed in each specimen was measured using a microscope.

Specimens used for analysis were in the form of beams with dimensions 50x10x3 mm. All specimens were prepared in the following way:

Using a saw, a sharp notch of depth 4.5mm was created in the middle of each beam.

A natural crack was then generated by tapping a razor blade into the bottom of the notch.

Cracks made by the razor blade were observed, by means of a microscope, in order to ensure they were approximately 0.5mm in depth.

Fracture toughness was expressed by means of critical stress intensity (K_{c}). As before, five to ten measurements were taken from each sample to obtain an average.

3.7 Dynamic mechanical analysis

Dynamic Mechanical Analysis (DMA) was carried out using a ‘Rheometrics Test Station’ in the condition of a dynamic temperature ramp and strain controlled three-point bending. A constant initial static force of 2.0N and 1 Hz frequency were applied. The temperature range was -10 to 160 °C and the ramp rate was 2 °C/min. Nitrogen was used as environmental agent below 50 °C, and air above 50 °C. The dimensions of the beams for DMA test were $50 \times 10 \times 3 \pm 0.3$ mm. The transition temperatures of the polymers were obtained according to the plot of $\tan\delta$ versus temperature.

The thermal deflection temperature of the pure polymer and composites was obtained from the graph of modulus versus temperature according to a data analysis method adopted from the ASTM International Standard D 648 and DMA Q800. The adoption was made in the following way:

Heat Deflection Temperature (HDT) is defined as the temperature at which a test bar reaches a deflection of 0.25mm under a stress of 1820 KPa or 455 KPa, applied at the centre of the bar. According to D 648, the dimensions of a standard sample should be 127mm in length, 13mm in thickness and 3-13mm in width. The length of span between two supports needs to be approximately 0.1m. Under a three-point bending geometry, deflection D can be expressed with the formula $D = \epsilon L^2 / 6h$, where ϵ , L and h represent strain, length of span and thickness of the testing specimen. Thus $\epsilon = 6hD / L^2$. Because elastic modulus $E = \sigma / \epsilon$, providing the stress (σ) is 1820 MPa, then,

$$\begin{aligned} E &= 1820 \times 10^6 / (6hD / L^2) \\ &= 1820 \times 10^6 / (6 \times 13 \times 10^{-3} \times 0.25 \times 10^{-3} / (0.1)^2) = 0.9333 \times 10^9 \text{ Pa} = 0.9333 \text{ GPa}. \end{aligned}$$

Thus, HDT is equivalent to the temperature where storage modulus has a value of 0.933 GPa.

3.8 Characterisation of the dispersion structure of reinforcements in composites

The quality of dispersion of fillers in composites were characterised by reflectance microscopy using a Leiz optical microscope. Specimens were cut from the cross-section of 50×10×3mm composite beams and mounted using Acryfix 2. Each specimen was polished with 6 then 3-micro alumina using a Buehler Powerpro 3000 grinder/polisher.

3.9 Characterisation of the crystallisation behaviour of the composites

Differential scanning calorimetric analysis and Polarised microscopy were applied to characterise the crystallinity and crystallisation behaviour of composites.

3.9.1 Differential scanning calorimetric analysis

Differential Scanning Calorimetric (DSC) Analysis was carried out using a Perkin-Elmer differential scanning calorimeter. About 10 mg of sample were exactly weighted into an aluminium autosampler pan and sealed by compressing a cover on top. This was then placed into the sample chamber of the calorimeter. A second sealed empty pan was put into the reference chamber. Temperature ranges of 0 to 270 °C for nylon composites and 0 to 250 °C for polypropylene composites were applied. In order to eliminate the thermal history of the specimens, a two-cycle procedure of heat-hold-cool followed by heat-cool was applied. In the first cycle the temperature ramp used was 50 °C/min for

heating and 10 °C/min for cooling. The temperature holding time employed was five minutes. A heating rate of 10 °C/min and a cooling rate of 50 °C/min were applied for the second cycle. Measurements were performed in a nitrogen atmosphere. The data obtained at temperature ramp 10 °C/min were used to evaluate the melting and crystallisation behaviour of the materials studied. The crystallinity, $X\%$, was calculated from the ratio of melt enthalpy of the sample, ΔH_m and crystallisation enthalpy of 100% crystalline polymer, ΔH_c^0 , using the equation $X\% = \frac{\Delta H_m}{(1-f)\Delta H_c^0}$ where f is filler content of the composite. The crystallisation enthalpy of 100% crystalline polymer was taken as 190 J/g for N6 and 210 J/g for polypropylene [178]-[180].

3.9.2 Polarised microscopy with hot stage

The crystallisation process and crystal size of sub-micro composites were investigated by means of a polarised microscope with a HMTS 600 hot stage and video camera. An 11×0.7 mm round slide cover was put in the silica crucible of the hot stage. A tiny piece of sample was put on the cover and the sample was heated until it melted at a ramp of 20 °C/min. The melt was then spread into a thin film by pressing another slide cover on top. The sample was held in the molten state for 3 minutes followed by cooling at 20 °C/min and then 2 °C/min when close to crystallisation temperature of the material. Crystallisation images were recorded approximately every 5 seconds once the first crystals started to appear. Crystal size was measured using imaging analysis. Fifty spherulites were measured in order to obtain the average size of each sample.

3.10 The rheological characterisation of the composites

Rheological properties were characterised using a Rosand RH7 twin-bore extrusion capillary rheometer made by Malvern Instruments Ltd. Tests were performed using a test sequence of 7 stages with shear rates of 3000, 2250, 1500, 750, 300, 150 and 60 s⁻¹. In order to remove air from the samples and to allow the samples to reach thermal equilibrium, a four-stage pre-test sequence was applied. The sequence consisted of an initial compression and pre-heat, followed by a second compression and pre-heat. The capillary die used is 16mm in length, 1mm in diameter and has an entry angle of 180°. The orifice die used has a length of 0.25mm, a diameter of 1mm and an entry angle of 180°. The test temperature used was 225 °C for polypropylene and its composites, 235 °C for N6 and its composites. Shear stress was corrected using Bagley correction combined with Cogswell convergent flow model. Each test was repeated twice to check reproducibility.

3.11 Electrical conductivity measurement of sub-micro graphite polypropylene composites

The electrical conductivity of sub-micro graphite/PP composites was tested using an Autobalance Universal Bridge B642 with an accuracy of 0.1% in measurement range. Measurements were carried out based on the ASTM D257 method. Figure 9 shows the experimental setup for volume conductivity measurement of the composites. The electrodes employed for testing were 10×10mm squares of self-adhesive copper tape. The test specimen was a 50×10×1.5mm film, cut from a plate moulded by means of hot compression of composite pellets. The volume conductivity is calculated using the equations $R_v = \rho_v \times \frac{T}{A} \times 2$ and $\sigma_v = \frac{1}{\rho_v}$, where ρ_v and σ_v represent volume resistivity

and conductivity. R_v is volume resistance of material, T , thickness of specimen, A , area of electrode. The results obtained were averaged from three tests for each sample.

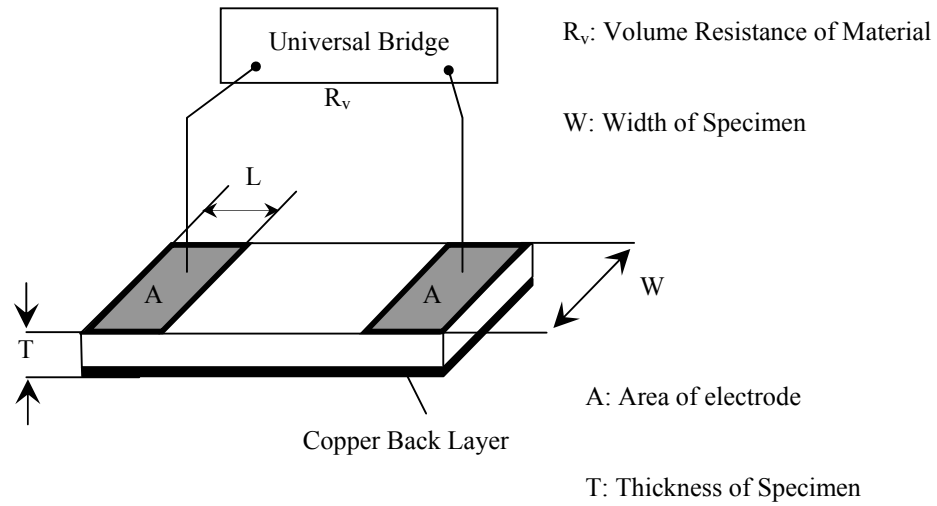


Figure 9: Schematic illustration of volume conductivity measurement

4 Prediction of Young's modulus and strength of N6 composites reinforced by sub-micro silica flakes

In order to predict the potential of sub-micro reinforcement, the modelling of Young's modulus and strength are conducted based on 350nm silica flakes and N6. In many aspects, the reinforcing structure of sub-micro silica flake/N6 composites can be considered similar to that of short fibre composites although they are in different reinforcement size regions. Theories and methods used for the modelling of short fibre composites were thus applied to investigate Young's modulus and strength of the sub-micro composites in this research. Modulus and strength prediction models of fibre composites are briefly reviewed in Section 4.1. Numerical aspects and the modelling of sub-micro reinforcement are given in Sections 4.2 and 4.3.

4.1 Theories of composite mechanical properties prediction

Rule of Mixtures, Halpin-Tsai and Shear Lag models are introduced for modulus prediction. Rule of Mixtures and a Modified Rule of Mixtures based on Shear Lag analysis are introduced for strength prediction.

4.1.1 Theories of modulus prediction

Many models have been developed to predict the elastic modulus and strength of short fibre composites since 1950s. These include the Rule of Mixtures, dilute Eshelby, Mori-Tanaka, Shear Lag, Halpin-Tsai, [129], [130], [181], [182] and their variations [183]-[185]. Amongst them, the Rule of Mixtures is the simplest model. The Shear Lag model is popular for longitudinal modulus prediction of unidirectional composites and others are used to predict the overall moduli of fibre composites. These models are also

applied in the prediction of mechanical properties of nanocomposites. [186]-[188]. Similar to their application in fibre composites, the Mori-Tanaka and Halpin-Tsai models are used for the overall elastic property prediction of nanocomposites. Shear Lag analysis is only used for axial modulus calculation of nanocomposites.

As the Rule of Mixtures, Halpin-Tsai and Shear Lag are three models in the simplest algebraic form for elastic modulus prediction, they were selected to predict the Young's modulus of sub-micro composites.

4.1.1.1 The Rule of Mixtures

The Rule of Mixtures model [5] considers a composite as a bi-component material where fibres are aligned in the same direction as shown in Figure 10. It is assumed that the relative thickness of fibre and matrix is in proportion to their volume. Both components exhibit the same strain response to the stress.

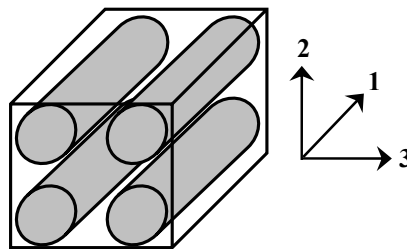


Figure 10: A schematic illustration of a unidirectional composite [5]

The modulus of a composite in the fibre direction, i.e. longitudinal modulus can be expressed as:

$$E_1 = (1 - f)E_m + fE_f \quad \text{Equation 1}$$

The transverse modulus of a fibre composite can be expressed as

$$E_2 = \left[\frac{1-f}{E_m} + \frac{f}{E_f} \right]^{-1} \quad \text{Equation 2}$$

Where f is the fibre volume fraction. Subscripts m and f represent the matrix and fibre respectively, E_f is the fibre stiffness in the axial direction and E_m is modulus of the matrix. In addition, $(1-f)E_m$ and fE_m represent the contributions to the elastic property of the composites by the matrix and fibres, respectively.

According to Equation 1, the longitudinal modulus of a composite is a function of fibre volume fraction only. The length and aspect ratio of fibres are not considered in this model. Therefore, the Rule of Mixtures is valid only if fibres are long enough and assumed to demonstrate equal strain to the matrix. In the Young's modulus prediction of fibre composites, Equation 1 is taken as a higher boundary. Due to the consideration of that all fibre aligns in transverse direction, Equation 2 underestimates the Young's modulus and is treated as a lower boundary for fibre composites [5]. In this section, only Equation 1 is applied to predict the modulus of sub-micro composites.

4.1.1.2 The Halpin-Tsai models

The Halpin-Tsai models were originally developed to compensate the strain magnification for the prediction of transverse modulus of fibre composites, which is neglected in the Rule of Mixtures, by introducing the geometric factor ζ into the models. The only assumption made in giving various values for ζ is that the modulus expressions for the composite are insensitive to the differences in Poisson ratios of fibre and matrix. The general Halpin-Tsai equation for short fibre composites is expressed as:

$$\frac{P}{P_m} = \frac{1 + \xi \eta f}{1 - \eta f} \quad \text{Equation 3}$$

$$\text{with } \eta = \frac{\frac{P_f}{P_m} - 1}{\frac{P_f}{P_m} + \xi} \quad \text{Equation 4}$$

Where P , P_m and P_f represent general properties of the composite, matrix and fibre. f is the volume fraction of fibres. Parameter ξ depends on the Poisson ratio of the matrix and the composite property. With geometric factor ξ in different expression, Halpin-Tsai models can be applied to predict not only elastic modulus but also transverse and shear moduli. For elastic modulus, P represents E and ξ is the aspect ratio of fibre multiplied by two i.e. $2\left(\frac{l}{d}\right)$. The Halpin-Tsai equation for calculating tensile modulus

of a composite can then be expressed as Equations 5 and 6, if $\left(\frac{l}{d}\right)$ is represented by s .

$$\frac{E}{E_m} = \frac{1 + 2s \eta f}{1 - \eta f} \quad \text{Equation 5}$$

$$\text{with } \eta = \frac{\frac{E_f}{E_m} - 1}{\frac{E_f}{E_m} + 2s} \quad \text{Equation 6}$$

According to Equations 5 and 6, the Halpin-Tsai model indicates that the elastic modulus of an aligned composite is a function of fibre fraction and aspect ratio.

4.1.1.3 Shear Lag analysis

Shear Lag analysis is most widely used for describing the effect of loading in aligned short fibre composites and was originally developed by Cox in 1950s. In Shear Lag analysis, a composite is considered to be a fibre with length l and radius r embedded in a matrix, as shown in Figure 11. The tensile stress is transferred from the matrix to fibre by means of interfacial shear stress [5], [68]. The interfacial shear stress and tensile strength in the fibre vary along the fibre. It is also assumed that the interfacial shear stress is proportional to the difference in displacement of the matrix in x-direction which is the fibre direction and there is no stress being transferred across the end faces of a fibre, i.e. $\sigma_f = 0$ at $x = 0$ and $x = l$.

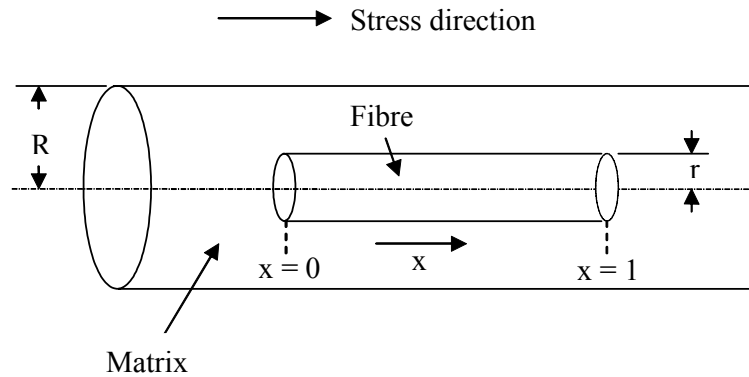


Figure 11: Schematic illustration of the fibre and matrix used in Shear Lag analysis [68]

For a fibre hexagonally arranged composite, the Shear Lag model is expressed as [5]:

$$E = fE_f \left(1 - \frac{\tanh \beta \cdot s}{\beta \cdot s} \right) + (1 - f)E_m \quad \text{Equation 7}$$

Where $\beta = \left(\frac{2E_m}{E_f(1+\nu_m)\ln(1/f)} \right)^{1/2}$, ν_m is the Poisson ratio of matrix.

$\left(1 - \frac{\tanh \beta \cdot s}{\beta \cdot s} \right)$ represents the effect of fibre aspect ratio on composite properties, if this

is represented by η_s Equation 7 can also be expressed as:

$$E = \eta_s E_f f + (1-f)E_m \quad \text{Equation 8}$$

Providing the influence of fibre orientation, η_o , is considered in the model, the Shear Lag model for elastic modulus prediction of short composites can be expressed as:

$$E = \eta_o \eta_s E_f f + (1-f)E_m \quad \text{Equation 9}$$

Both Equations 8 and 9 were used to compare the effects of filler orientation on modulus of sub-micro SF/N6 composites. Equation 8 is referred to Shear Lag I while Equation 9 is referred to Shear Lag II in later sections.

4.1.2 Theories for strength prediction

Models for strength prediction of composites are essentially the Rule of Mixtures and its variations in which the orientation and length distributions of fillers are considered. Sub-micro filler enhanced polymer composites involve both orientation and length distribution of fillers. Thus a modified Rule of Mixtures [68] is used to predict the strength of sub-micro SF/N6 composites and compared to the value from the Rule of Mixtures. The Rule of Mixtures for tensile strength is expressed as:

$$\sigma_1 = (1-f)\sigma_m + f\sigma_f \quad \text{Equation 10}$$

Where f is the fibre volume fraction, subscripts m and f represent the matrix and fibre respectively, σ_f and σ_m are failure strength of the fibre and matrix respectively.

$(1-f)\sigma_m$ represents the contribution from the matrix and $f\sigma_f$ is the strength contribution from the fibres.

The modified Rule of Mixtures for predicting the axial strength of a composite with efficiency factor of fibre orientation can be expressed as:

$$\sigma_1 = \eta_o \sigma_f f + (1-f)\sigma_m \quad \text{Equation 11}$$

When the distributions of fibre length/aspect ratio are concerned, uneven stress along the fibres has to be considered. This requires replacing σ_f with average fibre stress,

$\bar{\sigma}_f$ in Equation 10, thus,

$$\sigma_1 = \bar{\sigma}_f f + (1-f)\sigma_m \quad \text{Equation 12}$$

According to Cox analysis, for ductile matrices and large composite strains, average fibre stress $\bar{\sigma}_f$ can be given by:

$$\bar{\sigma}_f = \left(1 - \frac{l_c}{2l}\right) \sigma_f, \text{ for } l > l_c \quad \text{Equation 13}$$

where l_c is known as the fibre critical length and can be calculated using the formula

$$l_c = \frac{\sigma_f d}{2\tau_u}, \text{ where } d \text{ is the fibre diameter. } \tau_u \text{ represents the ultimate shear stress at the}$$

interface of fibres with matrices or the ultimate shear stress of the matrix. The axial strength of composites is then given by:

$$\sigma_1 = \left(1 - \frac{l_c}{2l}\right) \sigma_f f + (1-f)\sigma_m \quad \text{Equation 14}$$

When fibre length is shorter than l_c , the maximum fibre stress is determined by fibre length, fibre diameter and the ultimate interface shear stress or ultimate shear stress of the matrix, i.e. $\sigma_{\max} = \frac{2\tau_u \cdot l}{d}$. The average fibre stress is half of the maximum.

Therefore,

$$\bar{\sigma}_f = \frac{\tau_u \cdot l}{d} = \tau_u \cdot s, \text{ for } l < l_c \quad \text{Equation 15}$$

For composites containing fibres with both sub-critical length and super-critical length, Equation 14 is combined with Equation 15. The strength of composites is then given by:

$$\sigma_1 = \left[\sum_i \tau_u \cdot s_i \cdot \nu_i + \sum_j \sigma_f \nu_j \left(1 - \frac{l_c}{2l_j} \right) \right] \cdot f + (1-f)\sigma_m \quad \text{Equation 16}$$

Where ν_i represents the volume percentage of the sub-critical fibre with an aspect ratio of s_i . ν_j is the volume percentage of the super-critical fibre with a length of l_j . Adding the fibre orientation factor into Equation 16, the modified Rule of Mixtures strength model is expressed as:

$$\sigma_1 = \eta_o \left[\sum_i \tau_u \cdot s_i \cdot \nu_i + \sum_j \sigma_f \nu_j \left(1 - \frac{l_c}{2l_j} \right) \right] \cdot f + (1-f)\sigma_m \quad \text{Equation 17}$$

According to the modified Rule of Mixtures, axial strength of short fibre composites is determined by fibre content and fibre length distribution when fibre length is longer than the critical length. Fibre aspect ratio rather than length, however, becomes crucial when fibre is shorter than the critical length.

In sub-micro composite applications, Equation 10 is the expression for Rule of Mixtures and is taken as the higher boundary model for strength prediction. Equation 16 is the

modified Rule of Mixtures not considering filler orientation while Equation 17 is the modified Rule of Mixtures inclusive of the orientation efficiency factor. The model exclusive of the orientation efficiency factor is referred to Model I while the model inclusive of the orientation efficiency factor is referred to Model II in later sections.

4.2 Numerical aspects

Numerical aspects of this modelling study include the length of silica flakes, length distribution of silica flakes and orientation of flakes in composites. These details are discussed in the following sub-sections.

4.2.1 Length of flakes

According to SEM images, the silica flakes used in this study consisted of different shape particles including rectangular, triangular and disc-like as illustrated in Figure 12.

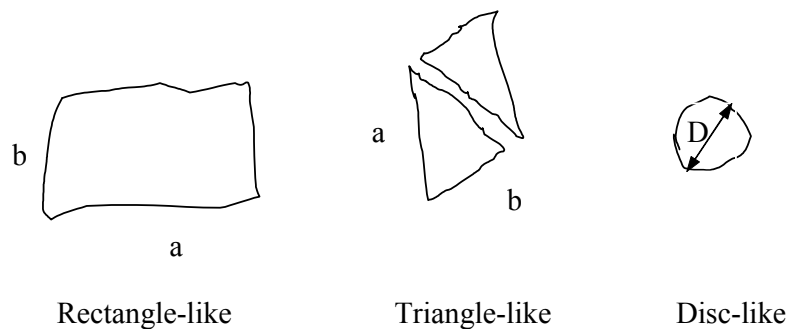


Figure 12: The shapes of silica flakes

To simplify calculations, two similar-sized triangle flakes are treated as one rectangle. All flakes were assumed to be aligned along their longest edges in the injection flow

direction. The length of flakes therefore can be taken as that of the longer side, a . The aspect ratio of flakes was defined as $\left(\frac{a}{t}\right)$, where t represents the thickness of silica flakes. For 350nm silica flakes, t is 350 nm.

4.2.2 Length distribution

The length distribution of fillers can be determined by number, weight or volume-based methods. In the literature [181]-[188], the length distribution of fillers is obtained either by number or weight-based method. The number-based length distribution, however, usually gives lower values of predicted elastic properties of composites than the weight-based length distribution [5]. SEM imaging is a simple and direct method to measure the length of materials which usually gives number-based length distributions. Because silica flakes have simple single-layered structure with simple shapes and consistent thickness, the volume of individual flakes is calculable. As a result of this, volume-based length distributions can be obtained via SEM images. The volume-based length distribution should be the most suitable method for the prediction of composite elastic properties because all model analysis is based on the volume fraction of fillers.

Furthermore, in order to avoid the complexity caused by the different shapes of flakes during the calculation of length distribution, the equivalent diameter of a rectangle is introduced and calculated using

$$D = 1.30 \left[\frac{(ab)^{0.625}}{(a+b)^{0.25}} \right] \quad [189] \quad \text{Equation 18}$$

Where a represents the length of the longer side of a rectangle and b represents the shorter edge. The volume fraction of flakes with a length of a_i is then given by:

$$v_i = \frac{n_i D_i^2 t}{\sum_j n_j D_j^2 t} = \frac{n_i D_i^2}{\sum_j n_j D_j^2} \quad \text{Equation 19}$$

where n_i is the number of flakes with length a_i . n_j is the number of flakes with length a_j , $j = 1, 2, 3 \dots$ and $i \in j$.

A hundred flakes were counted and measured by means of SEM imaging analysis. The volume-based length distribution of flakes is shown in Figure 13. The results show that the length range of 350nm silica flakes is 23 to 280 μm . Over 85vol% of the 350nm SF was found to be in the size range of 110 to 200 μm . The average length and aspect ratio of 350nm silica flakes was found to be 166.2 μm and 475 μm , respectively.

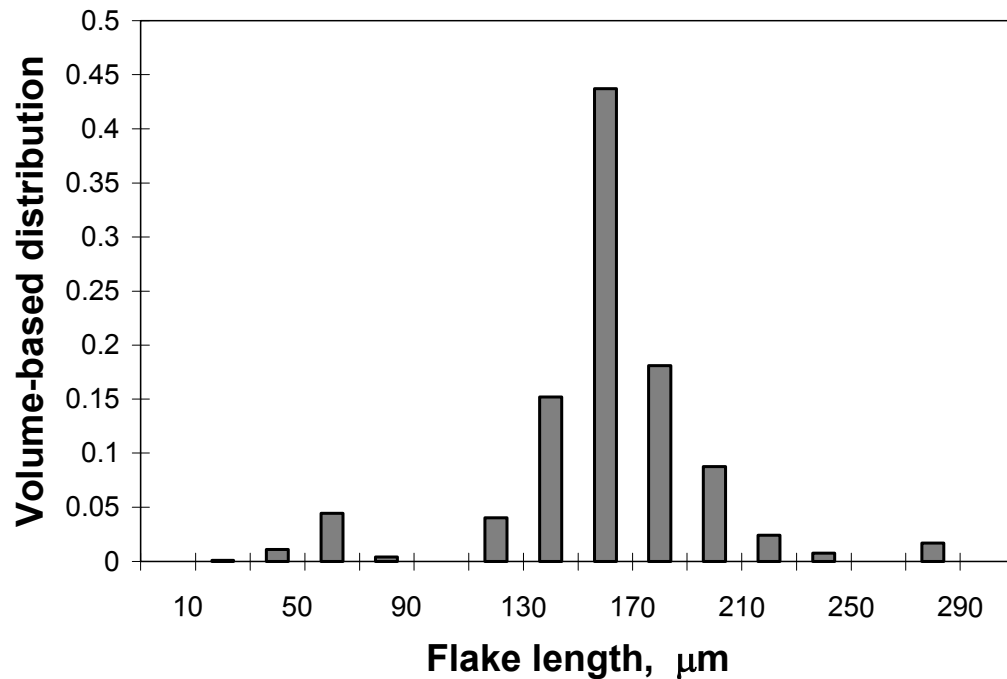


Figure 13: Length distribution of 350nm SF

4.2.3 The orientation of silica flakes in N6 composites

Similar to short fibre composites, injection moulded silica flake composites are partially orientated. The flake orientation in injection flow direction thus has to be investigated in order to predict Young's modulus and strength of sub-micro composites. A multi-layer analysis method adopted from [60] is applied to obtain the average orientation factor. The specimen was cut ten times evenly along its width resulting in eleven layers as shown in Figure 14. Following polish, acid etching and gold coating of the layers, six SEM-images were taken through the thickness of each layer at each of five regions. Five regions are evenly distributed along shaft length. A total of three hundred and thirty images were captured, six of which are shown in Figure 15 in order to illustrate the orientation structure of flakes in different sections.

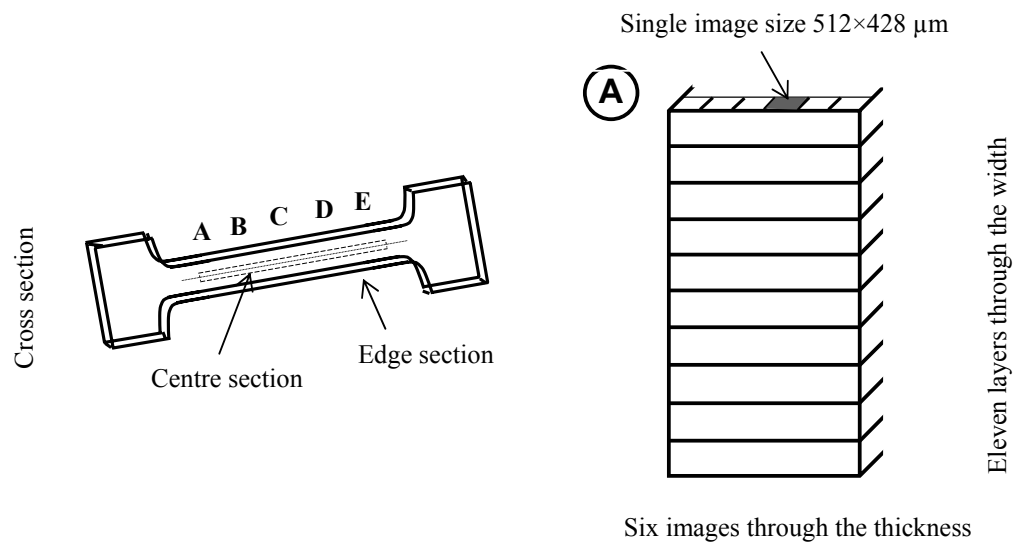


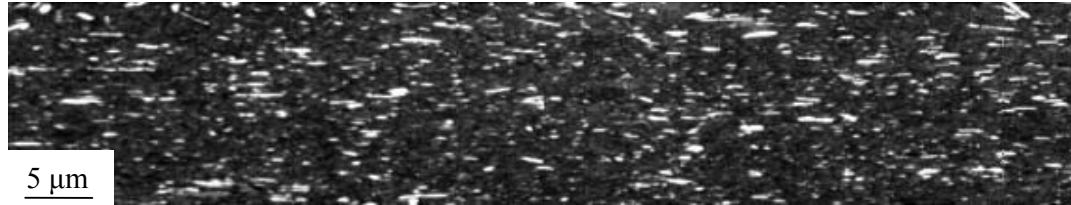
Figure 14: The scheme of image acquisition pattern

According to Figure 15, the injection moulded specimen of SF composites comprise of skin and core structures. In the skin area, flakes aligned more or less along the injection flow direction. By contrast, flakes are orientated randomly in the core area. When comparing Figure 15 with Figure 20b, the lengths of flakes in composites are far smaller than that of the original before extrusion. This is a clear indication of flake breakage during processing. The breakage of flakes generated large amounts of disc shaped particles with approximately equivalent length and width. In the central core section of test specimens these particles non-dimensionally aligned as seen in Figure 15d.

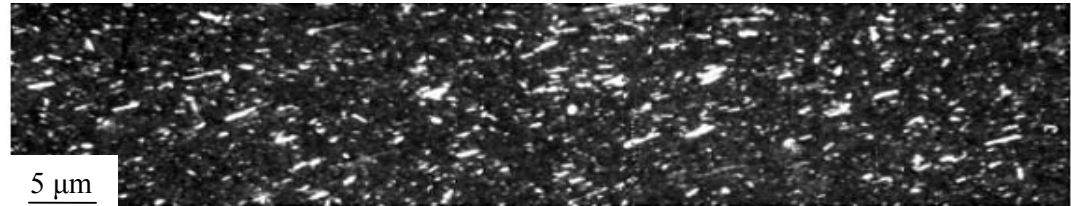
In order to analyse the alignment angle of flakes an image processing application was developed. The software is based on automated segmentation and bisection of flakes within an image. Orientation of a flake (θ_i) is determined by calculating the angle between flow direction and the longest bisector of a flake. In the event that the ratio of a flake length to width is between 0.95 and 1.05, the flake is considered as being at zero angle alignment. Flake orientation efficiency factor (η_o) is then calculated according to Equation 20. Before utilization, the software was proven reliable through testing five SEM-images and then comparing computed orientation factors with the results manually calculated based on the same images.

$$\eta_o = \sum_i c_i \cos^4 \theta_i \text{ with } \sum_i c_i = 1, \quad \text{Equation 20}$$

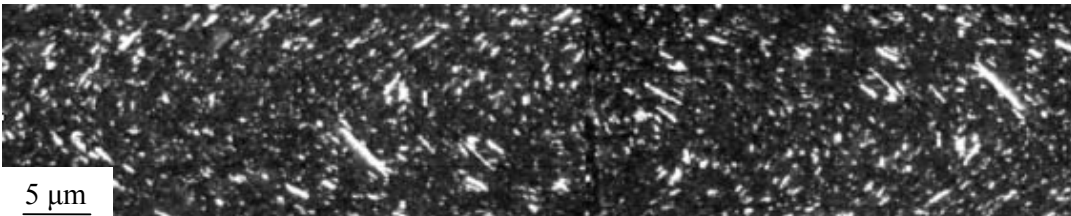
where c_i means the fraction of flakes aligned at angle θ_i .



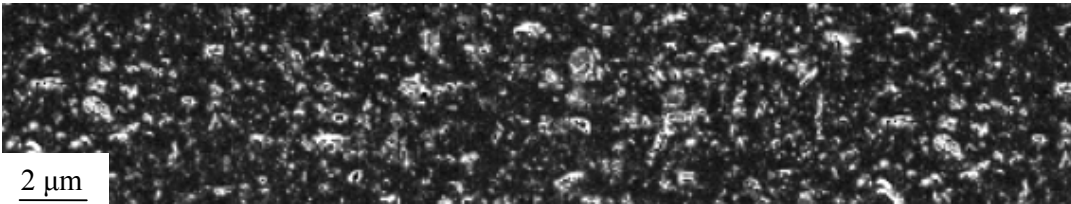
a. Skin area of cross-section



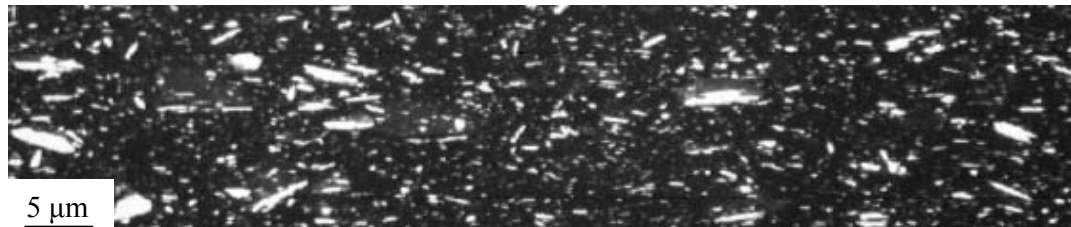
b. Skin-core junction of cross-section



c. Core area of cross-section



d. Core area of centre-section (layer 6), injecting flow direction →



e. Core area of edge-section (layer 1), injecting flow direction →



f. Skin area of edge-section, injecting flow direction →

Figure 15: Schematic orientation of 350nm silica flakes in N6 composites

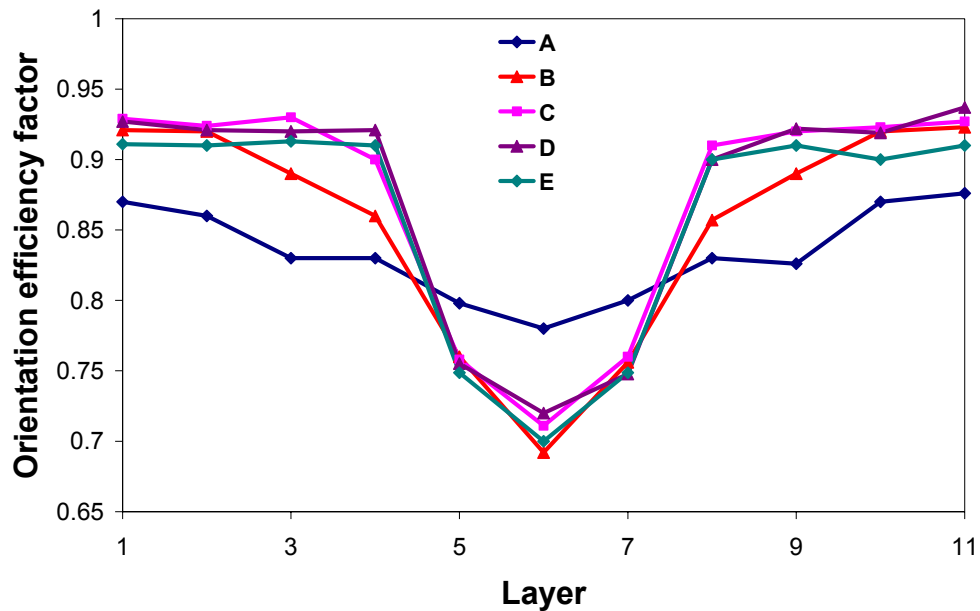


Figure 16: Orientation efficiency factors of eleven layers at five regions (A-E)

For each layer of a region, the flake orientation efficiency factor was averaged over all six images. The results of five regions, each containing eleven layers, are shown in Figure 16. According to the figure, the orientation efficiency factor of central layers (layers 5 to 7) is 0.683 to 0.78 while the edge layers (layers 1 to 4 and 8 to 11) have a factor range of 0.82 to 0.934. The relatively high orientation efficiency factors of centre layers are probably due to the non-dimensional alignment of small broken particles with equivalent length and width in the cores of centre section. Finally, the mean of fifty-five factors was calculated, a value of 0.836, and used for the prediction of Young's modulus and tensile strength.

4.3 Model prediction of the Young's modulus and strength of 350nm silica flake/N6 composites

The Young's modulus of 350nm SF/N6 sub-micro composites was predicted using the Rule of Mixtures (Equation 1), Halpin-Tsai (Equations 5 and 6) and Shear Lag model I and II (Equations 8 and 9). The prediction of tensile strength was carried out using the Rule of Mixtures (Equation 10) and modified Rule of Mixtures I and II (Equations 16 and 17). Physical parameters of the silica flake and N6 used to predict the Young's modulus and axial strength of SF/N6 composites are summarised in Table 6. In order to predict the potential of sub-micro flake in mechanical reinforcement, the original length distribution and aspect ratio flakes are used in this section. The calculated results are shown in Figures 17 and 18.

Table 6: The physical parameters of silica flakes and N6 for predicting the Young's modulus and strength of the composites

	Young's modulus, E GPa	Tensile strength, σ MPa	Ultimate Shear stress, τ_u , MPa	Poisson ratio, ν	Density, g/cm^3	Aspect ratio, s	Orientation efficiency factor, η_o
350nm silica flakes	76	2,000	–	–	2.6	475	0.836
N6	1.91	44.2	44.2	0.3	1.13	–	–

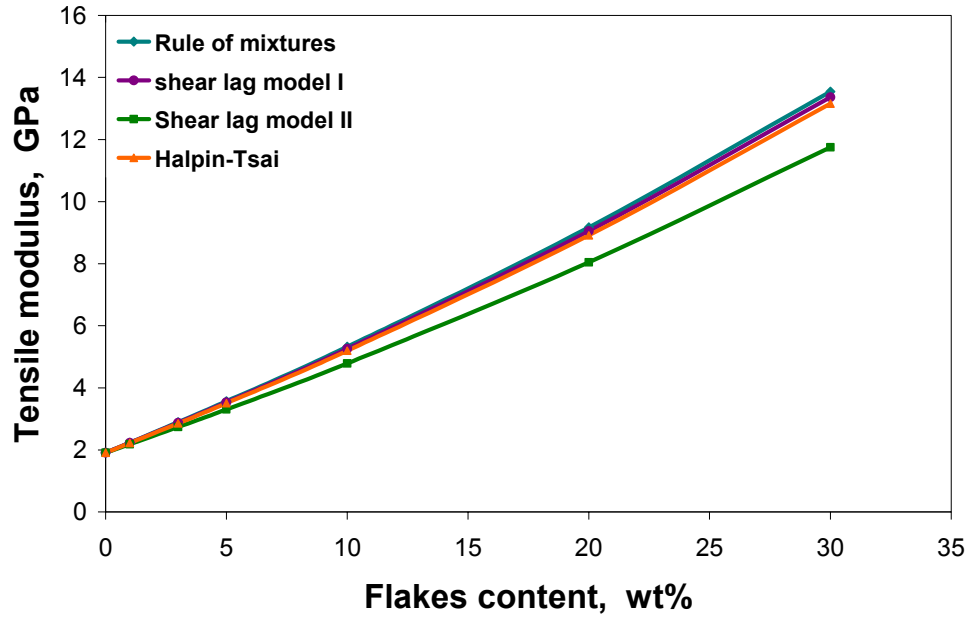


Figure 17: Dependence of the predicted longitudinal modulus of 350nm SF/N6 composites on silica flake content based on flake aspect ratio of 475 and average length of 166.2 μ m

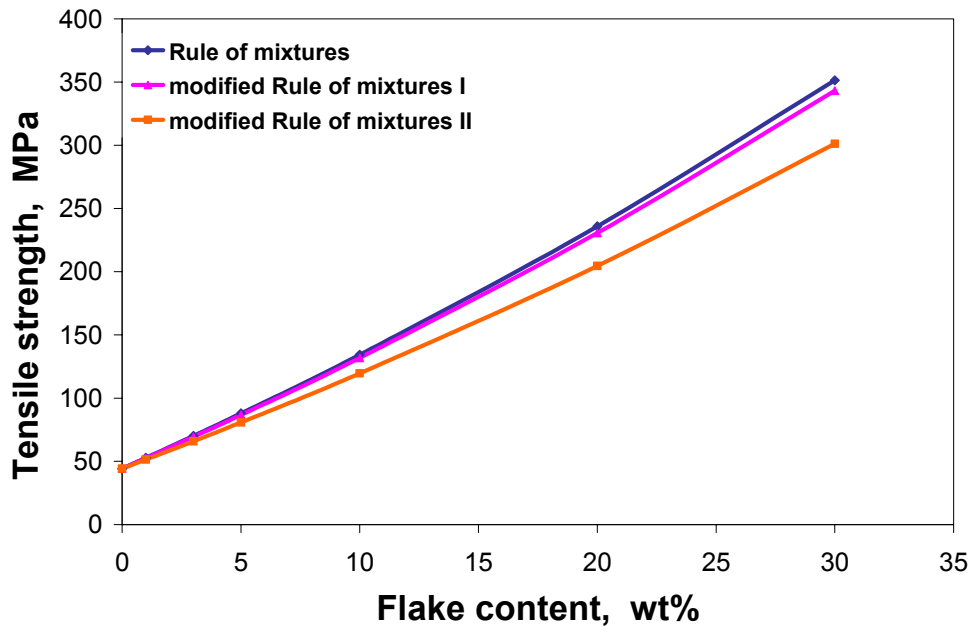


Figure 18: Dependence of predicted longitudinal strength of 350nm SF/N6 composites on flake content based on flake aspect ratio of 475 and average length of 166.2 μ m

Figures 17 and 18 show that the predicted Young's modulus and strength for all models increases with the flake content. There is little difference between the results calculated from all models when flake content is below 5wt%, and then the difference starts to be visible. The degree of this difference increases with flake fraction. At any filler content, the Rule of Mixtures gives the highest modulus value followed by Shear Lag model I and then the Halpin-Tsai model. Because the effects of both aspect ratio and orientation factor were included in the calculation, the Shear Lag model II gives the lowest values. For example, at 10wt% flake content, the calculated modulus from the Rule of Mixtures, Shear Lag model I, Halpin-Tsai and Shear Lag model II are 5.32, 5.26, 5.19, 4.79 GPa, respectively. There is 0.06 - 0.4 GPa difference between the adjacent two and 0.53 GPa different between the highest and lowest value. The calculated modulus of the composite from the Rule of Mixtures, Halpin-Tsai and Shear Lag model is 13.5, 13.36, 13.16, 11.75 GPa, respectively, with 30wt% flake content. This gives 0.14 – 1.41 GPa difference between the adjacent results and a 1.75 GPa difference between the highest and lowest value.

Similarly, the Rule of Mixtures gives higher strength than the modified Rule of Mixtures. For 5 and 30wt% flake reinforced composites, the calculated values from the Rule of Mixtures are 1.36% and 2.4% higher than those from modified Rule of Mixture I as well as 8.8% and 16.6% higher than those from the modified Rule of Mixtures II. Such results indicate that the higher the filler loading a composite has, the more significant the length distribution and orientation of fillers affect the strength of sub-micro composites.

Although the differences exist, the results calculated from orientation factor exclusive models are close to the Rule of Mixtures. Young's modulus and tensile strength calculated from orientation inclusive models, in contrast, are 7.9% to 15.2% and 8.8% to 16.6% lower than those calculated using the Rule of Mixtures in the range of flake content 5 – 30wt%. This is a clear indication that flake orientation has a major influence on the mechanical performance of sub-micro SF composites when flakes are long enough to allow of an effective stress transfer from matrix to flakes.

It is well known that calculated modulus and strength based on the Rule of mixtures are highly precise if fibres are long enough and well-aligned which virtually represents the case of long fibre reinforced unidirectional composites. Sub-micro filler reinforced polymer composites can therefore potentially achieve around eighty percent the longitudinal mechanical properties of unidirectional long fibre composites at 30wt% flake content.

5 Experimental results and discussion

In order to achieve the aims of this project, candidates for sub-micro composite application were identified. Silica flakes were selected as single-layered sub-micro fillers while expanded graphites (EG) were synthesised as multi-layered fillers for sub-micro composite enhancement. In this chapter, the experimental results of tensile modulus and strength of silica flake/N6 composites are presented in Section 5.2. Based on N6, a comparison of mechanical properties amongst glass fibre microcomposites, clay nanocomposite and silica flake sub-micro composites is outlined in Section 5.3. In Sections 5.3-5.8, investigations into key factors for mechanical reinforcement, rheology, crystallisation, impact toughness and dynamic thermal mechanical properties of silica flake composites are presented. The synthesis of expanded graphite, graphite structure in polypropylene and the mechanical properties of expanded graphite/PP composites are discussed in Sections 5.9 and 5.10 respectively. In Section 5.11, the rheology and crystallisation behaviours of EG/PP composites are explored. Finally, the relationship between the conductivity of EG/PP composites and the structure of expanded graphite in PP are investigated in Section 5.12.

5.1 The identification of fillers as the candidates for sub-micro composite application

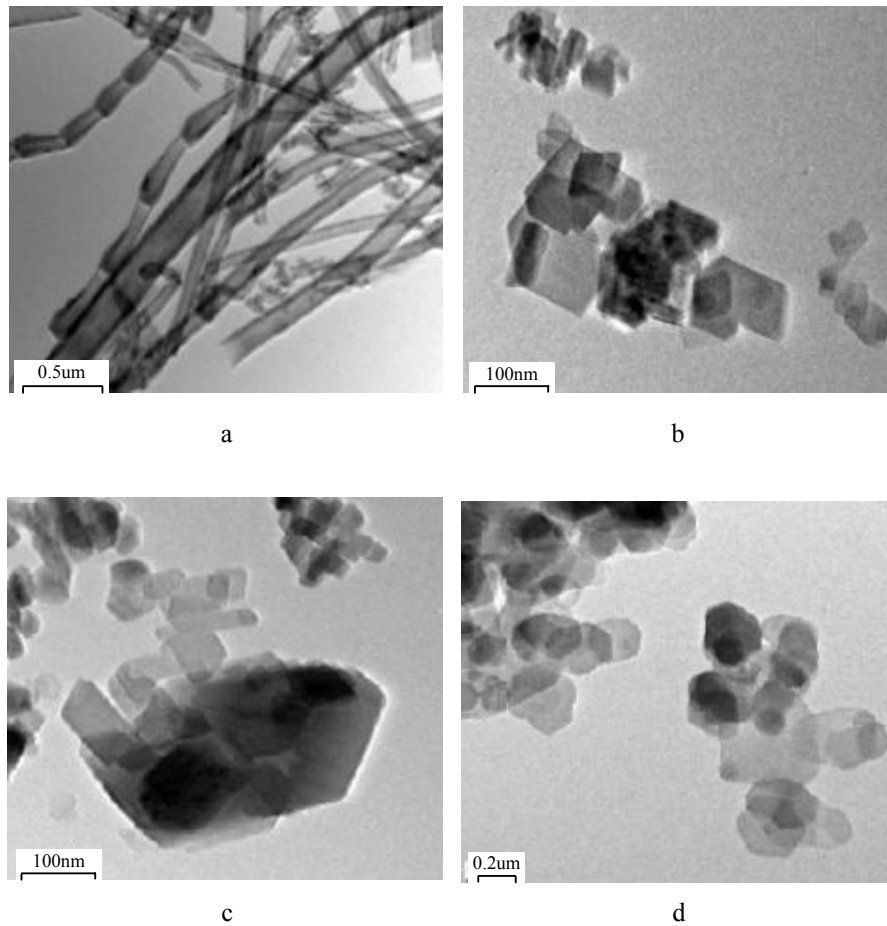
In this section, potential reinforcing fillers for sub-micro composite application are examined. The materials investigated include graphite, nano-fibres (Pyrograf III), four boehmites (dispersal 40, 80, OS 1 and MG61HT), two types of silica flakes (SF I and SF II) expanded graphite and individual graphite sheets. Their structure and surface properties were investigated using SEM and TEM.

Figure 19 shows TEM images of pyrograph III, MG61HT, dispersal 40 and 80. Figure 20 shows SEM micrograph of dispersal OS 1, expanded graphite, graphite sheets and silica flakes. Table 7 described the thicknesses and diameters of these filler particles.

Table 7: Thicknesses and diameters of candidate fillers for sub-micro application

	Pyrograf III	Dispersal 40	Dispersal 80	MG61HT	Dispersal OS1	SF I	SF II
Thickness /nm	~ 30	20-50	20-40	100-200	--	750-860	350-365
Diameter /nm	50-280(exter)	50-150	80-180	300-500	30-500 μm	50-150 μm	50-150 μm

Since carbon nanofibres and some boehmites are small, TEM was used to investigate these materials. The TEM morphology of Pyrograf III revealed a mixture of single-walled, multi-walled and bamboo-shaped carbon tubes. Their external diameters were between 50 and 280 nm, which make them partially overlap with the sub-micro range. Boehmite dispersal 40, 80, and MG61HT exhibit layered-structure with thicknesses of 20-50, 20-40 and 100-200nm respectively. Their corresponding diameters were 50-150, 80-180 and 300-500nm respectively. Dispersal 40 and 80 thus are classified as nano-size range particles while MG61HT is a sub-micro particulate filler.

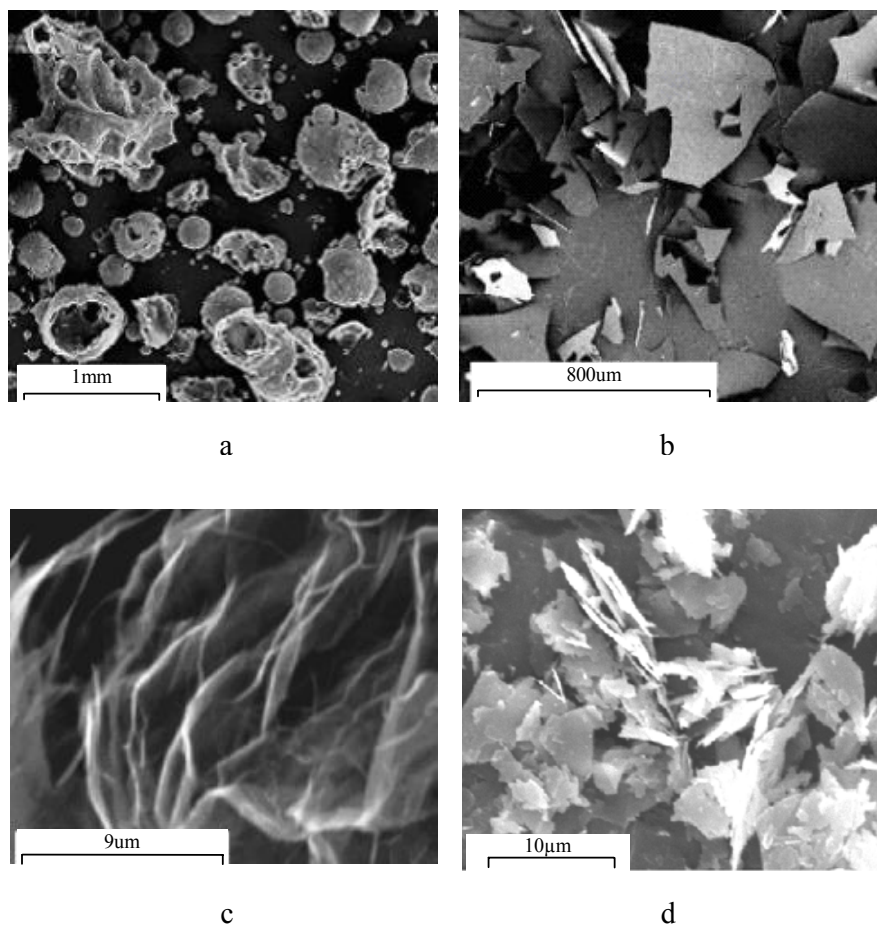


a) Carbon nanotube Pyrograf III. b) Dispersal 40. c) Dispersal 80. d) MG61HT.

Figure 19: TEM micrograph of carbon nanotube pyrograf III and boehmites

The other fillers studied are much larger and therefore were investigated using SEM. Boehmite OS1 consists of hollow spheres. The product also contains a great number of broken particles as shown in Figure 20a. As a consequence, this structure is not suitable for mechanical reinforcement. Two types of silica flakes were observed to have similar shapes and single layered structures. The layer thicknesses of silica flakes (SF) were between 750 and 860nm for silica flake I and 350 to 365nm for silica flake II. They are

thus referred as 850nm silica flakes and 350nm silica flakes. These silica flakes have a similar distribution of diameter which is in the range of 50 to 150 μ m.



a) Dispersal OS 1. b) Silica flakes. c) Expanded graphite. d) Graphite sheets.

Figure 20: SEM micrograph of beomite, silica flakes and sub-micro graphite

As shown in Figure 20c, expanded graphite has a honeycomb structure within worm-shaped strands. The layer thickness of expanded graphite was 50 to 150 nm with a diameter of 5 to 18 μ m. Graphite sheets were made from expanded graphite but the honeycomb structure has been broken resulting in individual sheets. The thickness of

sheets was between 280 and 360nm with a diameter of 5 to 15 μ m. Both expanded graphite and graphite sheets possessed multi-layered structures.

Based on the morphology and dimensions of the particles examined, MG61HT was selected as a zero dimensional sub-micro particle filler and Pyrograf III as a one dimensional filler. The two silica flakes and two graphite products were used as two dimensional reinforcing fillers. In accordance with their thicknesses, silica flakes are classified as 350nmSF and 850nmSF. Because of their structure, expanded graphite and graphite sheets are referred to multi-layered sub-micro fillers. Amongst these sub-micro fillers, MG61HT has small aspect ratios of approximate 1.5 to 5. Pyrograf III has a complex mixture of different structural carbon-tubes. Therefore, only the silica flakes and two graphite products were used in sub-micro composite during this project.

Since the silica flakes have single sheet structure, there is no need for exfoliation. This advantage makes silica flakes a suitable model materials for exploring the potential of sub-micro reinforcement. Due to their narrow thickness distribution, silica flakes were also considered suitable for the investigation of aspect ratio effects on sub-micro reinforced polymer composites. Sub-micro graphite products because of their electrical conductivity, they were used not only to reinforce mechanical properties of the composites but also to synthesise conductive polypropylene composites. The results of this work are discussed in following sections under the heading of reinforcement with single-layered sub-micro fillers and enhancement with multi-layered sub-micro fillers, respectively.

Part I: Reinforcement with single-layered sub-micro fillers

Based on the single-layered 350nm silica flakes and N6, the relationship of Young's modulus and strength of the 350nm silica flake/N6 composites with filler fractions was studied. A comparison of mechanical properties was conducted for the clay/N6 nanocomposites, 350nmSF/N6 sub-micro composites and glass fibre composites. Furthermore, the key factors in sub-micro composite enhancement, rheology, crystallisation behaviour and fracture toughness and thermal dynamic mechanical properties of silica flake/N6 composites were explored. Detailed discussions are given in Sections 5.2 to 5.8.

5.2 Tensile modulus and strength of sub-micro silica flake/N6 composites

Sub-micro N6 composites studied were based on 350nm silica flake produced by the melt blending method as described in Section 3.5.1. The filler fractions in the composites were 1, 3, 5, 10, 20 and 25wt% respectively. The tensile modulus and strength of the composites were measured according to the method as described in Section 3.6.1. Figures 21 and 22 show the dependences of tensile modulus and strength of 350nm silica flake/N6 composites on filler fractions.

Figure 21 shows that the tensile modulus of silica flake sub-micro composites increases with filler loading. The greatest increase occurred below 3wt% after which there was a steady increase up to 20wt%. The rate of increase, however, decreased in the range of 3 to 20wt% filler content. At 3wt% flake loading, the modulus of the composite reached 2.98GPa which was an increase of 56% compared with the base polymer. The tensile

modulus of the composite only rose by 24% from 3 to 20wt%. The possible reason for this is that above 3wt% filler content the low aspect ratio distribution of silica flakes, generated by the breakage of silica flakes during composite processing, have increased significantly, which is evidenced by Figures 26 to 29. Over 20wt% flake fraction, the rate of modulus improvement increased again and achieved 4.13 GPa at 23.72wt% silica flake fraction. This is 116% higher than the pure N6.

Figure 22 shows that the tensile strength of 350nm silica flake/N6 sub-micro composites had a drastically improvement of 55.6% at 1wt% silica flake content with respect to the pure polymer. Above 1wt% flake loading, the tensile strength of composites kept slow rising until flake fraction of 20wt% was reached and then slightly dropped. The highest strength of sub-micro silica flake/N6 composites produced was 77.13 MPa obtained at 20wt% filler loading which is an increase of 74.5% compared to the pristine polymer.

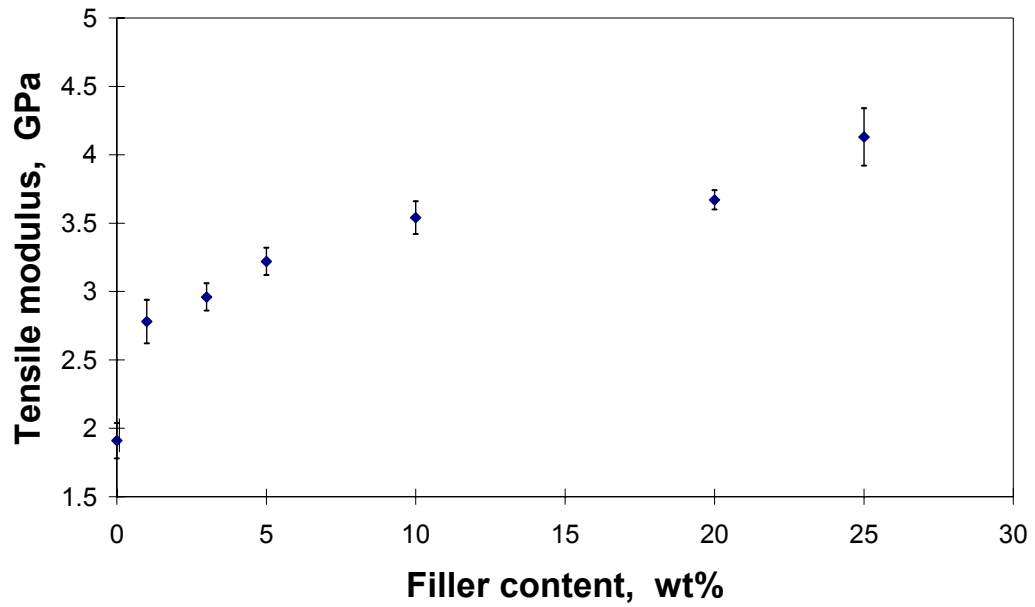


Figure 21: The dependence of tensile modulus of 350nmSF/N6 sub-micro composites on filler contents

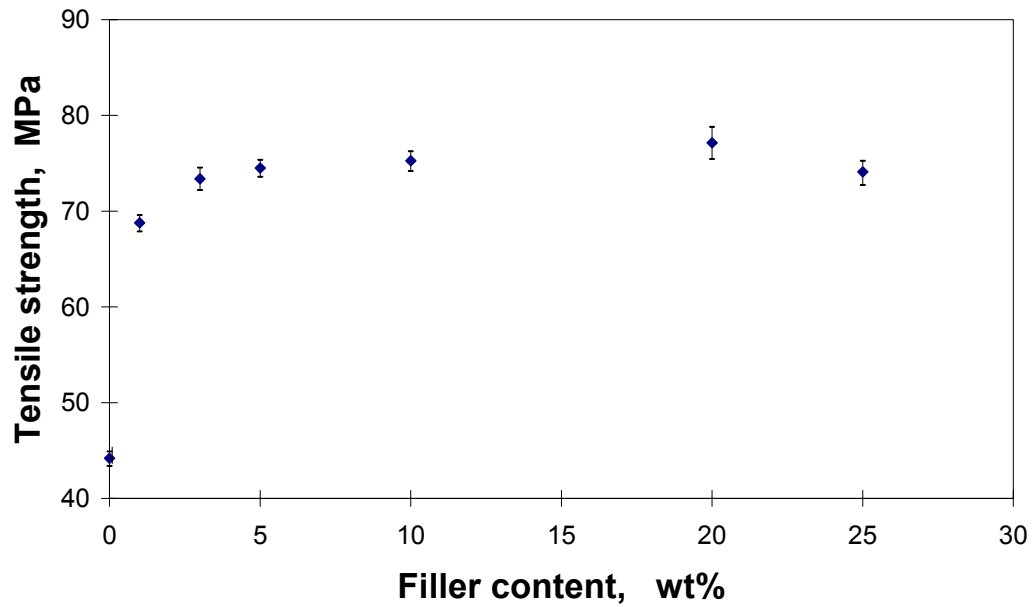


Figure 22: The dependence of tensile strength of 350nm silica flake/N6 composites on filler contents

5.3 A comparison in mechanical properties amongst the sub-micro filler reinforced composites, nanocomposites and short fibre composites

For a comparison, clay93a/N6 nanocomposites were also prepared via the same melt blending method. The filler content of nanocomposites was between 1 and 20wt% after which the products become dark and brittle. Over 20wt%, clay/N6 composites could not be produced using the extrusion technology. The tensile modulus and strength of the nanocomposites were measured using the same method used for the sub-micro composites. The tensile modulus and strength of 5, 15 and 30wt% short glass fibre reinforced N6 were adapted from references [81], [93] and [186]. All results were normalised using the ratio of a composites property to the equivalent matrix polymer properties, i.e. E_c/E_m and σ_c/σ_m , and plotted in Figures 23 and 24. The failure stress of a composite is known to reduce if fibre content is below the critical fibre volume fraction. The critical fibre volume fraction of glass fibre/N6 composites is around 9% according to the equation $V_f' = \frac{\sigma_m^*}{\sigma_f^* - \sigma_f' + \sigma_m^*}$ [5]. Where V_f' represents the fibre critical volume fraction while σ_m^* and σ_f^* are the ultimate tensile strength of matrix and fibre respectively. σ_f' is the fibre stress when the matrix fails. Five percent glass fibre content is below the critical fraction and thus not practical. Such glass fibre content is used in this research for comparison purposes only.

According to Figure 23, in the low filler fraction range, the nanocomposite performed the best in tensile modulus, amongst the clay93a/N6 nanocomposites, sub-micro silica flakes enhanced N6 and 6mm glass fibre reinforced N6. An improvement of 103% in

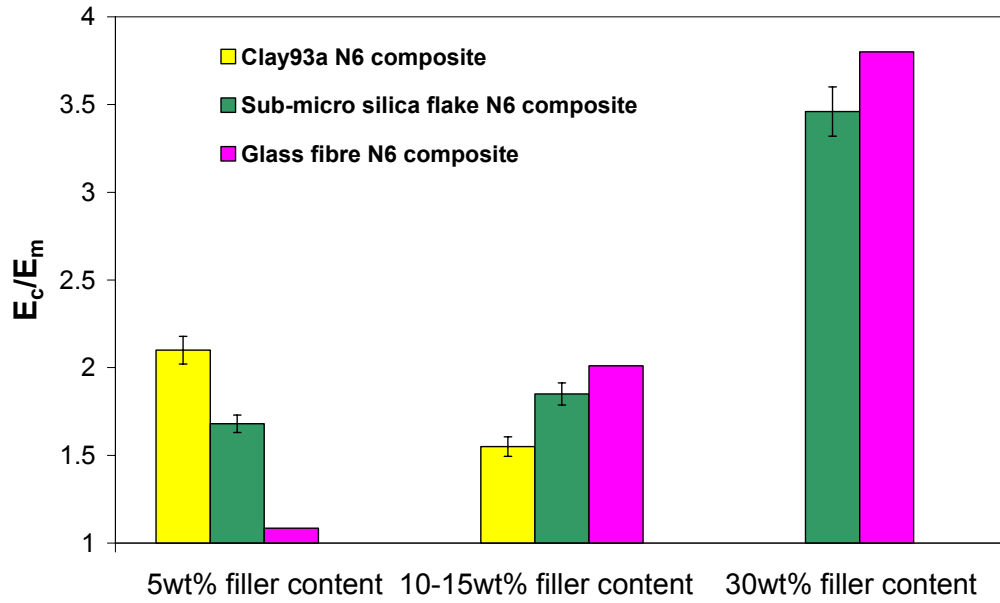
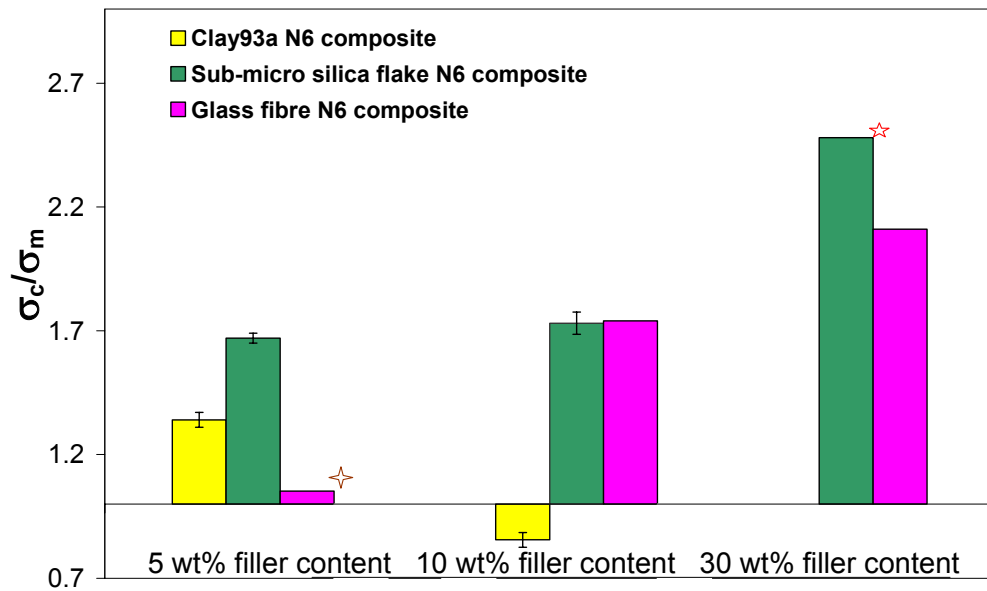


Figure 23: Tensile modulus comparison of sub-micro, micro and nano composites



✦ Predicted strength by the Rule of Mixture.

★ Predicted strength using modified Rule of Mixtures with an aspect ratio of silica flakes of 12.

Figure 24: Tensile strength comparison of sub-micro, micro and nano composites

Young's modulus was achieved by the nanocomposite at a low filler loading level of 5wt% compared with the pristine polymer. The 5wt% sub-micro silica flakes/N6 composite was second best with a tensile modulus 68% higher than the matrix polymer. The 5wt% glass fibre reinforced composite only had a modulus increment of 5.4% with respect to the pure N6, which is far lower than the corresponding nano and sub-micro silica flake composites.

The tensile modulus of nanocomposites, however, started to deteriorate when over 7wt% clay content due to the poor dispersion and agglomeration of clay layers in the polymer. This is indirectly evidenced by X-ray diffraction analysis as shown in Figure 25. The X-ray pattern of clay93a showed a peak at 2-theta angle of 3.9789 degree which represents the clay93a has an interlayer $d_{(001)}$ -spacing of 2.229nm. This peak disappeared in the pattern of 5wt% clay93a/N6 composite indicating the exfoliation of the clay in the polymer. However, the peak shifted back to a 2-theta angle of 5.316 degree in the pattern of 10wt% clay93a/N6 composite leading to a clay interlayer d_{001} -spacing of 1.665nm, in the composite. This narrowed $d_{(001)}$ -spacing of the clay in the composite is a clear indication that agglomeration of clay nanolayers has occurred resulting a poor dispersion of the clay in the polymer.

In contrast, the modulus of sub-micro composites continuously increased with flake fraction. At 10wt% of filler loading, the modulus improvement of the sub-micro SF/N6 composite was close to that of a 15wt% 6mm glass fibre reinforced N6 composite. With 30wt% filler fraction, both glass fibre and sub-micro SF/N6 composites achieved significant improvement in Young's modulus of over 240% compared to their matrix

polymers. This is 53% higher than the best clay/N6 nanocomposites produced in this study.

Figure 24 shows that at 5wt% filler fraction, the sub-micro SF/N6 composites exhibited the best improvement in tensile strength which was 60% higher than a model-predicted value of 5wt% glass fibre filled N6 composites. This was also 34% and 67% higher than that of the 5wt% clay93a nanocomposites and the pure N6 respectively. Interestingly, if comparing 10wt% filler reinforced composites, the tensile strength of the clay93a/N6 nanocomposite was deteriorated and 14.5% worse than the base polymer. In contrast, the 350nm SF enhanced composite achieved the same improvement in tensile strength as that of a 15wt% glass fibre reinforced N6 composite. The calculated tensile strength of 30wt% 350nm silica flakes reinforced N6, based on aspect ratio of 12 and the modified Rule of Mixtures II (Equation 17), showed a strength improvement 25% higher than the 30wt% glass fibre counterpart and an increase of 148% compared to the pure N6.

In summary, the tensile strength of the 350nm silica flake composite is 38% higher than that of nanocomposites at 5wt% filler loading although the corresponding tensile modulus is 35% lower than that of nanocomposites. Importantly, both strength and modulus of 350nm SF/N6 composites are superior to nanocomposites at medium and high filler fractions and also comparable with glass fibre/N6 composites in high filler fractions. Therefore, in theoretical and practical terms, the sub-micro composite approach has the potential to fill the gap between nano and micro composite reinforcement.

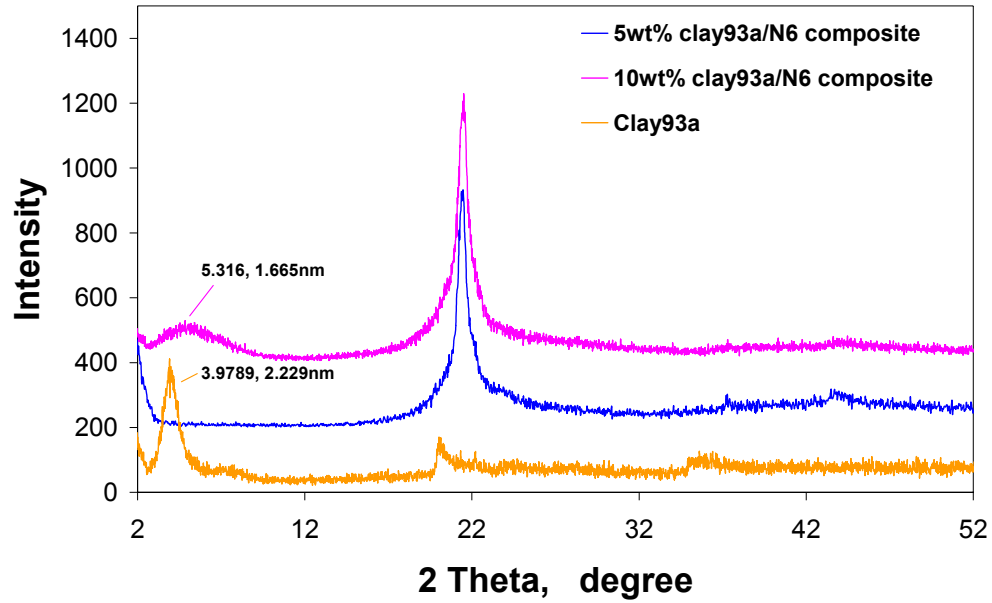


Figure 25: XRD patterns of clay/N6 composites

5.4 Key factors of sub-micro silica flake enhancement

As discussed in Section 5.2, sub-micro silica flake composites have outstanding tensile modulus and strength both at low and high filler loading. However, when comparing experimental results with predicted data, the experimental results are far lower than the predicted modulus and strength when flakes content is over 5wt%. It was found that silica flakes were broken during the extrusion process, especially in composites with high filler loadings (seen by comparing Figure 13 with Figures 26 to 29). This led to the length and aspect ratio of silica flakes being drastically reduced and resulted in significant deviation of the experimental results from the predicted values. To understand the effects of filler length and aspect ratio on sub-micro enhancement, the virtual length distributions of silica flakes after extrusion were investigated. The

influences of extrusion conditions and filler surface treatment on flake breakage were explored. Furthermore, the compatibility of silica flakes with matrices was also studied.

5.4.1 The effect of aspect ratio on tensile modulus and strength of sub-micro silica flake composites

In this section, an investigation into length distributions and aspect ratios of broken silica flakes in the composites is conducted. The Young's modulus and strength of composites based on the real distributions of length and aspect ratio of the broken flakes are calculated. The Shear Lag models I and II were used for the modulus calculation while the modified Rule of Mixtures I and II were applied to calculate strength.

Due to the uneven dispersion of flakes with different lengths along the width of a tensile test specimen, as seen by comparing Figure 15 d and e, it is difficult to carry out image analysis and to calculate flake length distribution based on the injected moulds. An alternative method was therefore used to investigate length distribution of silica flakes after extrusion. The method was based on composite pellets burning for one hour at 400 °C in a muffle oven, followed by SEM image analysis. One, three, five and twenty five percent of flakes reinforced composites were studied. The flake length distribution in each composite is shown in Figures 26 to 29. It is found that the length of the longest flakes in each composite shortened from 23 to 8.3 μm when filler content increased from 1 to 25wt% while the length of shortest flake in each composite did not change. In the 1wt% 350nm silica flakes filled N6 composite, the major flake length distributions were in 19-21, 8-9 and 4 μm . The average length and aspect ratio of flakes was 10.8 μm

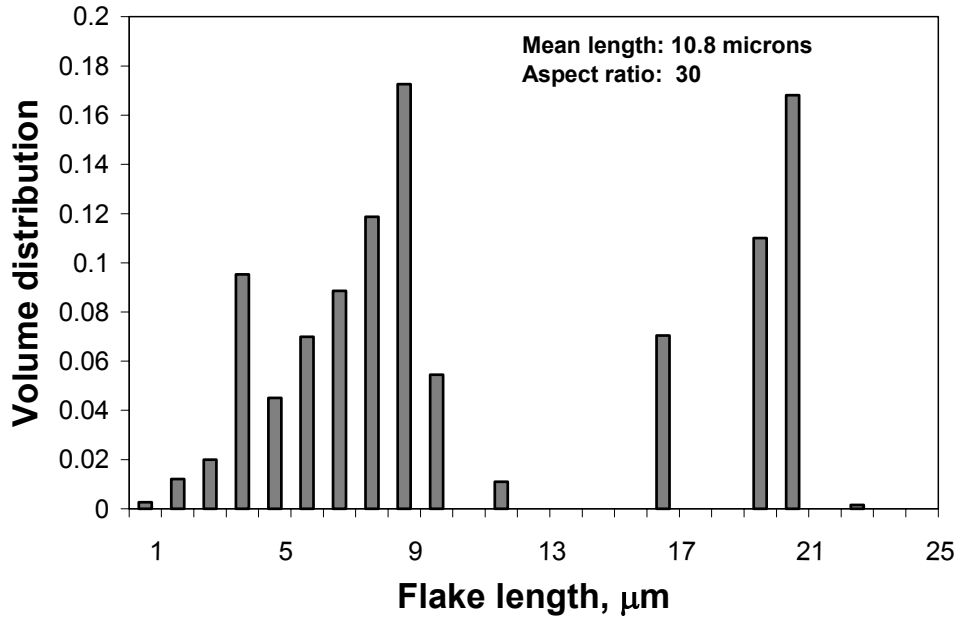


Figure 26: Length distributions of silica flakes in 1wt% SF/N6 composites

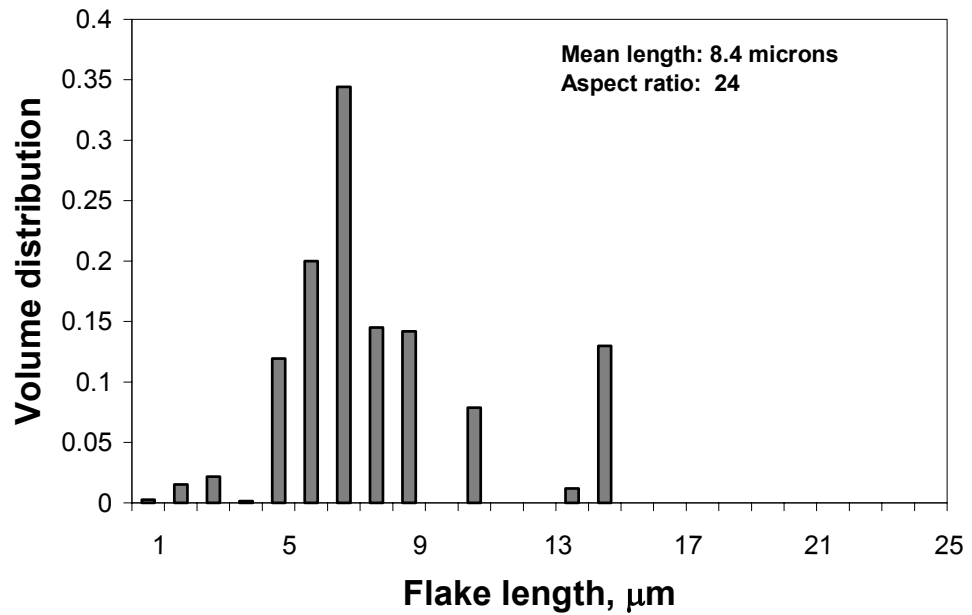


Figure 27: Length distributions of silica flakes in 3wt% SF/N6 composites

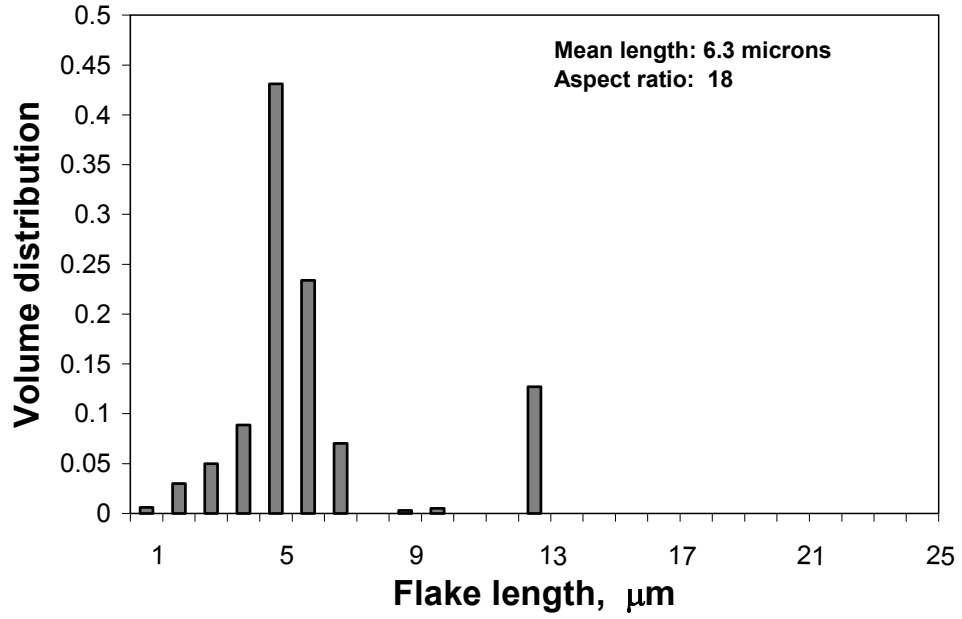


Figure 28: Length distributions of silica flakes in 5wt% SF/N6 composites

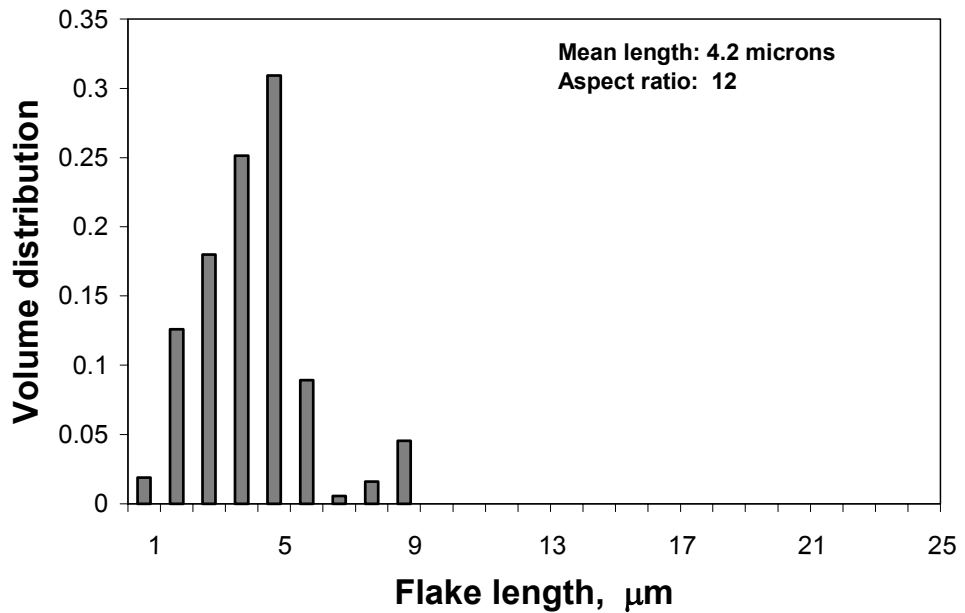


Figure 29: Length distributions of silica flakes in 25wt% SF/N6 composites

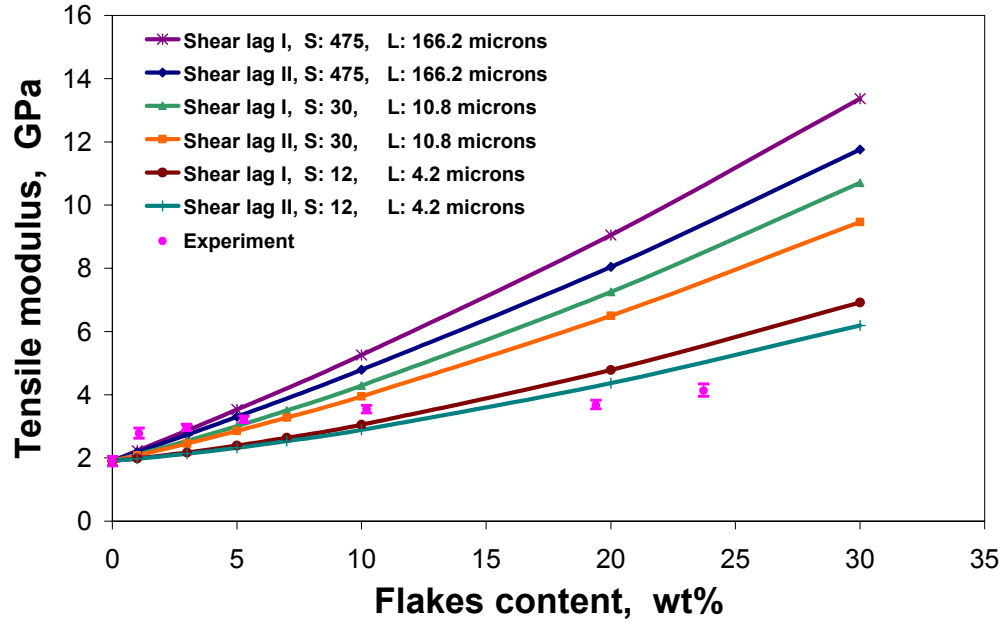
and 30, respectively. With 3wt% filler loading, the major flake length distribution reduced to around 7 μm whereas approximately 13vol% flakes still remained a length of 14-15 μm . The average flake length and aspect ratio was 8.4 μm and 24, respectively. In 5wt% 350nm silica flakes filled N6 composite, the major flake length distribution reduced to 4-5 μm while approximately 12vol% flakes remained a length of 12-13 μm . The mean length and aspect ratio was 6.3 μm and 18, respectively. With 25wt% flake filled N6, the major length distribution was 4.89 μm , similar to that of the 3wt% composite. The longest and average flake length, however, significantly decreased to 8.3 μm and 4.2 μm respectively which gave an average aspect ratio of 12.

In order to clarify the effects of such breakage on the mechanical properties of sub-micro silica flake composites, the elastic modulus and strength of 350nmSF/N6 composites were re-calculated using real flake length and aspect ratio distributions of broken silica flakes. The calculation was based on two Shear Lag and two modified Rule of Mixtures models and designed to investigate the effects of both aspect ratio and filler orientation. The re-calculated results are plotted in Figures 30 and 31. For all models applied, the tensile modulus and strength of composites significantly reduced with the decrease of filler aspect ratio. In terms of Shear Lag modulus model II, the modulus of the 20wt% 350nmSF composite dropped by 19.3% and 45.8% from 8.04 to 6.49 and 4.36GPa, when the aspect ratio of flakes was reduced from 475 to 30 and 12 respectively. In terms of the modified Rule of Mixtures strength model II, the strength of the 20wt% 350nmSF composite dropped by 37% and 58.9% from 204.6 to 129.8 and 84.8 MPa, when the aspect ratio of flakes was reduced from 475 to 30 and 12, respectively.

The re-calculated modulus and strength based on aspect ratio 30 and 12 are very close to experimental results. With a flake aspect ratio of 12, all models give similar results to the experimental data for high loading levels such as 10, 20 and 25wt%. With a flake aspect ratio of 30, the models gave similar results to the experimental data for low SF loaded N6 composites, such as 3 and 5wt%. The main reason for this being that the aspect ratio of silica flakes reduced with the increase of filler loading leading to a lower flake aspect ratio in high filler loaded composites, as seen in Figures 26 to 29.

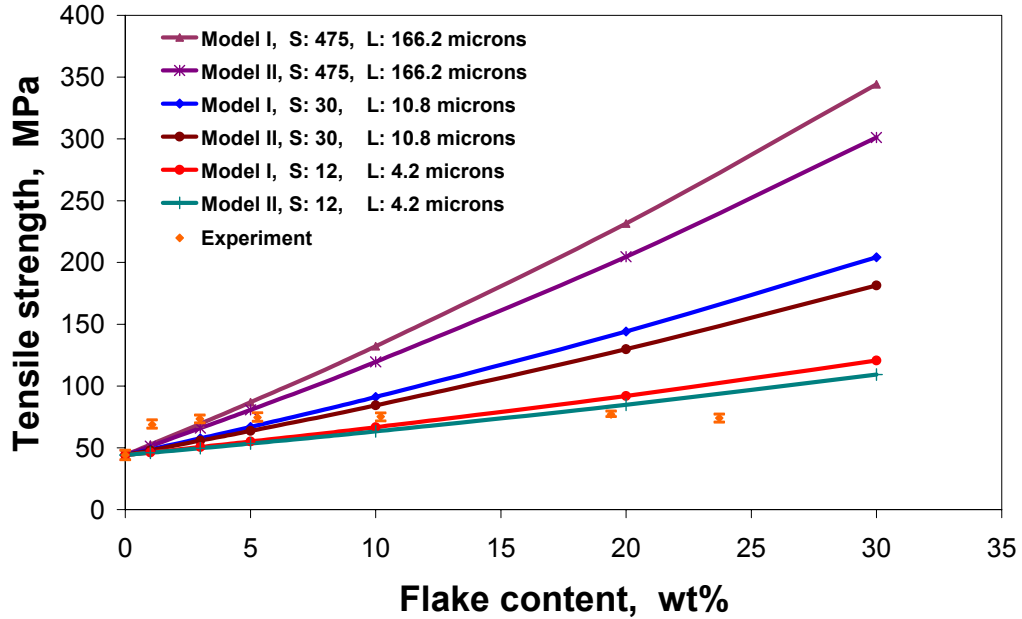
Comparing Model I to Model II, the effect of filler orientation on both tensile modulus and strength tend to decrease with the reduction of flake aspect ratio. When aspect ratio is reduced to 12, the influence of flake orientation becomes insignificant, as shown in Figures 30 and 31.

Based on the results above, the aspect ratio decrease of silica flakes is a major reason why the tensile modulus and strength of highly filled silica flake/N6 composites is limited.



Shear Lag I is referred to η_0 exclusive and Shear Lag II is referred to η_0 inclusive

Figure 30: Dependence of elastic modulus of sub-micro SF/N6 composites on the fraction, aspect ratio and orientation of flakes based on Shear Lag models



Model I is referred to η_0 exclusive and Model II is referred to η_0 inclusive

Figure 31: Dependence of tensile strength of sub-micro SF/N6 composites on the fraction, aspect ratio and orientation of flakes based on modified Rule of Mixtures

5.4.2 Extrusion speed and surface protection of silica flakes

As a major condition of the extrusion process, the effect of screw speed on flake breakage was studied. Amino-silane, epoxy-silane and vinyl-silane surface modified flakes were employed in the investigation of flake surface protection. The SEM morphology of flakes burnt from various composites is shown in Figures 32 and 33.

Figure 32 illustrates four SEM images. The first three images represent non-modified 350nm silica flakes in 5wt% N6 composites at 100, 250 and 400rpm screw speed respectively. The final image is the flakes from 5wt% 350nm amino-silane coated silica flakes/N6 composite at 400rpm screw speed. According to the images of non-modified flakes in the composites, the degree of flake breakage increases with screw speed. On comparing the flake image after a 100 rpm screw speed extrusion with that of after 250 rpm, it can be seen that their diameter of large particles is similar while the diameter of small particles has decreased after 250 rpm extrusion. As a consequence, the average aspect ratio of silica flakes is reduced. Unsurprisingly, extrusion at 400 rpm resulted in a reduction of flake diameter and a significant increase in small particles.

When comparing the non-modified with amino-silane modified flakes in the corresponding composites at 400rpm screw speed, the results in Figure 32 show that surface treatment can protect the flakes from breakage to a certain degree. After amino-silane surface treatment, large particles remained while the fraction of small particles decreased. Furthermore, the effect of different modifiers is explored as illustrated in Figure 33. The figure shows that epoxy-silane coated 350nm silica flakes in the composite have the largest particle diameter followed by vinyl-silane treated flakes. The diameter of amino-silane silica flakes is slightly smaller than that of vinyl-silane

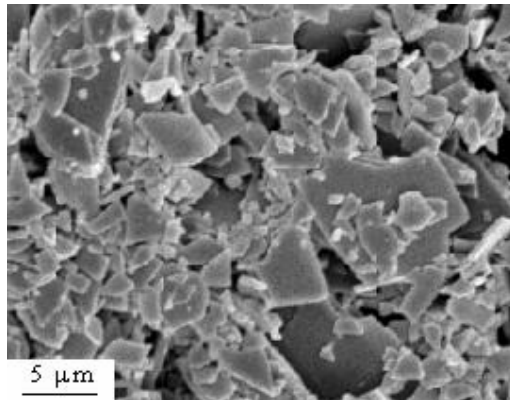
modified flakes. This is an indication that epoxy silane provides the best protection for silica flakes in N6 matrix. However, considering the compatibility of the coupling agent with N6, amino-silane modified 350nm silica flakes were selected for the later study.

In summary, low extrusion speeds and surface modification are beneficial in the maintenance of large aspect ratio silica flakes. However, the size of surface treated flakes after extrusion is still far smaller than the original flakes, when comparing Figure 33 with Figure 20b. Surface coating thus is not an effective method to prevent flakes' break. Low extrusion speeds, in addition, results in longer residence in the extruder as shown in Table 8, leading to the degradation of materials. This in turn reduces the mechanical properties of the product.

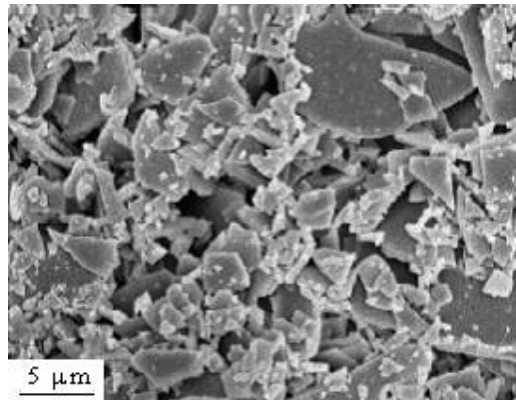
Table 8: The dependence of residence time on screw speed of the extrusion at 20vol% feeding rate

Screw speed rpm	250	300	350	400	450
Residence time s	39	31	26	22	22

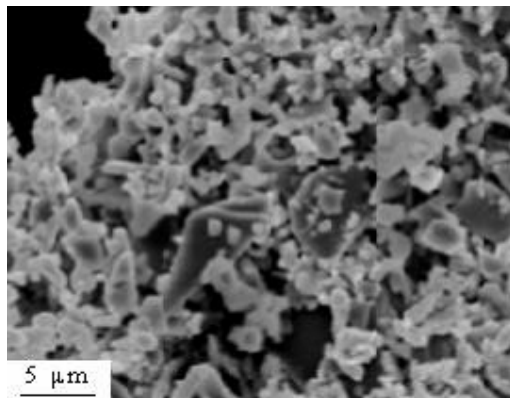
Residence time was measured by adding five grams of coloured additive during polymer extrusion. The period time from addition to removal of the additive from the extruder was taken as the residence time.



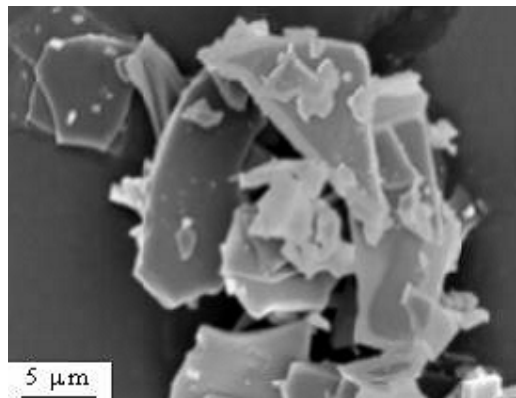
5 wt% 350nmSF/N6 composite
Screw speed: 100 rpm



5 wt% 350nmSF/N6 composite
Screw speed: 250 rpm

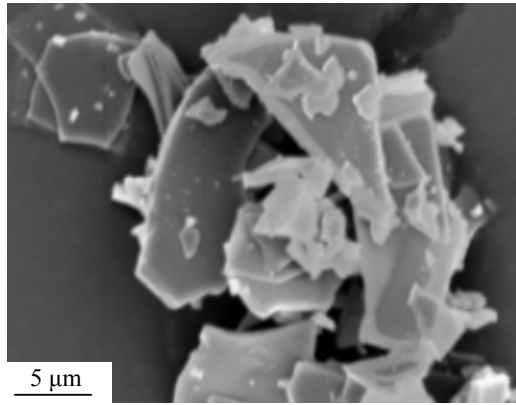


5 wt% 350nmSF/N6 composite
Screw speed: 400 rpm

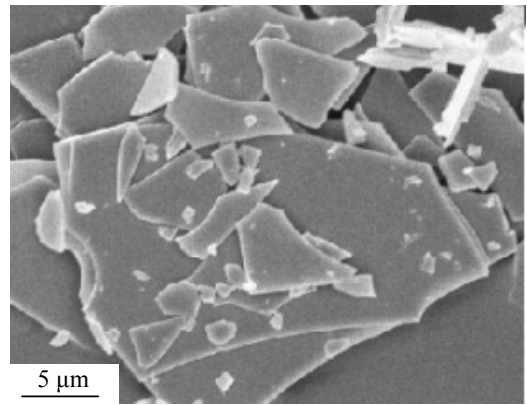


5 wt% 350nm
Amino-silane modified SF/N6
composite

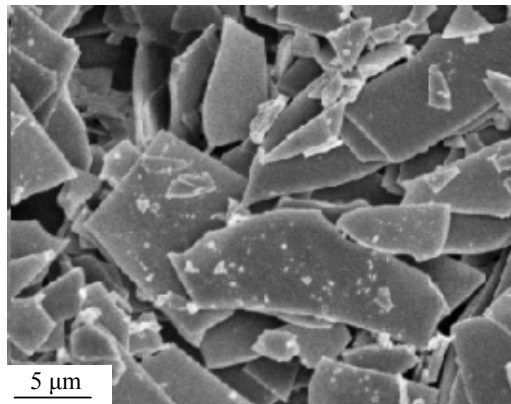
Figure 32: The effect of extrusion speed and surface modification on silica flake breakage



5 wt% 350nm
Amino-silane modified
SF/N6 composite



5 wt% 350nm
Epoxy-silane modified
SF/N6 composite



5 wt% 350nm
Vinyl-silane modified
SF/N6 composite

Figure 33: The effect of different silanes on flake surface protection

5.4.3 Degradation of materials during composite processing

Investigation into thermodegradation of materials and effect of the degradation on mechanical properties of composites were carried out using amino-silane modified SF reinforced PP and N6. The effect of extrusion speed on degradation of the composites, visible as change in colour, is shown in Figure 34. At a process temperature of 225 °C feed rate of 20vol% and extrusion speed of 400rpm, the pellets of PP composite have similar colour to the PP but become dark brown when extrusion speed below 400rpm, due to the degradation of surface modifier. The pellets of N6 composite are brown even at 400rpm extrusion speed as the higher processing temperature caused amino-silane degradation during the extrusion.

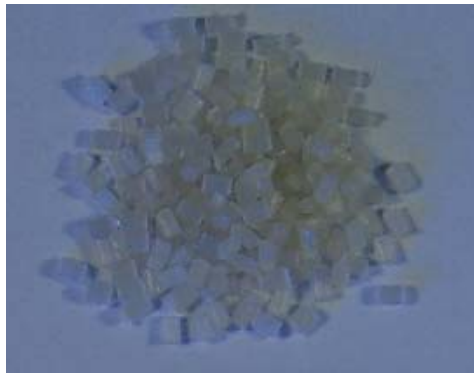
The degradation led to a decrease in tensile strength of the composites. Table 9 shows the influence of degradation on the mechanical properties of sub-micro composites. With 25wt% 350nm flakes surface modified by amino-silane, the modulus of N6 composites increased by 47% from 4.13 to 6.11 GPa, when compared with 30wt% non-modified 350nmSF/N6 composite. This increase benefited from the larger aspect ratio of flakes after surface treatment. However, due to the degradation of amino silane, tensile strength decreased from 74.1 to 68.32 MPa rather than increases with the improved aspect ratio. Details on this will be explained in the rheology section of this thesis. As a result, the use of high temperature resistant modifier to perform silica flake surface protection is an important objective for N6 sub-micro composites in future research.



Amino-silane modified SF/PP composite
Temperature: 225 °C, Feed rate: 20 %
Screw speed: 350 rpm



Amino-silane modified SF/PP composite
Temperature: 225 °C, Feed rate: 20 %
Screw speed: 400 rpm



Amino-silane modified SF/N6 composite
Temperature: 235 °C, Feed rate: 20 %
Screw speed: 400 rpm

Figure 34: The effect of extrusion speed on degradation of sub-micro composites

Table 9: Tensile modulus and strength of 30wt% 350nm SF/N6 composite with and without surface modification

	Tensile modulus GPa	Tensile strength MPa
350nmSF/N6 composite	4.13 ± 0.21	74.1 ± 1.16
Amino-silane modified 350nm/N6 composites	6.11 ± 0.34	68.32 ± 0.8

5.4.4 The compatibility of silica flakes with polymer

Polypropylene and N6 were selected as matrices to investigate the effects of compatibility of silica flakes with polymers on mechanical properties of sub-micro composites. Due to the highly hydrophobicity of polypropylene, coupling agent modified 350nm silica flakes were used to improve the compatibility of flake with PP, including vinyl-silane, amino-silane and epoxy-silane coated 350nm silica flakes. The chemical structure of polypropylene and three silanes are shown in Figure 35 while the tensile modulus and strength of PP composites are shown in Table 10.

As a non-polar polymer, PP is highly hydrophobic and not compatible with hydrophilic fillers. As a consequence, a weak interface bonding between silica flakes and PP occurs. This is reflected by the significant tensile strength decrease of the 30wt% non-modified 350nm SF/PP composite. By using silane compatiliser treated silica flakes, the strength of composites was improved with respect to the non-modified SF/PP composite. The

improvement increased with the compatibility between silane coupling agents and the matrix.

Table 10: Tensile modulus and strength of 30wt% 350nm SF/PP composite with and without surface modification

	PP	350nm SF/PP	Amino-silane modified 350nmSF/PP	Epoxy-silane modified 350nmSF/PP	Vinyl-silane modified 350nmSF/PP
Tensile modulus GPa	1.41±0.1	2.24±0.09	2.91±0.1	2.33±0.12	3.6±0.18
Tensile strength MPa	32.63±0.82	26.72±0.31	28.69±0.64	25.65±0.4	31.12±0.42

With 30wt% vinyl-silane modified SF, the strength of the composite was compensated and reached a similar value to that of non-filled polypropylene. The results in Table 10 also show that tensile modulus of sub-micro composites increase with the improvement of compatibility between filler and matrix. With 30wt% vinyl-silane modified SF, the tensile modulus of the composite increased by 155% from 1.41 to 3.6 MPa when compared with polypropylene.

Furthermore, with N6, polymer molecules are bonded with silica flakes through hydrogen bond as shown in Figure 36. The compatibility of the filler with matrix is thus much higher than that of silica flakes with PP. A significant mechanical property improvement in both modulus and strength is achieved in SF/N6 composites as discussed in Section 5.2. Therefore, for hydrophobic polymers, the compatibility of polymers with flakes is an essential factor for sub-micro composite mechanical enhancement, especially in strength reinforcement.

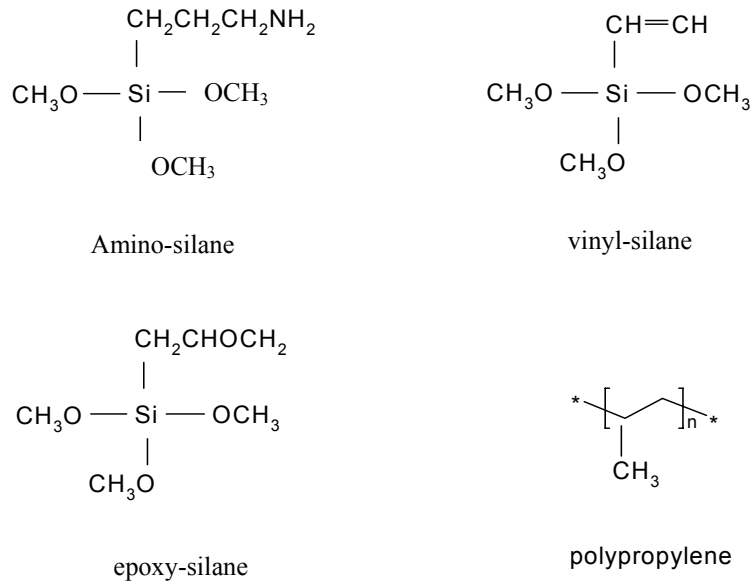


Figure 35: Chemical structure of polypropylene and silane coupling agents

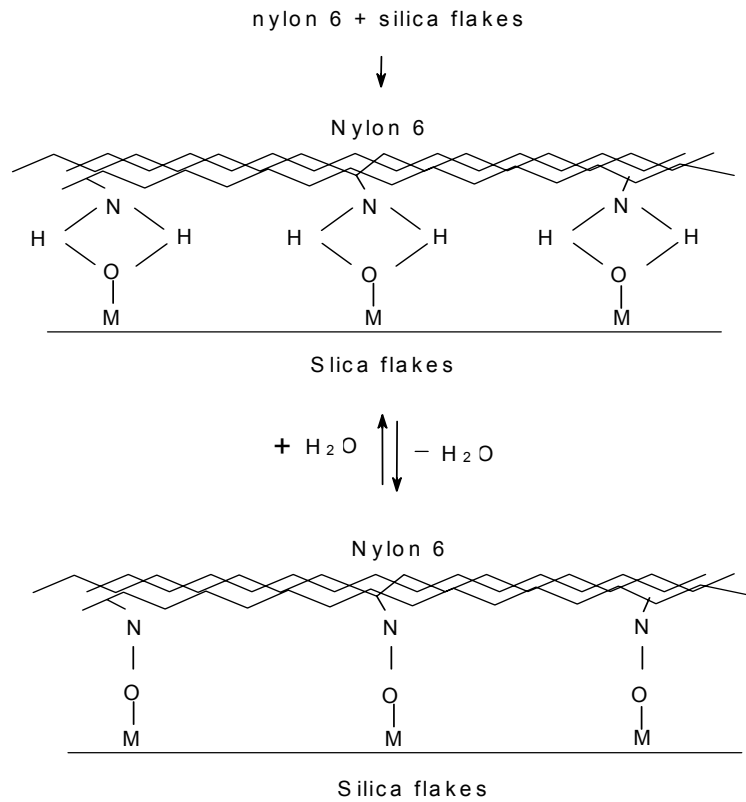


Figure 36: The possible mechanism of chemical bonding between silica flakes and N6

5.5 Rheology of glass flake polymer composites

Rheological properties are important to polymers and polymer composites in processing, mould design and so on. The analysis of the rheology of a polymer involves two types of flow, namely shear and extensional flow. For each flow, viscosity and elasticity can be characterised. Shear viscosity is defined by the ratio of shear stress to shear rate in Pascal seconds while elasticity is usually inferred from die-swell data. With a capillary rheometer, the flow of a molten composite through a capillary die exhibits shear behaviour. A strong extensional flow, however, occurs when the melt flows from the reservoir of a capillary rheometer. Thus, viscosity and elasticity of a flow type can be obtained.

The rheological properties of sub-micro composites were measured using a twin-bore extrusion capillary rheometer. Details of the measurements have been described in Section 3.10. In this section, shear viscosity and its dependence on shear rate are discussed. The effects of flake fraction, filler surface treatment and matrix type on the shear viscosity of sub-micro composites are also discussed in detail. Other rheological properties will be studied as part of future work. The results obtained are shown in Figures 37 to 39. The graphs clearly show that shear viscosity decreases with shear rate for all materials investigated. This can be explained by the different existing morphology of polymer molecules, at different shear rates. At a low shear rate, polymer molecules are entangled and inter-diffused resulting in limited mobility and a relatively high viscosity. With shear rate increases, molecules are stretched by shear force leading to the decrease in molecular entanglement. Understandably, under these conditions viscosity is reduced.

As shown in Figures 37 and 38, polypropylene silica flake composites and pristine polymer have the same shear viscosity over 150 s^{-1} shear rate. The only exception to this was the 30wt% flake reinforced composite which produced slightly higher viscosity than polypropylene. In contrast, apparent differences in shear viscosity were observed at the low shear rate range below 150 s^{-1} among composites with different flake fraction above 5wt%. It was found that non-modified 350nm silica flake polypropylene composites with 1 to 5wt% filler loading have the same shear viscosity. The shear viscosity of composites started to increase when loaded flakes were above 5wt%. The shear viscosities of 1 to 7wt% 350nm SF reinforced PP composites, however, are unusually lower than that of original PP. At 10wt%, composite viscosity reached that of PP while over 10wt% shear viscosity is slightly higher than that of PP.

Interestingly, of all the SF/PP composites studied this unusual low viscosity of composites was only observed with 350nm silica flakes without surface coating. The phenomenon did not occur with the clay nanocomposite, 850nm and vinyl-silane surface modified 350nm silica flake composites according to Figure 38. Neither do fibre composites demonstrate such rheological response. In general, the viscosities of fibre composites are higher than the base polymer and increase significantly with fibre fraction [68].

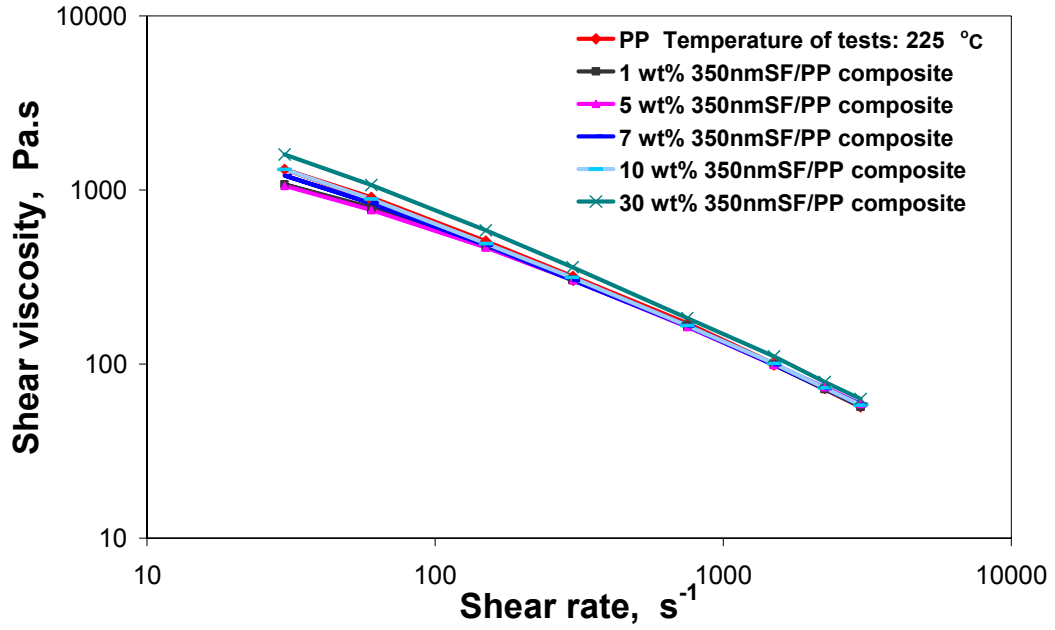


Figure 37: Shear viscosity and shear rate of 350nm SF/PP composites with different filler fractions

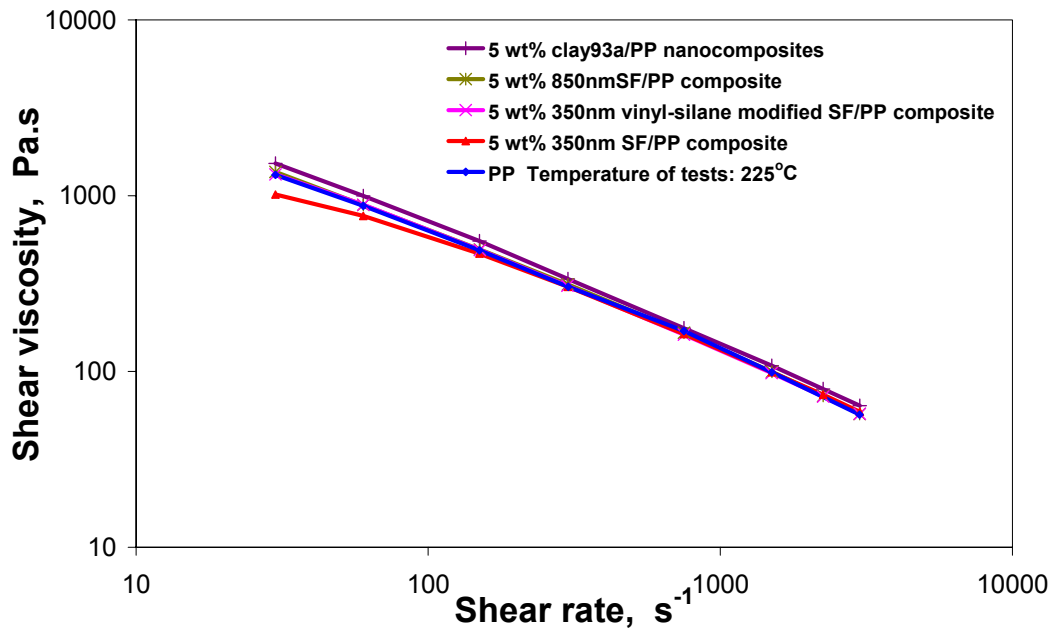


Figure 38: Effect of filler thickness and flake surface treatment on PP sub-micro composites

In order to explain this unique rheological phenomenon of sub-micro composites, a lubrication mechanism is proposed. 350nm silica flakes have smooth surfaces. In the case of weak bonding between flake surface and polymer molecules, the flakes and polymer slide passing each other when a shear force is applied. This slipperiness leads to an increase of molecular mobility. The shear viscosity of silica flake composites thus decreased.

As the increase in filler loading, the free space between flakes reduces. With shear rate increase, the collision probability of molecules increases. Resistance to the freedom of polymer molecules thus increases with the filler loading and shear rate. As a result of this, such sliding effects decrease with flake content increase and are only apparent at low shear rates, which is consistent with the results shown in Figure 37.

Improvements in flake and polymer bonding, through the use of surface modified flakes or a compatible matrix, will decrease the lubrication effect. This is the reason that 5wt% vinyl-silane modified 350nm SF/PP and Non-modified 350nm SF/N6 composites did not exhibit the slippery phenomena.

With sub-micro N6 composites, the addition of silica flakes led to increase in viscosity. According to Figure 39 increasing the flake content of SF composites, results in increased viscosity. This is simply because the more flakes a composite contains, the lower the molecular mobility a composite possesses. The shear viscosity of the 5wt% amino-silane treated 350nmSF/N6 composite, however, was observed to be lower than that of 5wt% non-treated 350nm flake/N6 composite, throughout the entire shear rate range. A possible reason for this is that thermal degradation of amino-silane occurred

during processing. The degradation weakened or damaged the interface bonding between the silica flakes and N6 molecules, resulting in the slippery effect. The damage of such interface bonds results in the reduced mechanical properties of composites. This corresponds to the decrease in tensile strength of the 30wt% 350nm amino-silane surface coated silica flake reinforced N6 composite when compared with its non-modified 350nm SF reinforced composite, as discussed in Section 5.4.3. Because slippery effect reflects the interface bonding of sub-micro silica flakes with polymer, it can be possibly applied to evaluate the interfacial bonding property and guide the design of sub-micro composites.

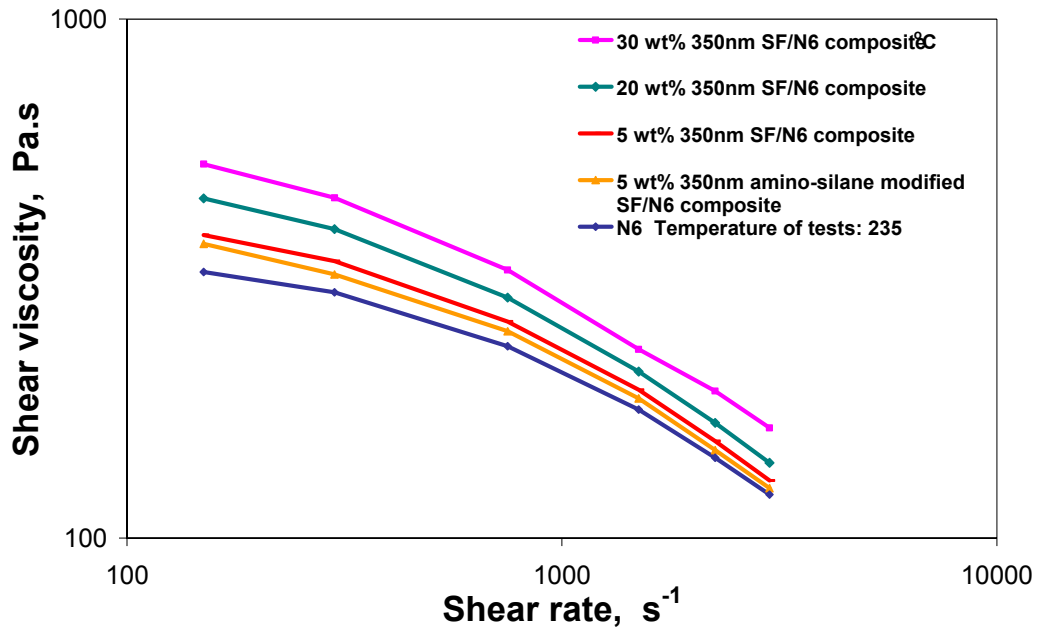


Figure 39: Effect of filler content and flake surface treatment on N6 sub-micro composites

5.6 Crystallisation behaviour of glass flake polymer composites

It is well known that the properties of a composite are determined by the properties of filler and matrix, filler fraction, filler aspect ratio and interface bond between filler and matrix. Furthermore, in the cases of crystalline/semicrystalline polymers used as matrices, the mechanical properties of composites are also depended on their crystallisation behaviour [156]. The crystallisation behaviour of sub-micro silica flake composites is therefore discussed in this section. The effects of flake fraction and surface treatment on crystallisation are studied. Investigations conducted include nucleation, crystal growth and crystal size as well as melting behaviour, crystallisation temperature, crystallinity and crystallisation rate. Nucleation, crystal growth and crystal size were evaluated using polar microscopy combined with hot-stage. Measurements of melting point, crystallisation temperature, crystallinity and crystallisation rate were carried out by means of DSC analysis. Micrographs of the crystallising processes of sub-micro SF/N6 composites are shown in Figures 40 and 41. Similarly, micrographs of the crystallising processes of sub-micro SF/PP composites are shown in Figures 42 and 43. The results of crystal size are listed in Table 12. Results obtained from DSC analysis of composites are summarised in Table 12. They include the crystallisation rate, crystallisation temperature, onset and end of crystallisation temperature. The melting point, onset and end of melting temperature of the composites studied are also listed in Table 12.

In accordance with Figure 40, the crystallisation process of N6 consists of nucleus formation, nucleus growth and the formation of polycrystal. In accordance with Table 12, the average diameter of N6 spherulites is 38.34 μm . The results in Table 12 show that the crystallisation temperature of N6 significantly increased to 188.6 – 192.6 $^{\circ}\text{C}$

from 176.2 °C after the addition of 350nm silica flakes. Correspondingly, Figure 40a shows the significant increments in nucleation rate of the silica flake/N6 composites with respects to pure N6. Such results provide clear evidence on nucleation effect of silica flakes in N6. The nucleation effect resulted in the total crystallisation rate of composites increasing to 3.27-4.25 mg/min from 1.86 mg/min of the N6 as shown in Table 12. The average crystal size of composites dramatically reduced to 17-22 μm in diameter according to Table 12. This is typical due to the increase of crystallisation rate resulting in smaller crystalline size.

When compared to the 5wt% 350nmSF/N6 composite, the further increase of filler content and surface treatment of flakes did not result in a considerable effect on the nucleation. The total crystallisation rate of composites, however, increased with filler content and slightly decreased after flake surface coating. Consequently, the crystal size of the 20wt% 350nm SF/N6 composite is, smaller than the 5wt% 350nmSF/N6 composite as shown in Table 12. The decrease in crystallisation rate caused by surface treatment, however, is not significant resulting in a similar crystal size of 5wt% surface treated 350nm SF/N6 composite to that of the 5wt% 350nmSF/N6 composite.

Due to the nucleation effect of silica flakes, the crystallisation temperature of SF/N6 composites increased by 12 to 16 °C compared to pure N6. Melting point, onset and the end of the melting temperature range, however, did not change significantly. The 350nm SF N6 composites showed a difference in their melting peak from the base polymer as shown in Figure 44. In general, all composites showed a small shoulder on the endothermal peak at approximate 220 °C, this was also observed in the clay N6 nanocomposites [190]. The most reasonable explanation for this is the formation of γ -

crystals in the N6. There are two types of N6 crystal, α and γ -form. The α -crystals are thermal dynamically stable while the γ -form represents a heterophase which is relatively unstable. The presence of silica flakes increased crystallisation temperature and crystallisation rate of the composites. High temperature crystallisation and high crystallisation rate induced less stable nucleation of γ -phase. Consequently, a small amount of γ -crystal was formed.

According to Table 12, the crystallisation temperature and onset crystallisation temperature of silica flake/PP composites increased by 2.3 - 5.4 °C and 3.5 - 7.2 °C respectively. This indicates the nucleation effect of silica flakes in polypropylene. According to Figure 42a, the addition of 5wt% 350nm silica flakes, however, did not cause apparent increase in the nucleation rate of polypropylene at the beginning of crystallisation. The total crystallisation rate of the composite only had a small increase to 2.83 mg/min from that of PP 2.42 mg/min. A probable reason of this is the poor compatibility of flakes with the matrix suppressed the nucleation effect at the beginning of crystallisation. The 5wt% 350nmSF reinforced PP composite thus has similar crystal size to that of neat PP. The average diameter of the 5wt% 350nmSF/PP composite and neat PP is 64.06 and 71.33 μm respectively as shown in Table 12.

Both increases in flake fraction and improvement in compatibility can initiate the nucleation effect at the beginning of crystallisation. Therefore, the nucleation rate of 20wt% and 5wt% 350nm vinyl-silane modified SF/PP composites significantly increased when compared with that of the N6 and 5wt% 350nmSF/PP composite as shown Figure 42a. The total crystallisation rate of 20wt% and 5wt% 350nm vinyl-silane

modified SF/PP composites considerably increased to 3.69 and 3.63 mg/min, respectively and their crystal size in turn dramatically decreased to 32 - 35 μm .

In accordance with Table 12, the crystallinity of SF reinforced N6 and PP composites were similar or lower than the pristine polymers. This was caused by the increase of crystallisation end temperature. Crystallising at a higher temperature led to less crystal formation from the molten polymer. This can be evidenced by the data of crystallinity and $T_{c,end}$ listed in Table 12. The higher $T_{c,end}$ a composite has, the lower crystallinity it possesses.

In general, an increase in crystallinity improves the elastic modulus and strength of a polymer. The crystallinity in 350nm silica flake/N6 and PP composites is either similar or lower than the pure polymers. Therefore, the tensile modulus and strength improvements, which have been achieved in 350nm silica flakes reinforced N6 and PP composites, are primarily due to the filler contributions.

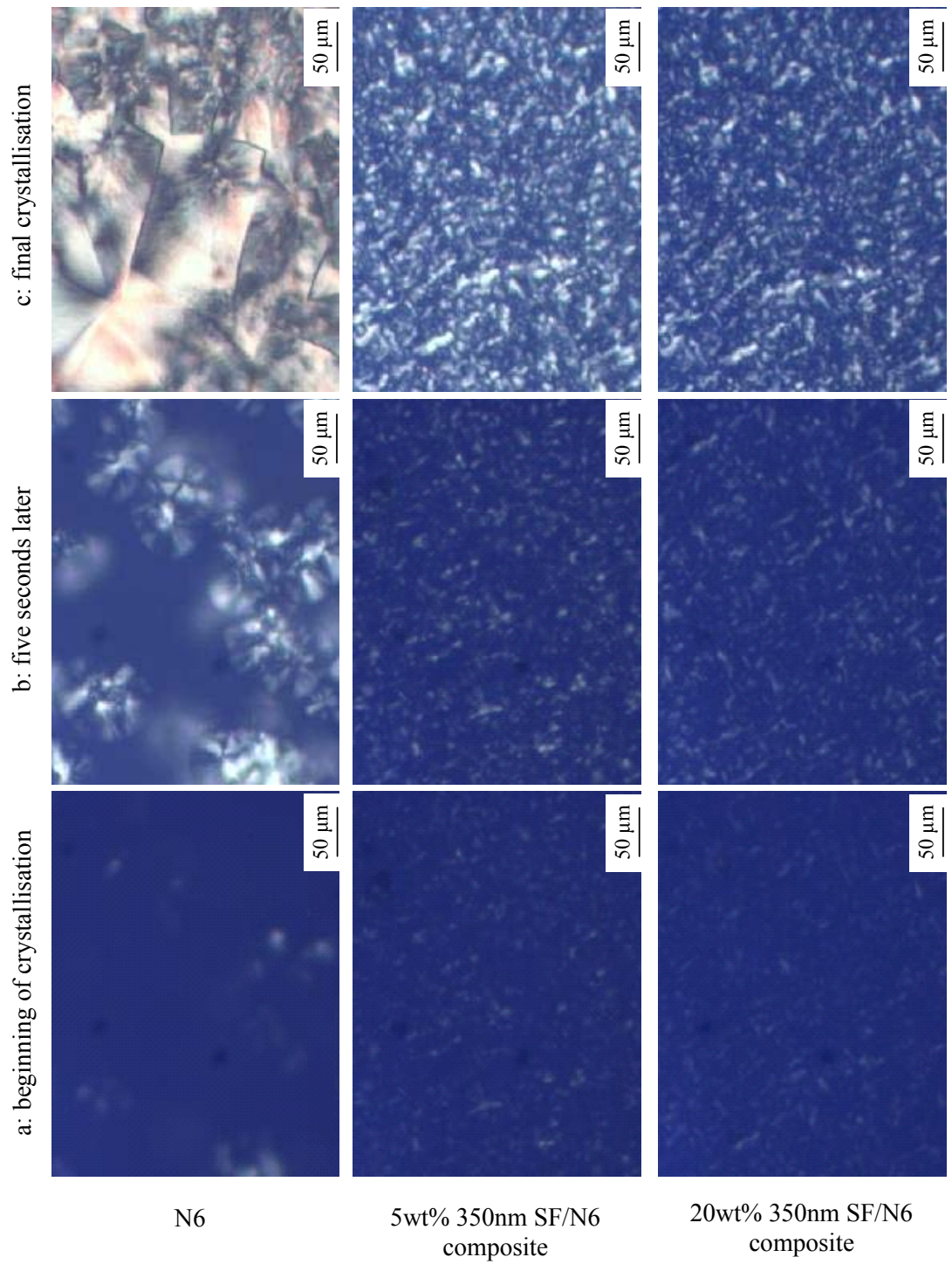


Figure 40: The effect of flake fraction on sub-micro SF/N6 composite crystallisation

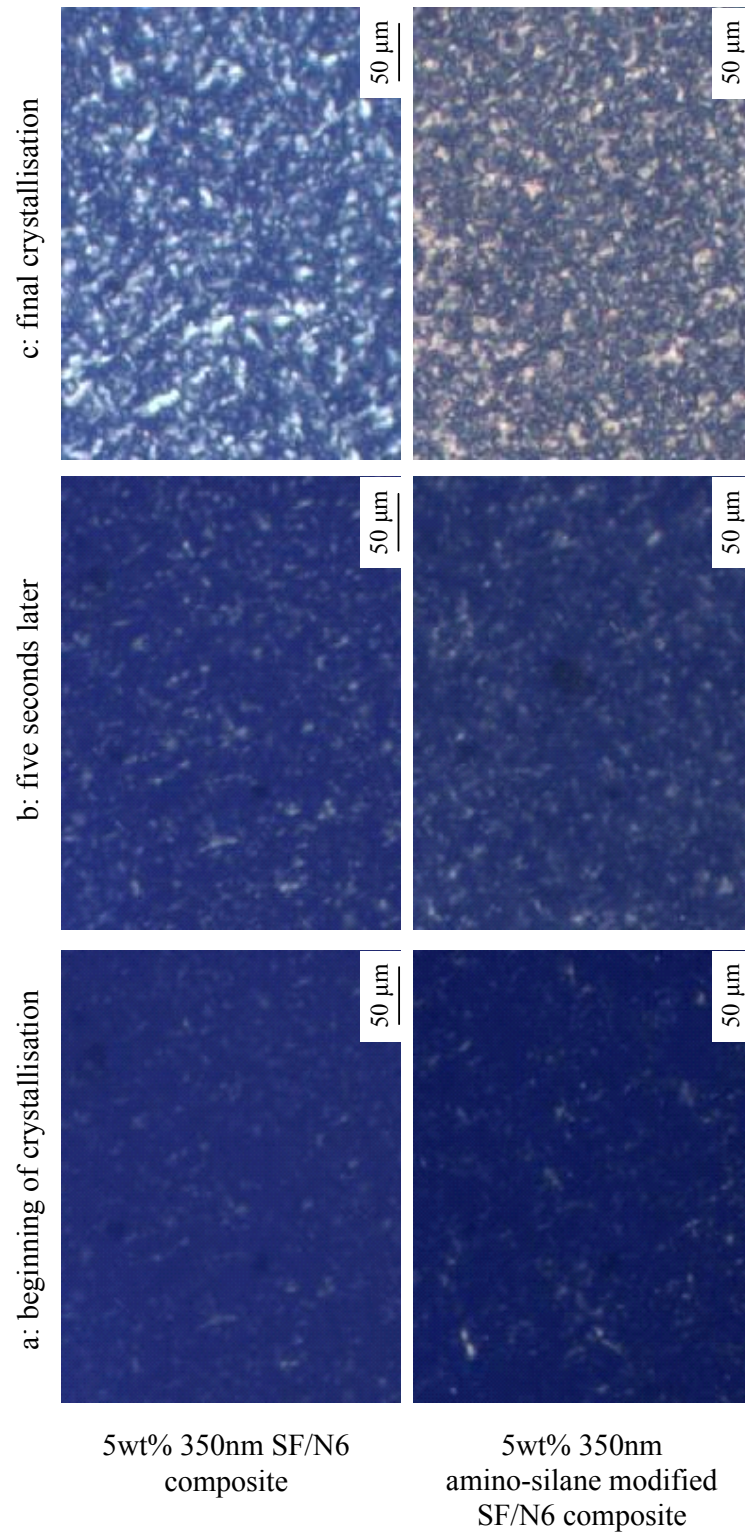


Figure 41: The effects of flake surface treatment and thickness on sub-micro SF/N6 composite crystallisation

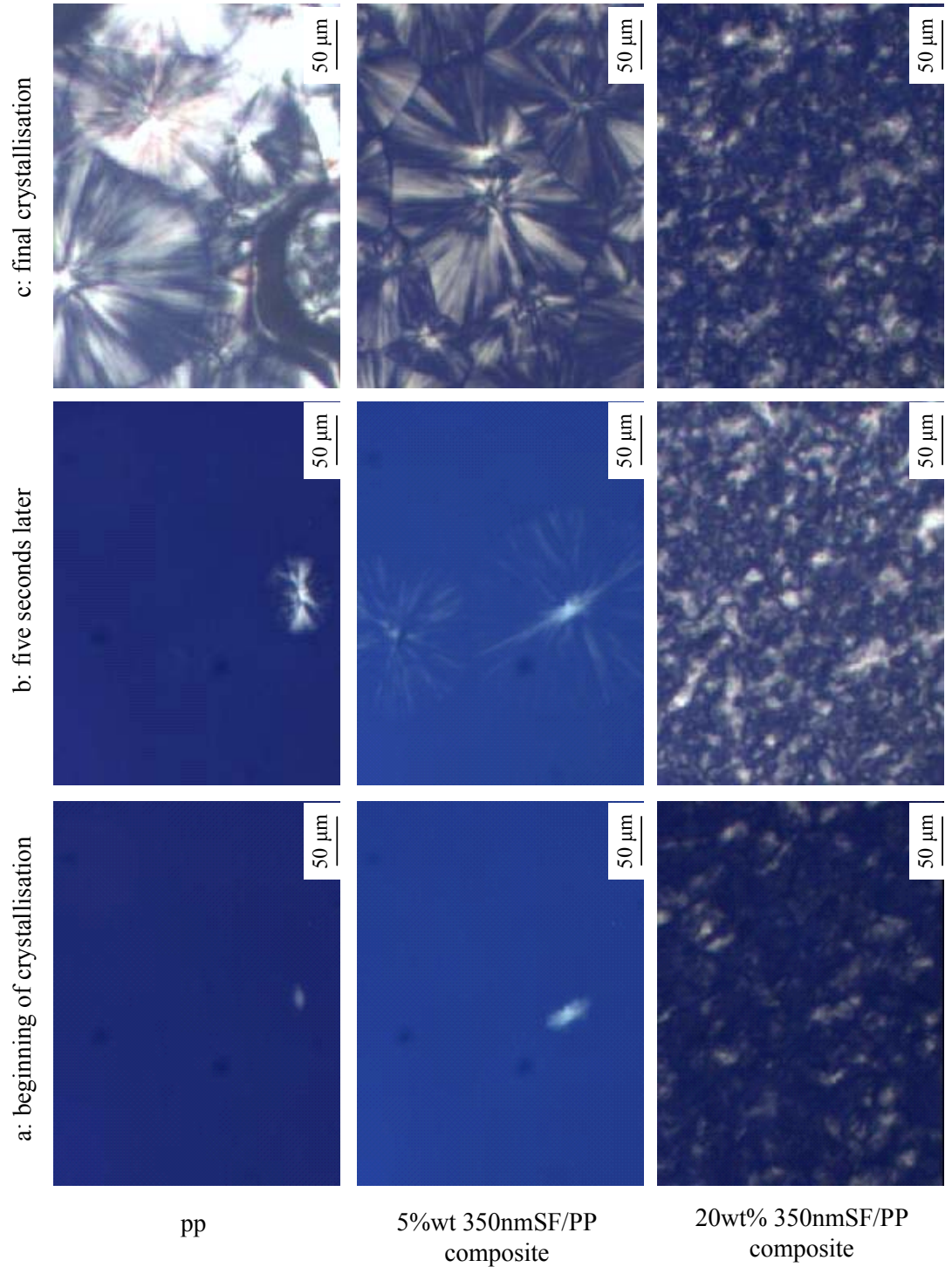


Figure 42: The effect of flake fraction on sub-micro SF/PP composite crystallisation

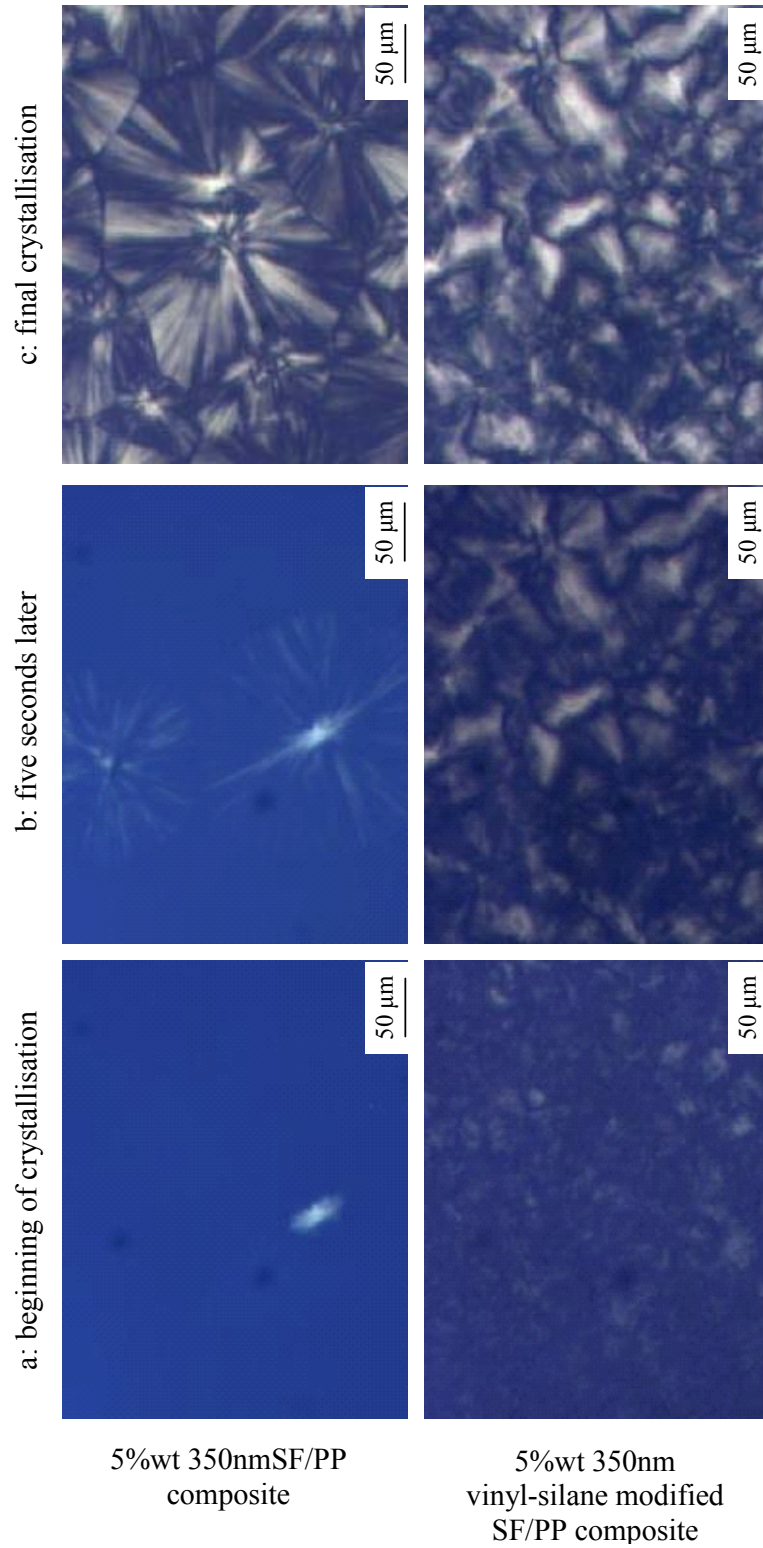


Figure 43: The effects of flake surface treatment and thickness on sub-micro SF/PP composite crystallisation

Table 11: Crystal diameters in sub-micro silica reinforced N6 and PP composites

	N6	5wt% 350nm SF/N6	20wt% 350nm SF/N6	5wt% amino-silane modified 350nm SF/N6
Average diameter of crystals μm	38.34	20.93	17.1	21.64
	PP	5wt% 350nm SF/PP	20wt% 350nm SF/PP	5wt% amino-silane 350nm SF/PP
Average diameter of crystals μm	71.33	64.06	32.87	34.9

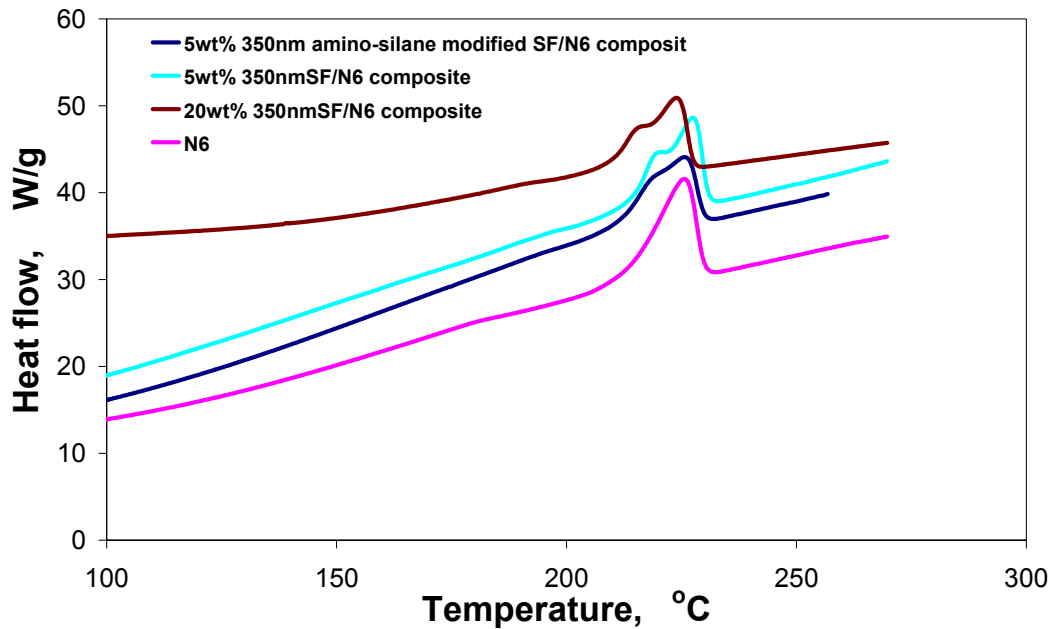
**Figure 44: DSC melt curves of 350nm silica flake/N6 composites**

Table 12: Summary results DSC analysis of sub-micro SF composites

	Crystalline temperature $T_c, ^\circ\text{C}$	$T_{c,onset}$ $^\circ\text{C}$	$T_{c,end}$ $^\circ\text{C}$	Melt point $T_m, ^\circ\text{C}$	$T_{m,onset}$ $^\circ\text{C}$	$T_{m,end}$ $^\circ\text{C}$	Crystallinity x%	Crystallisation rate v, mg/min
N6	176.2	186.4	168.8	225.4	212.6	229.9	23.94	1.86
5wt% 350nm SF/N6	192.4	195.6	188.9	227.4	215.6	230.7	17.86	3.88
20wt% 350nm SF/N6	188.6	192.0	184.6	224.8	211.7	227.5	23.9	4.27
5wt% 350nm amino-silane modified SF/N6	192.63	195.6	187.9	225.7	212.9	229.8	21.0	3.25
PP	115.89	120.2	112.0	166.3	160.6	171.8	33.9	2.42
5wt% 350nm SF/PP	121.3	125.4	113.9	167.6	159.8	173.5	33.3	2.83
20wt% 350nm SF/PP	119.6	123.7	115.9	166.9	158.9	171.7	30.6	3.69
5wt% 350nm vinyl-silane modified SF/PP	118.17	127.4	114.0	168.1	159.3	173.0	29.5	3.63

5.7 Impact fracture and dynamic thermal mechanical analysis of sub-mico silica flake composites

In addition to tensile modulus and strength, the impact fracture and dynamic thermal mechanical analysis of silica flake/N6 composites were also carried out to evaluate the fracture toughness and thermal mechanical properties of sub-micro composites. The detailed results are discussed in following sub-sections.

5.7.1 Impact fracture of sub-micro silica flake/N6 composite

The fracture toughness of sub-micro SF/N6 composites was assessed using the critical stress intensity (K_c). K_c was measured in accordance with the method described in Section 3.6.2. As a general rule, the bigger the value of K_c the tougher a composite is. 350nm and 850nm flake reinforced N6 composites were tested in order to investigate the effect of flake thickness on the impact property of sub-micro composites. The results obtained are shown in Figure 45. It was found that K_c of 5wt% 350nm and 850nm silica flakes reinforced N6 increased by 17.2 and 19% respectively, when compared with the pure polymer. With the composites studied, flake thicknesses did not show apparent effect on fracture toughness. An investigation into 100nm and 2 μ m flake reinforced N6 should be carried out as part of future work.

The impact toughness improvement of composites is substantially contributed by interfacial frictional sliding between filler and matrix during the fracture. In general, the toughness is greater when fillers have a larger aspect ratio and diameter [5]. The 350nm flakes are thinner but have a larger aspect ratio than the 850nm flakes. As a consequence, their 5wt% SF/N6 composites exhibited the similar improvement in

fracture toughness. Moreover, the reduction in crystal size of the N6 due to addition of silica flakes also has a positive effect on the toughness of sub-micro SF/N6 composites.

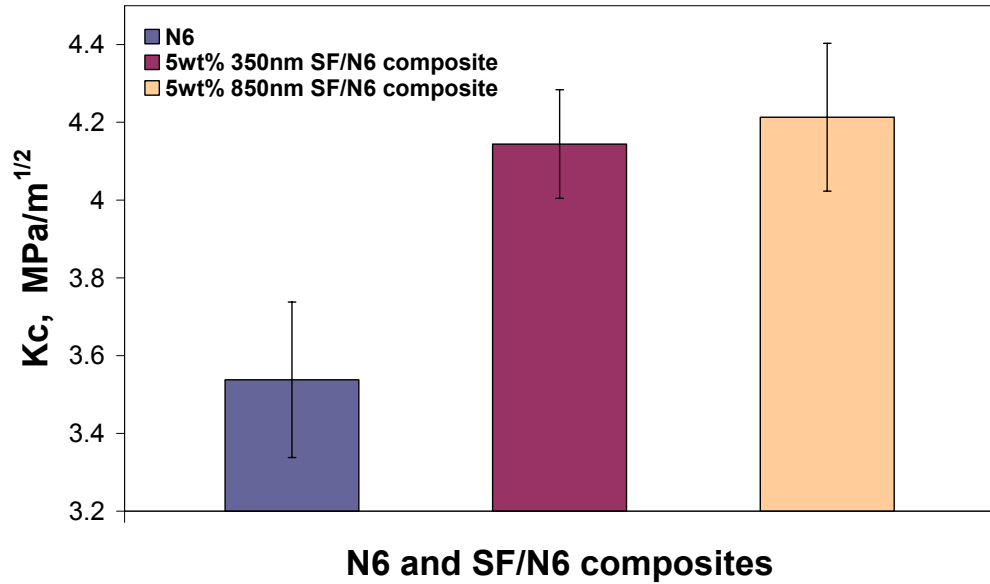


Figure 45: impact fracture toughness of N6, 350nmSF/N6 and 850nmSF/N6 composites

5.7.2 The dynamic thermal mechanical properties of glass flakes composites

Dynamic thermal mechanical analysis is a technique used to investigate the viscoelastic properties of a material including complex modulus, storage/elastic modulus (E'), loss/viscous modulus and loss tangent ($\tan\delta$). Using the plot of E' versus temperature, the change of storage modulus with temperature can be evaluated. Using the plot of $\tan\delta$ versus temperature, the glass transition temperature (T_g) can be obtained. These properties are important factors in plastic engineering applications in high temperature environments.

In this section, modulus-change with temperature, glass transition temperature based on loss tangent and Heat Deflection Temperature (HDT) of sub-micro silica flake reinforced N6 are investigated. Results obtained are shown in Figure 46, Figure 47 and Table 13 respectively.

Figure 46 shows that the elastic modulus of all materials was steady in the range of -10°C to room temperature. They exhibited a consistent tendency with their tensile modulus at room temperature i.e., the storage modulus of SF composites is always higher than that of the pristine polymer and increases with filler fraction but decreases with flake thicknesses. Within the temperature range from 23 to 50°C , the modulus of N6 and SF composites rapidly decreased with temperature increases. The modulus of the SF composites, however, remained 20 to 40% higher than N6. Within the range 50 to 125°C , the modulus of materials became steady and only a slightly decline occurs. In this temperature range, the modulus of 10wt% 350nmSF composite was higher than 5wt% 350 and 850nmSF composite while the modulus of 5wt% 850nmSF was higher than that of 5wt% 350nmSF composites. It is indicated that in the post-transition temperature range, the loading-bearing capability of sub-micro SF/N6 composites increases with flake loading and thickness. At 120°C , the storage modulus remained at 656 MPa for 10wt% 350nmSF composite, 544 MPa for 5wt% 350nmSF composite and 585MPa for 850nm SF composites. These values are 62%, 34% and 44% higher than non-filler N6 respectively.

Figure 47 shows that the addition of flakes had little influence on the glass transition temperature of N6. The glass transition temperature of 5wt% and 10wt% 350nm SF reinforced N6 was observed to be 45.54 and 46.5°C respectively both of which are

similar to the N6 transition temperature 45.9 °C. The glass transition temperature of 5wt% 850nm SF/N6 was 50.3 °C and 4.4 °C higher than $T_{g, N6}$.

According to Table 13, the heat deflection temperature of sub-micro SF/N6 composites increased with flake fraction. Flake thickness did not make apparent difference in HDT of the composites. With 10wt% 350nm silica flake reinforced composite, the HDT (at 1.82 Mpa stress) increased by 20.3 °C from 45.99 °C of pristine polymer, which is an improvement of 44%.

According to the literature [26] and [28], with 6wt% filler content the HDT of clay/N6 nanocomposites at 1.82 MPa stress can be improved by 125-154% with respect to the neat polymer. This improvement is much higher than that of silica flake sub-micro composites achieved. One possible explanation is that the interaction of nanoclays with polymer molecules is higher than that of sub-micro silica flakes due to the large surface area of the nanoclays. Interfacial interaction of sub-micro silica flakes with polymer can be improved by means of surface treatment using compatibilisers which would give sub-micro silica composites further improvements in thermal dynamic properties. It could be difficult, however, to reach the level that clay nanocomposites have achieved due to the smaller surface area of sub-micro fillers. Further investigation is considered as part of future work.

Table 13: Thermal deflection temperature of sub-micro SF/N6 composites

	N 6	5 wt% 350nmSF/N6	10wt% 350nmSF/N6	5 wt% 850nmSF/N6
Heat Deflection Temperature at 1.82MPa, °C	45.99	54.6	66.3	54.17

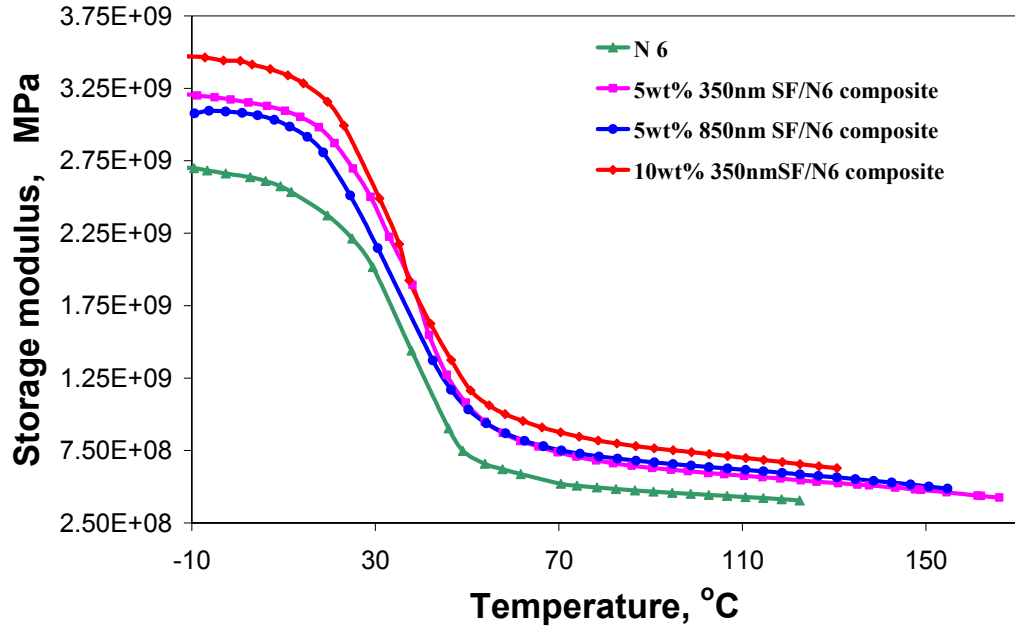


Figure 46: Storage modulus & temperature of sub-micro SF/N6 composites

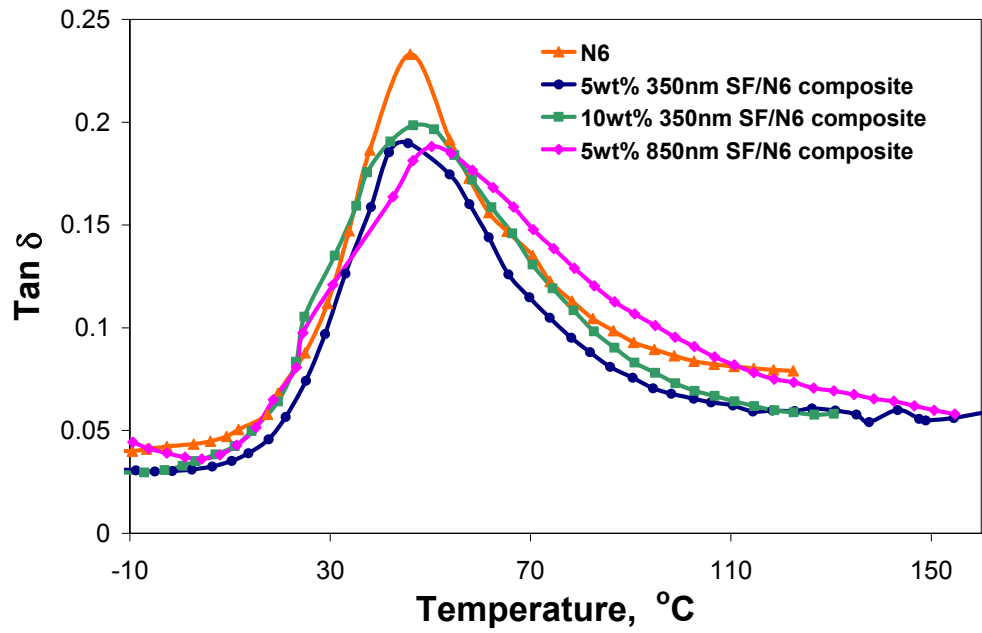


Figure 47: Tan δ & temperature of sub-micro SF/N6 composites

Part II: The enhancement with multi-layered sub-micro fillers

In this research, two different structures of expanded graphite were investigated. One is layer interlinked structure. Another is individual sheet structure. Considering the effect of dispersion level and filler orientation on the mechanical properties of composites, the individual sheet structure was studied for mechanical reinforcement purpose. The relationship between filler exfoliation and mechanical properties of the composite was explored. The layer interlinked structure has potential to form an effective conductive graphite network in the composites. It thus was used to enhance electrical conductivity for polypropylene.

5.8 Developing multi-layered sub-micro fillers

Expanded graphite (EG) was prepared from expandable graphite. Expandable graphite is the graphite flakes intercalated by various chemicals at defects along the edges of the graphite layers [138], [191]-[194]. Thus, they are also known as intercalated graphite. When an intercalated graphite is exposed to high temperatures, its layers are forced to separate due to rapid vaporisation of the intercalants. Direct heat treatment by flame or furnace heating is traditionally used for expanding expandable graphite [192]. In this study, a microwave irradiation method was explored as a new approach in the preparation of expanded graphite. Three out of the four expandable graphite grades used were commercial products provided by the Branwell Graphite Ltd with trade names ES350, ES120 and ES100 respectively. The remaining expandable graphite named IG230 was synthesised in our own laboratory via acid treatment using nitric and sulphuric acids according to reference [193]. Extent of the graphite expansion was assessed by expansion volume. Expansion volume is defined as the increase in volume of one gram expandable graphite after expansion with unit ml/g [194]. For each type of

expandable graphite, the optimum conditions of expansion were determined by identifying the highest expansion volume achieved.

The microwave irradiation of expandable graphite was carried out in a microwave oven with heating time between 10 and 60 seconds. The relationship between expansion volume and expansion time is shown in Figure 48.

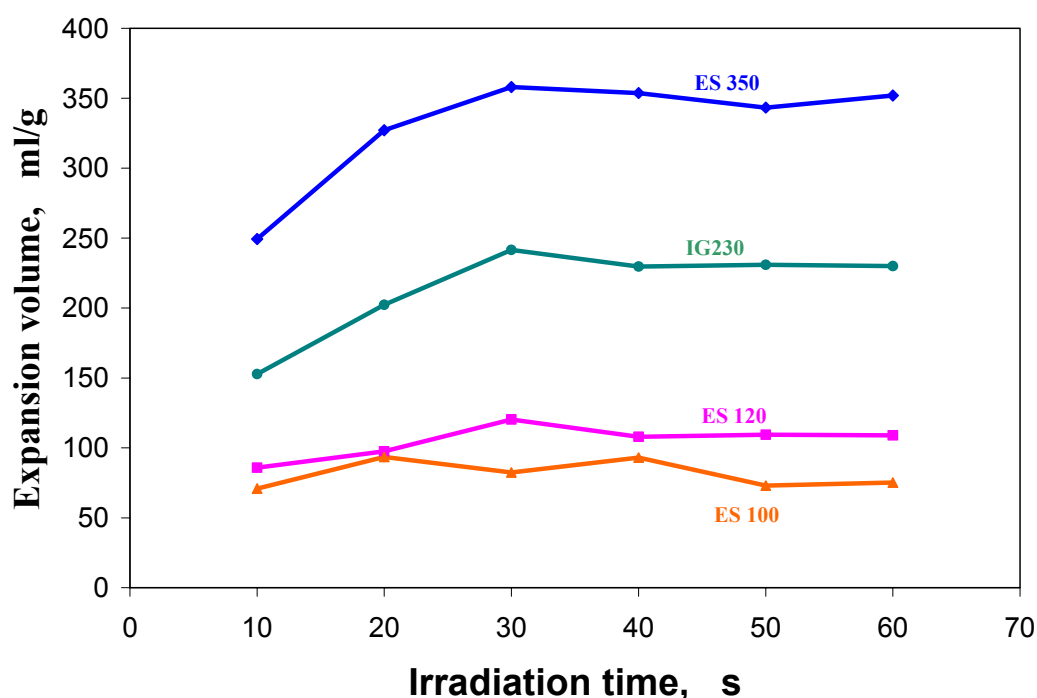


Figure 48: The relationship between expansion volume of expandable graphite and microwave irradiation time

Figure 48 shows that the expansion volume increased with expansion time of up to 30 seconds for ES350, IG230 and ES120 and up to 20 seconds for ES100. After that no further expansion occurred. The commercial expandable graphite ES350 had the highest expansion volume of 358 ml/g, which is one third higher than IG230 and almost three

times higher than ES120 and ES100. This may be associated with the different particle thickness of the expandable graphites. Thicker flakes tend to result in higher expansion volume. As shown in Figure 49, ES350 has the thickest and ES100 has the smallest thickness amongst the expandable graphites used. The dependence of expansion volume on particle thickness was then investigated and show in Figure 50. According to the figure, the expansion volume has a good linear relationship with the thickness of

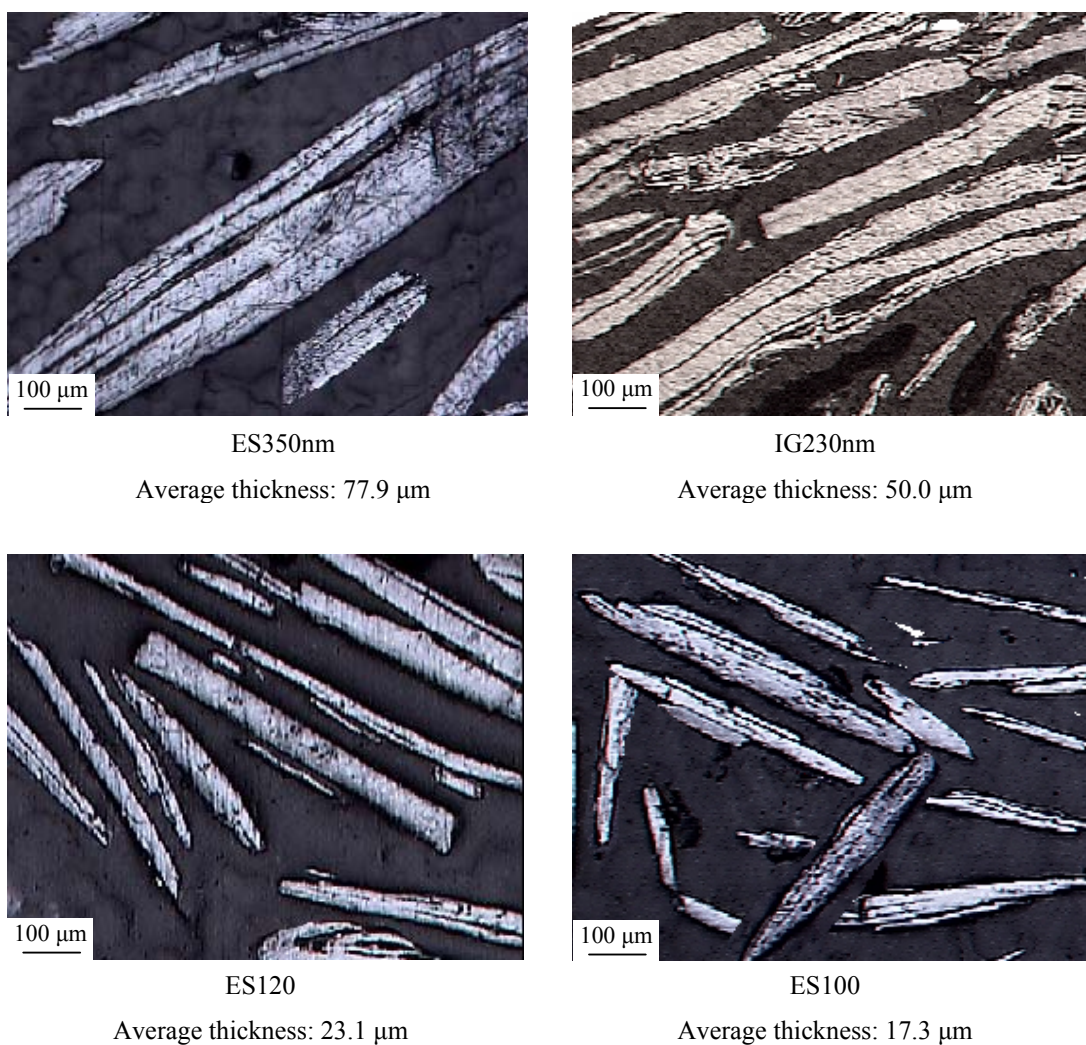


Figure 49: Micrograph of the cross-section of the expandable graphites under optical microscopy

expandable graphite. The regression results in an equation: $y = 4.3706x + 19.434$ with an R^2 of 0.9996. The equation can be used to quantify the relationship between expansion volume and particle thickness of the expandable graphite products studied. The possible reason for the formation of such linear relationship is associated with the number of natural defects possessed by graphite flakes. In general, defects are distributed at random along the edges of flakes. The number of defects, however, proportionally increases with the particle thickness of expandable graphite resulting in a correlation between quantity of intercalant in expandable graphite and graphite flake thickness. Consequently, a linear relationship between expansion volume and particle thickness of expandable graphite occurs.

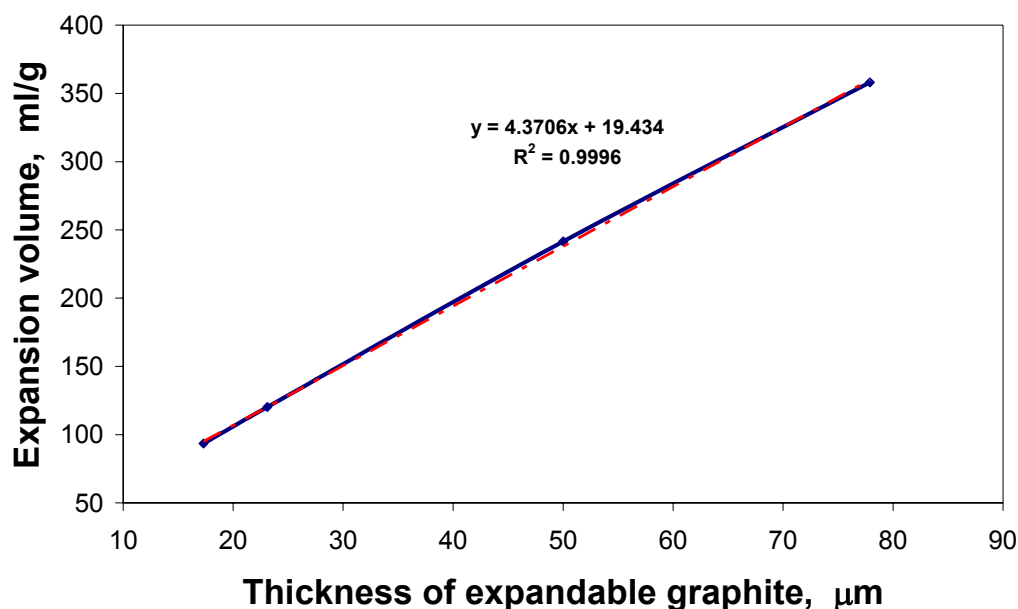


Figure 50: Dependence of expansion rate on particle thickness of expandable graphite

The micro-structures of graphite before and after expansion are shown in Figure 51. After expansion, graphite flakes change into a porous structure with layer thicknesses

approximately 50 to 150 nm. When comparing expanded ES350 with expanded ES100, where the former achieved the highest expansion volume and the latter had the lowest, there are not noticeable differences in the layer length and thickness between two products.

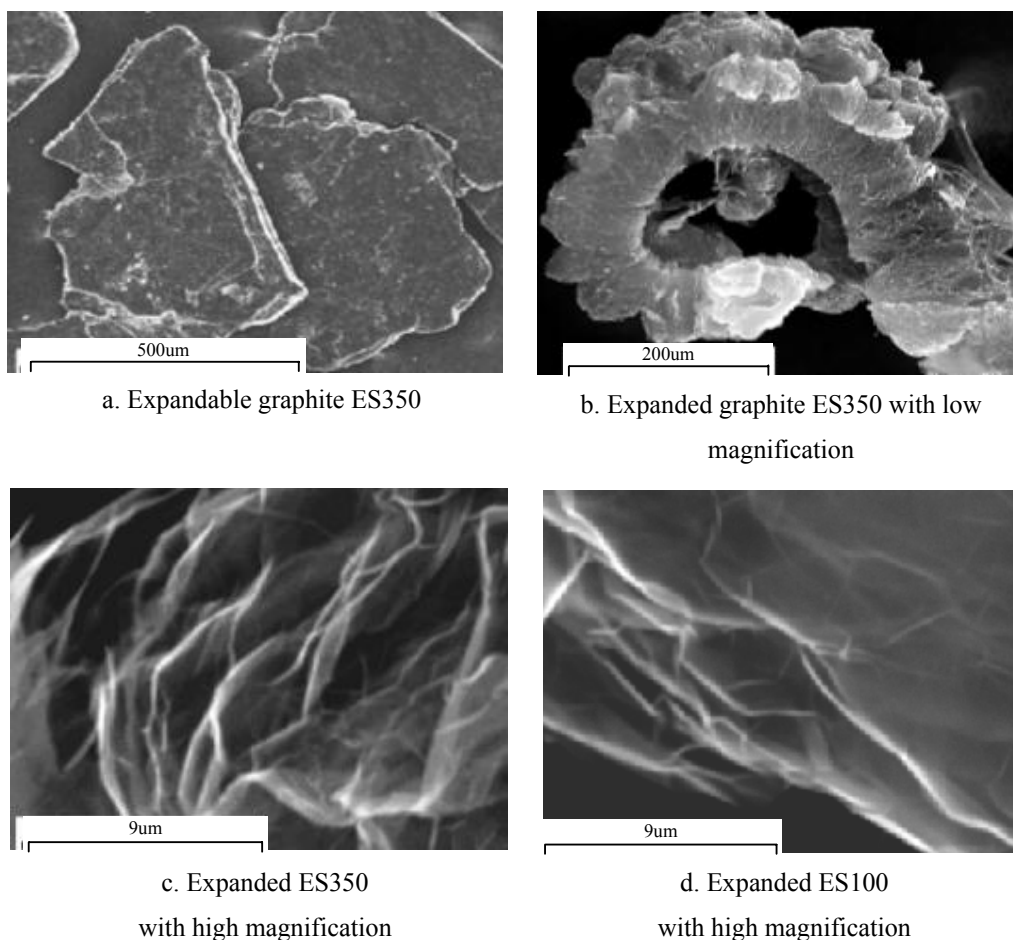


Figure 51: SEM morphology of graphite before and after expansion

Moreover, as show in Table 14, expanded ES350 and ES100 have a similar specific surface area. The apparent volume of expanded ES350, however, is much higher than that of expanded ES350. Such high volume has caused high volume ratio of expanded

graphite to base polymer resulting in high viscosity flow during the preparation of expanded ES350 polymer composites. As a consequence, Expanded ES100 was chosen as a sub-micro multi-layered reinforcement throughout this research.

Table 14: BET specific surface area of graphite before and after expansion

	ES350	ES100
Specific surface area before expansion cm^2/g	0.58	2.93
Specific surface area after expansion cm^2/g	27.9	30.6
Apparent volume after expansion cm^3/g	326	95.6

5.9 The dispersion of expanded graphite and the mechanical properties of sub-micro graphite PP composites

The porous structure of expanded graphite allows polymer molecules to enter its layer galleries to form expanded graphite polymer composites. However, similar to other layer-structured fillers such as clays, expanded graphite has dispersion problem. The expanded layers tend to agglomerate rather than further exfoliation during melt blending process. It is well known that for multi-layered reinforcements, the extent of layer dispersion within a composite is a crucial factor for the reinforcement of mechanical property. The dispersion of expanded graphite in polymer and the effect of dispersion structure on tensile modulus and strength of sub-micro composites are therefore investigated in subsequent sections.

5.9.1 The dispersion of expanded graphite in polymers

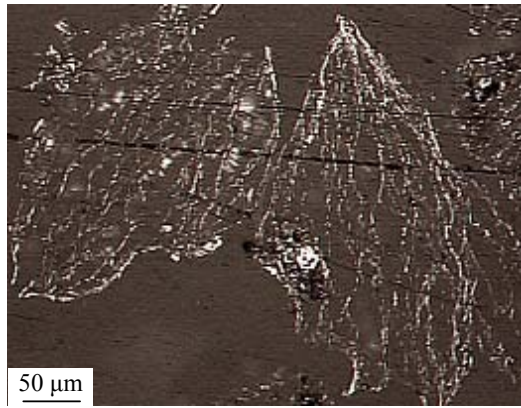
Different from clay/polymer nanocomposites, the extent of graphite dispersion cannot be investigated using X-ray diffraction technique because the crystal structure of graphite does not change during the graphite expansion and layer exfoliation process. Optical microscopic analysis was therefore applied to study the dispersion of multi-layered sub-micro filler within their polymer composites.

The structures of expanded graphite in low viscosity cyanoacrylate resin and polypropylene were investigated and are discussed in this section. A room temperature curing processing was used for cyanoacrylate resin while both the solution method and the melt blending were employed for polypropylene composites. Details of these methods are described in Section 3.5. The morphology of graphite structures under these conditions is shown in Figure 52. As can be seen, expanded graphite exists in the layered interlinked structure in cyanoacrylate resin and the polypropylene-compatible xylene solution. This is primarily due to the low viscosity of the resin and solution which allows them to flow into the pores of the expanded graphite. Once the pores of the graphite are occupied, the expanded layers cannot be compressed by applied external forces such as stirring. As a consequence, the expanded structure of the graphite remains after curing. The situation is different in melt blending, in which the expanded layers of the graphite have been compressed back to their original unexpanded state. This may be associated with extensive collision in the feeding zone of the extruder where polymer pellets have not been molten. These pellets squeezed the expanded graphite resulting in expanded gap closure. In order to overcome this problem and to enable the melt blending method to be suitable for the development of sub-micro graphite composites, a method with two-feeder combined with multi-extrusion was

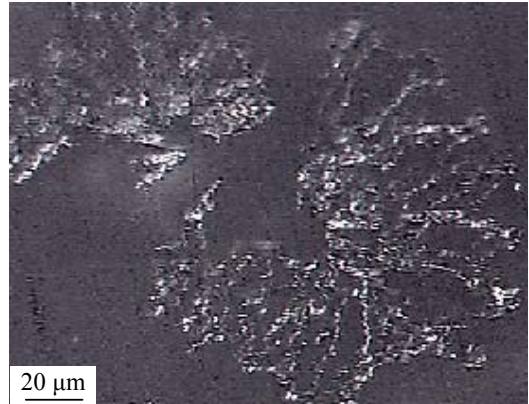
designed. The principle of this method is that polymer is fed first and expanded graphite is fed later via a second feeder where the pellets have been molten. Thus extensive collision of pellets with the graphite can be avoided, allowing the molten polymer to flow into the pores of the expanded graphite. The resulting morphology in Figure 53a shows that expanded layered-structure of the sub-micro graphite remains whereas the layers are not well dispersed. By applying high shear stress generated during multi-extrusion, well dispersed and orientated individual graphite sheets in polypropylene composites were obtained as shown in Figure 53b.

Multiple-extrusion may cause polymer degradation so that an alternative method has been developed. In this method, sub-micro graphite sheets were produced by breaking the interlinked structure of expanded graphite using sonication. Expanded graphite was sonicated in an ultrasonic bath containing water. The sonication time required to separate layers of expanded graphite into individual sheets is shown in Table 15. From the results obtained it is clear that the sonication time needed to break the honeycombs of expanded graphite into individual sheets increases with the amount of sonicated graphite. Sonicating one gram of expanded graphite required a total of 6 hours whereas five grams took 18 hours. Sonication is therefore not practical for the large scale production of sub-micro graphite.

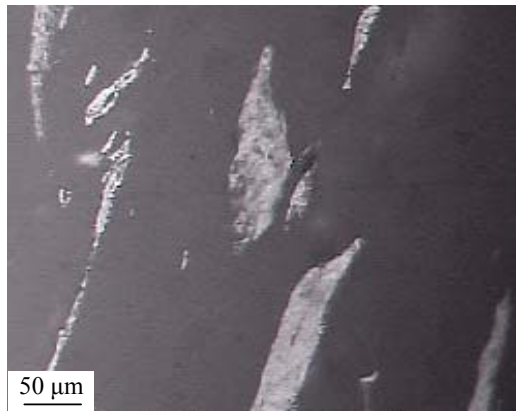
Figure 54 shows the morphology of sonicated graphite and multi-extruded graphite obtained by burning the melt blending processed EG/PP composite following six cycles of extrusion. The individual sheets obtained from two methods demonstrate similar thickness and length.



a Structure of expanded graphite in cyanoacrylate resin



b Structure of expanded graphite in PP-compatibiliser-xylene solution



c Dispersion structure of expanded graphite in PP via melt blending

Figure 52: Structures of expanded graphite in cyanoacrylate and PP under different processing methods

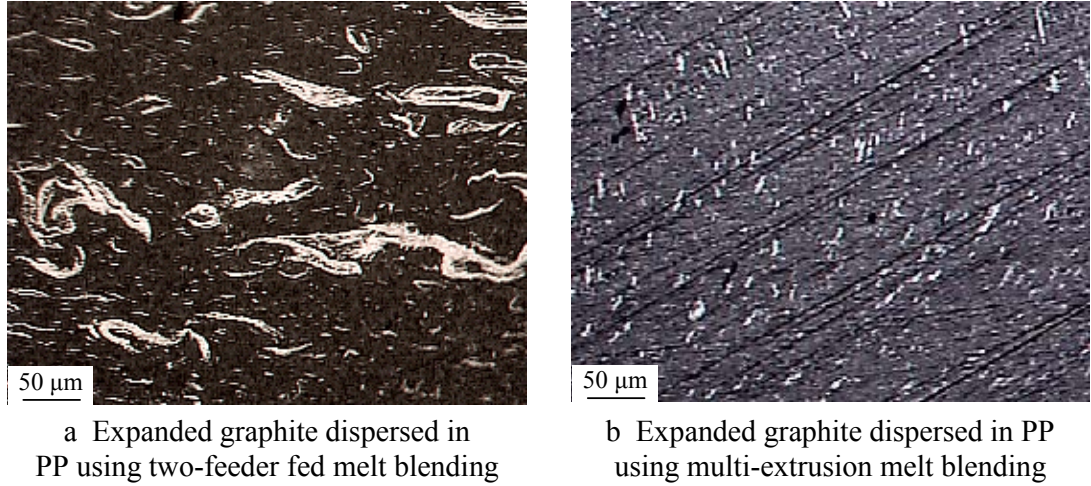


Figure 53: The optical microscopic morphology of expanded graphite dispersions in PP under the two-feeder fed and multi-extrusion methods

Table 15: The sonication time for separating the layers of expanded graphite into individual sheets

Amount of graphite g	1	5
Sonication time hrs	6	18

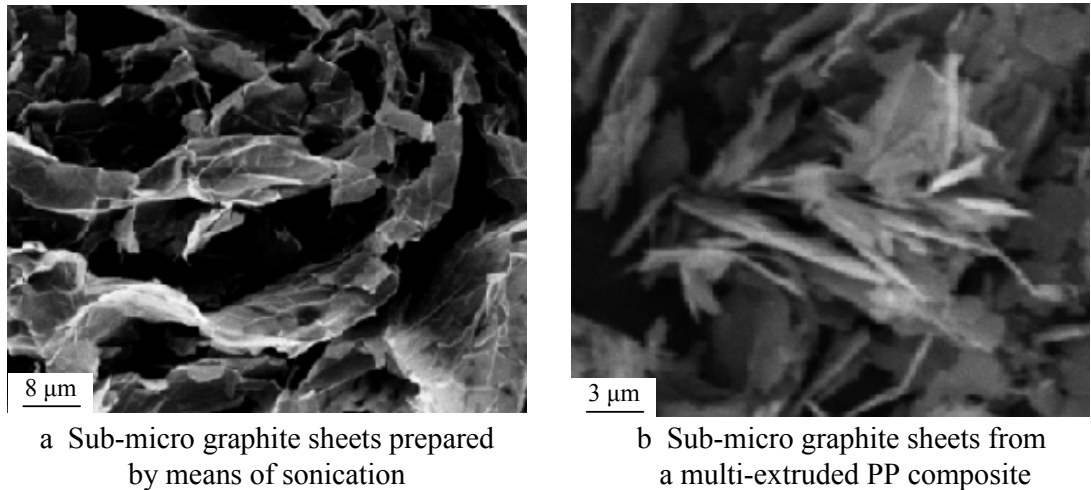


Figure 54: Individual graphite sheets produced via the sonication and multi-extrusion

5.9.2 The mechanical properties of sub-micro graphite reinforced polypropylene composites

The mechanical properties of sub-micro graphite reinforced polypropylene depend on the structure of graphite in the composites and the extent of filler dispersion. As discussed before, with the traditional extrusion method, the expanded layers of EG are essentially agglomerated. With two-feeder multi-extrusion methods, the interlinked structure in the expanded graphite worms remains in PP composites in the first cycle extrusion. The graphite worms are chopped down during further extrusion cycles. After six extrusion cycles for 5wt% reinforcement and ten cycles for 20wt% reinforcement, the interlinked structure of expanded graphite is broken down to a satisfactory level similar to what is obtained using the sonication method. The tensile modulus and strength of EG/PP composites with different reinforcement structures are given in Table 16. In order to rule out the effects of multi-extrusion on pure PP, the tensile strength and modulus of PP after the 6th and 10th extrusion were also studied.

According to the results obtained, multi-extrusion does not affect the tensile strength of polypropylene but slightly reduces PP tensile modulus. When comparing the EG/PP composite produced using the traditional melt processing method with the pristine polymer, at 5wt% filler fraction, the tensile modulus of the composite is improved by 6.4% but tensile strength decreases by 6.8% from 30.9 to 28.8 MPa. The interlinked structure of expanded graphite neither enhances nor degrades the tensile modulus and strength of polypropylene. Due to poor disperse of expended graphite at high filler loading, the tensile strength of one-cycle extruded 20wt% EG/PP composite is worse than that of the corresponding 5wt% EG/PP composite. However, when interlinked layers were exfoliated into individual sub-micro sheets, the tensile modulus and strength

of expanded graphite PP composites significantly increases. The degree of improvement increases with the number of extrusion cycle. At 5wt% expanded graphite content, tensile modulus increased by 23.5% and 31.4% while tensile strength rose by 6.7% and 10% after six and ten cycles of extrusion, respectively, compared with the data obtained from one cycle extruded composite. With 20wt% expanded graphite content, after six and ten cycles, the tensile modulus increased by 33% and 45.2% while tensile strength increased by 9.4% and 21.82% respectively, compared to the one-cycle extruded composite.

The improvement in tensile modulus and strength of graphite/PP sub-micro composites is also a function of the filler loading. When comparing the ten-cycle extruded composites with the pristine polypropylene, at 5wt% filler fraction, the tensile modulus and strength of EG/PP composites increased by 28.8% from 1.56 to 2.01 GPa and 8.3% from 30.9 to 33.48 MPa. At 20wt% graphite content, tensile modulus increased to 3.31 GPa and is improved by 112.2% while tensile strength raised to 34.39 MPa and is improved by 11.3%.

These results are a clear indication that the improvements in tensile modulus and strength of multi-extruded EG/PP composites are caused by the changes in expanded graphite structure within the composites. When expanded graphite exists as a layer-aggregated structure and layer-interlinked structure in composites, the weak interaction between graphite layers can be detrimental to the mechanical properties of composites. After interlinked layers are exfoliated into individual graphite sheets, the layers are connected by polymer molecules resulting in a relatively stronger interaction than graphite layers alone. Due to the incompatibility of graphite with polypropylene, the

degree of improvement in tensile strength is not significant. Tensile modulus, however, improved by 112.2% at 20wt% graphite fraction, when compared to the pure polypropylene.

Table 17 shows the degree of tensile modulus and strength improvement of the 20wt% 350nm vinyl-silane treated silica flake/PP composite and 20wt% EG/PP composite with 10-cycle multi-extrusion. When comparing with the silica flake/PP composites, the individual graphite sheet/PP composites demonstrated better improvement in both modulus and strength. This may be associated with the better mechanical properties that graphite sheets possess.

Table 16: Tensile modulus and strength of sub-micro graphite/PP composites

	PP	5wt% EG/PP one-feeder fed after 1 st extru.	5wt% EG/PP two-feeder fed after 1 st extru.	20wt% EG/PP two-feeder fed after 1 st extru.
Tensile strength MPa	30.9 ± 0.94	28.8 ± 0.67	30.43 ± 0.3	28.23 ± 0.43
Tensile modulus GPa	1.56 ± 0.35	1.66 ± 0.1	1.53 ± 0.07	2.28 ± 0.25
	PP after 6 th extru.		5wt% EG/PP two-feeder fed after 6 th extru	20wt% EG/PP two-feeder fed after 6 th extru.
Tensile strength MPa	30.62 ± 0.24	–	32.46 ± 0.68	30.87 ± 0.31
Tensile modulus GPa	1.48 ± 0.15	–	1.89 ± 0.13	3.04 ± 0.19
	PP after 10 th extru.		5wt% EG/PP two-feeder fed after 10 th extru	20wt% EG/PP two-feeder fed after 10 th extru.
Tensile strength MPa	30.76 ± 0.17	–	33.48 ± 0.10	34.39 ± 0.28
Tensile modulus GPa	1.43 ± 0.21	–	2.01 ± 0.13	3.31 ± 0.11

Table 17: A comparison of the mechanical property improvement between 20wt% single and multi-layered sub-micro filler reinforced polypropylene

	20wt% 350nm vinyl-silane modified silica flake/PP composite	20wt% EG/PP composite two-feeder fed 10-cycle multi-extrusion.
The improvement in tensile strength, σ/σ_m	0.97	1.11
The improvement in tensile modulus E/E_m	1.61	2.12

5.10 The rheology and crystallisation behaviour of sub-micro graphite composites

5.10.1 Rheology of sub-micro graphite polypropylene composites

The dependence of rheology behaviour of sub-micro graphite composites on the structure and exfoliation level of graphite in polypropylene are investigated in this section. The EG/PP composites containing an interlinked structure of the expanded graphite were obtained from one-cycle extrusion. Exfoliated graphite PP composites, in which the structure of graphite in PP is individual sheets, were produced via the multi-extrusion method. The shear viscosities of these composites under different shear rates are shown in Figures 55 and 56. Similarly to 350nm silica flakes polypropylene composites, the lubrication effect was demonstrated by exfoliated graphite PP composites. For 5wt% EG/PP composite after the 6th extrusion cycle and 20wt% EG/PP composite after the 10th extrusion cycle, the shear viscosities are lower than that of polypropylene at any shear rates tested. The shear viscosities of the first and the 10th cycle extruded PP are almost exactly the same as the pure polypropylene. It can thus be

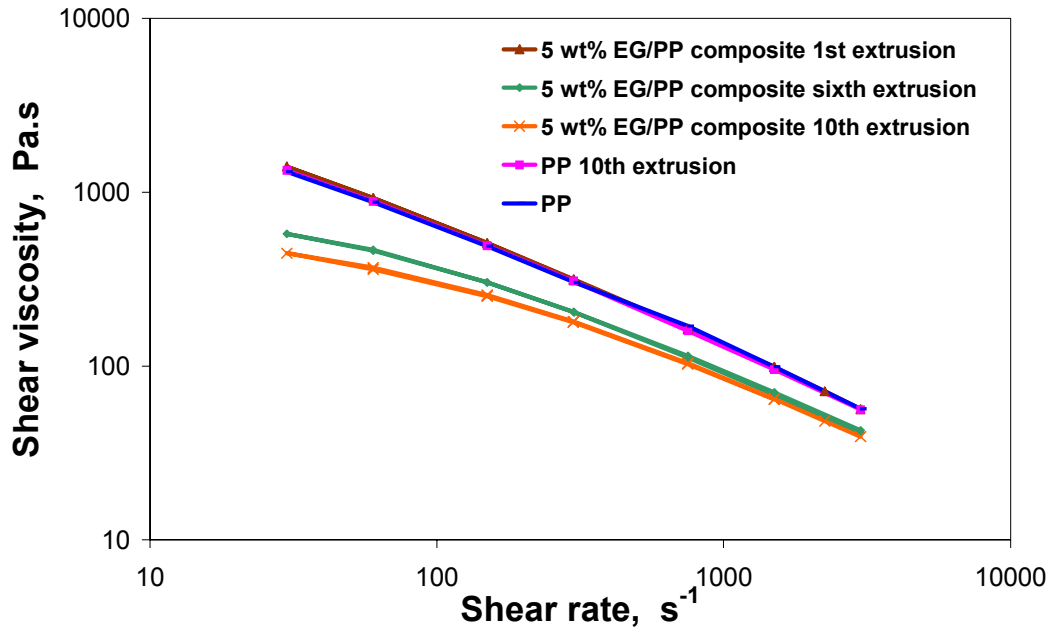


Figure 55: The dependence of shear viscosity of sub-micro graphite PP composites on the shear rate and structure of reinforcements

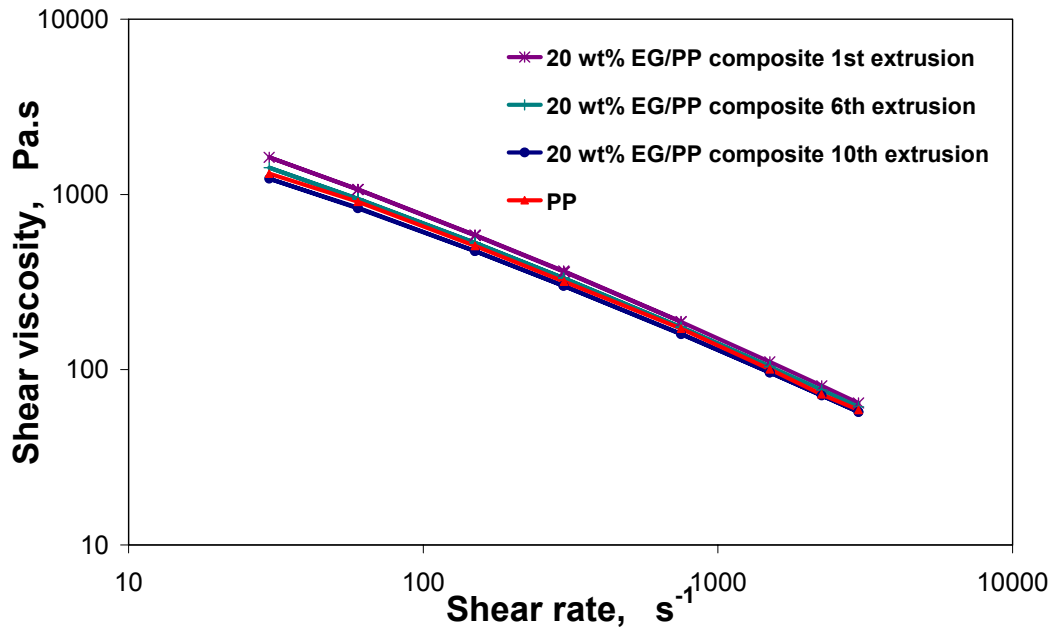


Figure 56: The dependence of shear viscosity on the shear rate of 20wt% sub-micro graphite PP composites

concluded that these low viscosities are caused by the slipperiness of exfoliated graphite rather than the degradation of polypropylene. Significantly, viscosities of the 10th cycle products are lower than that from the 6th cycle. This is a clear indication that the more extrusion cycles an EG/PP composite has, the higher the exfoliation level of sub-micro graphite can be achieved and the thinner the sub-micro graphite sheets produced are, as shown in Table 18.

Table 18: the dimensions of expended and exfoliated graphite

	Original expanded graphite	6 th cycle extruded graphite	10 th cycle extruded graphite
Thickness, nm	50 - 150	274-570	280 - 360
Length, μm	5 - 18	5 - 15	5 - 15

Throughout testing the lubrication effect, observed with sub-micro composites, did not occur with the EG/PP composites containing interlinked structure. The shear viscosity of these composites are either similar or slight higher than that of polypropylene.

In general, the shear viscosities of sub-micro graphite composites decreases with the increases in shear rate, the reason for this being the improved molecular mobility associated with higher shear rates. Shear viscosities did, however, increase with filler content. This is because molecular moving space is reduced with filler fraction increases. In addition, the shear viscosity of sub-micro graphite composites significantly decreases with multi-extrusion cycles. This is caused by the change of graphite structure in the PP. When the inter-linked structure is broken, the molecular mobility in the system rapidly increases leading to a decrease in viscosity. When graphite is exfoliated into individual sheets, the slippery effect appears resulting in a lower shear viscosity than the pure PP.

5.10.2 Crystallisation of sub-micro graphite composites

The crystallisation of sub-micro graphite polypropylene composites is studied in this section. The materials studied are the same as those used for the rheology investigation. The results obtained from differential scanning calorimeter tests are summarised in Table 19. When comparing polypropylene with multi-extruded polypropylene, the results show that multi-extrusion has little influence in the crystallisation behaviour of PP under 10 extrusion cycles. After 10 cycles of multi-extrusion, the melt temperature and onset melt temperature drop by 1.8 °C and 3.6 °C from 166.3 °C and 160.6 °C respectively, with respect to PP. This indicates that minor thermal degradation of polypropylene has occurred around the 10th extrusion cycle. For this reason, 10 cycles was determined as the maximum number of extrusions allowed for the preparation of sub-micro graphite PP composites.

Table 19 also shows that the addition of 5wt% expanded graphite results in an increase in crystallisation temperature, onset and end of crystallisation temperature of polypropylene of approximate 9 °C respectively. Melting temperature, onset and end of melt temperature also increased by 5 °C respectively. Apart from the 10-cycle extruded EG/PP composite, all crystallisation and melt temperatures increased with filler contents and multiple extrusion cycles. This result implies that sub-micro graphite has a nucleation effect on polypropylene. The nucleation effect is enhanced by the increase of fraction and exfoliation of sub-micro graphite. For EG/PP composites extruded for 10 cycles, onset-melt temperatures are lower than their 6-cycle extruded counterparts which confirmed the minor degradation of PP in the 10th extrusion cycle.

When compared with PP, the crystallinity of sub-micro graphite composites slightly decreased. Multi-extrusion does not have apparent influence on crystallinity of polypropylene and its sub-micro graphite composites. Based on this, the mechanical property improvement of individual graphite sheet/PP composites is contributed by filler other than crystallisation of the polymers.

Table 19: Summary of DSC results of sub-micro graphite polypropylene composites

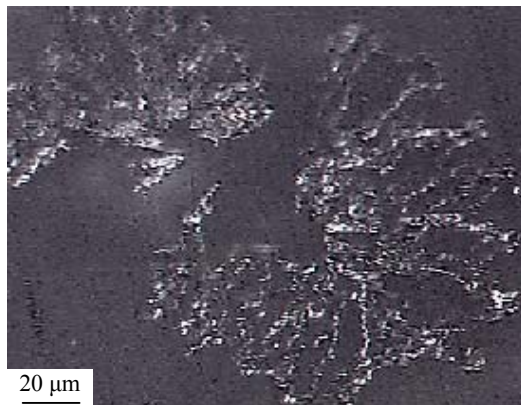
	Crystallisation temperature T_c , °C	$T_{c,onset}$ °C	$T_{c,end}$ °C	Melt point T_m °C	$T_{m,onset}$ °C	$T_{m,end}$ °C	Crystallinity x%
PP	115.9	120.2	112.0	166.3	160.8	171.5	33.9
PP 6 th extrusion	115.2	119.9	110.4	166.2	160.6	171.8	33.3
PP 10 th extrusion	115.8	120.2	112.3	164.6	157	170.9	33.7
5wt% EG/PP composite 1 st extrusion.	125.3	129.9	121.5	169.2	163.8	173.0	30.78
5wt% EG/PP composite 6 th extrusion.	130.3	135.1	126.2	167.0	162.0	173.8	30.21
5wt% EG/PP composite 10 th extrusion.	131.6	136.9	126.6	171.6	155.3	175.8	30.79
20wt% EG/PP composite 1 st extrusion.	132.7	137.6	120.3	173.2	163.8	176.5	31.2
20wt% EG/PP composite 10 th extrusion	134.6	139.8	129.8	170.8	155.9	175.2	30.7

5.11 Conductive sub-micro graphite composites

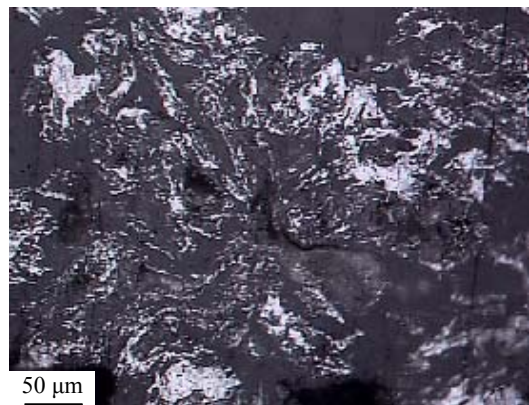
According to the literature, a number of researchers have reported on the electrical conductivity of expanded graphite polymer composites [134]-[148]. The effects of expanded structure and interfacial properties on the conductivity of expanded graphite composites, however, have not been well understood. In this research, the dependences of electrical conductivity of EG/PP composites on graphite structure in PP and the interfacial compatibility of PP with EG are explored. Three sets of expanded graphite polypropylene composites were synthesised. Amongst them two groups were synthesised using a solution method while the others were prepared using the two-feeder extrusion melt blending method as described in Section 3.5. With one group of solution synthesised composites, 5wt% maleic anhydride-grafted-PP (E43) was added as a compatiliser to improve compatibility between PP and graphite. By using different synthesis methods, different structures of expanded graphite in PP were achieved. Micrographs of these structures are shown in Figure 57. The conductivities of the composites were measured using the method described in Section 3.11 while results are shown in Figures 58 and 59.

From the results obtained, it is clear that the structure of expanded graphite in PP has a significant effect on the conductivity of composites. With the inter-linked structure of expanded graphite in PP, both composites synthesised via the solution method achieved higher conductivity and lower percolation threshold than the composite produced using the two-feeder extrusion method. With the E43/EG/PP composites, conductivity achieved 10^{-4} and 1.3×10^{-3} S/cm at 5wt% and 20 wt% filler content respectively. With solution synthesised EG/PP composites, conductivity reached 1.42×10^{-8} , 3.9×10^{-6} and 8.91×10^{-6} S/cm at 5wt%, 10wt% and 20wt% graphite content respectively. The

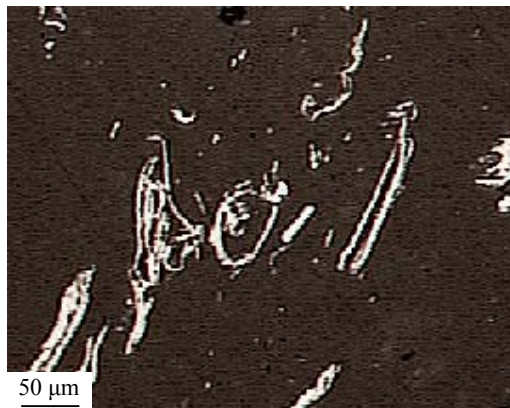
extruded EG/PP composite at 20wt% EG fraction, in contrast, exhibited an electrical conductivity of 5.79×10^{-9} S/cm which is static dissipative rather than conductive. The E43/EG/PP composite had a lowest critical percolation value of 0.8wt%. This is followed by the solution synthesised EG/PP composites which possess a percolation threshold of 4.2wt% and the EG/PP composites produced by two-feeder extrusion had percolation threshold of 14wt%. This is because the higher the dispersion density of expanded graphite, the lower a percolation value can be achieved. According to Figure 55, the graphites in E43/EG/PP and solution synthesised E43/PP composites have much higher dispersion density than the ones in extruded E43/PP composites. Furthermore, when comparing Figure 55 a and b, layer agglomeration along the edge of expanded graphite worms is observed with the solution synthesised EG/PP composite. Such agglomeration, however, does not occur in the E43/EG/PP composite. A possible reason for this is that the addition of E43 improved the compatibility of graphite with polypropylene. Consequently, the interfacial contact between PP and expanded graphite layers is enhanced and the agglomeration of expanded graphite in the polymer is decreased. This leads to a better conductive network within composites and hence the highest conductivity was achieved amongst E43/EG/PP composites. According to the results, volume conductivity of E43 is 6.24×10^{-14} S/cm which is slight higher than that of the PP, 10^{-16} S/cm. The improvement in conductivity of the E43/EG/PP composites, when compared with solution synthesised EG/PP composites, is therefore a result of the improved conductive network rather than the conductivity of E43.



a Structure of expanded graphite in 5wt% E43 + 5wt% EG/PP composite synthesised via solution method



b Structure of expanded graphite in 5wt% EG/PP composite synthesised via the solution method



c Expanded graphite dispersion structure in two-feeder fed extruded 5wt% EG polypropylene composite

Figure 57: The structure of expanded graphite in PP composites synthesised via the solution method with and without compatiliser as well as the two-feeder extrusion

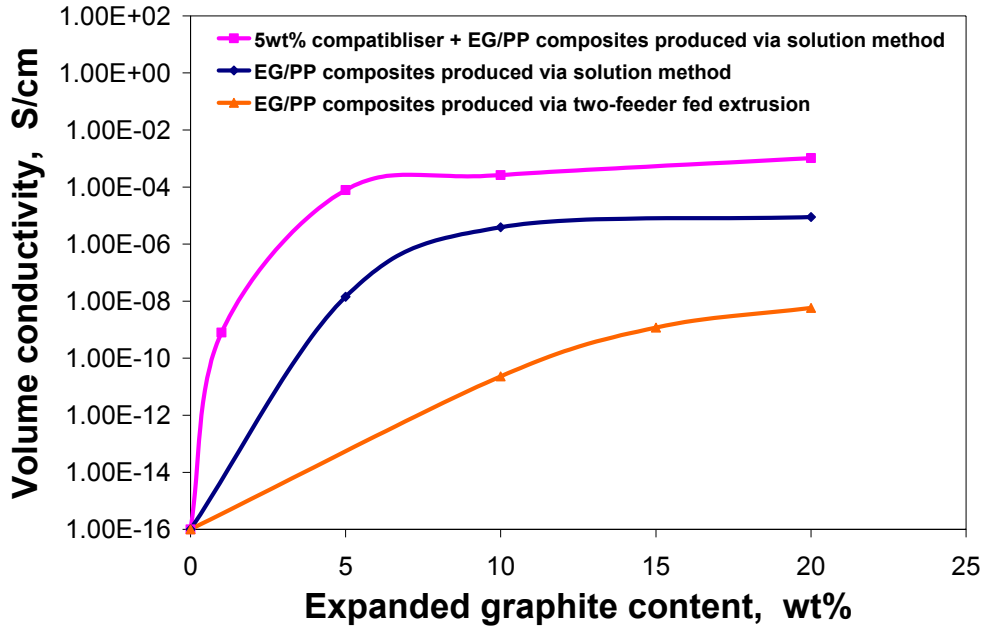


Figure 58: The conductivity dependence of sub-micro graphite enhanced PP on structures and content of the fillers

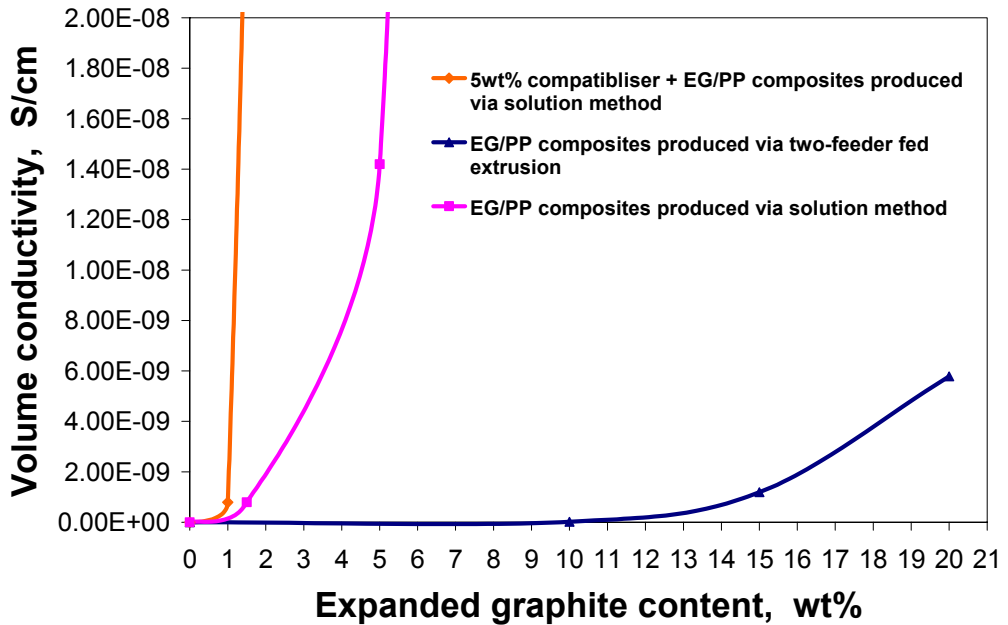


Figure 59: The critical percolation threshold of different structural sub-micro graphite/PP composites

6 Conclusions

In this study, sub-micro polymer composites have been developed based on silica flakes with thickness 350nm and graphite sheets with thickness 280-360nm. The potential and problems encountered in sub-micro composite reinforcement have been investigated.

Single-layer structured silica flakes and multi-layered graphite flakes were selected as sub-micro reinforcing fillers since they are in sub-micro region, strong in layered directions and have high aspect ratios, which are preferred properties for mechanical reinforcement. The potential of sub-micro fillers was explored based on the model filler composites, i.e., single-layered silica flakes reinforced nylon-6 sub-micro composites. The predicted Young's modulus and strengths of the composites are as high as 3.3 GPa and 81 MPa at 5wt% flake content as well as 11.75 GPa and 301MPa at 30wt% filler fraction, respectively. Experimental results show similar improvements to the predictions in filler loading below 5wt% but far lower than the calculated values in higher filler content. It is found that this low efficiency of reinforcement at high filler contents was caused by the breakage of silica flakes during extrusion resulting in significant reduction of the aspect ratio of silica flakes. The mean aspect ratio before extrusion is 475. The mean flake aspect ratio in 30wt% SF/N6 composite, however, is only 12.

Even for composites with broken flakes, the tensile modulus and strength of 5wt% silica flake reinforced N6 is improved 68% and 67% respectively, when compared with the N6. These improvements are 38% higher in tensile strength but 35% lower in tensile modulus than that achieved by the 5wt% clay/N6 nanocomposite. The tensile modulus of 30wt% silica flake reinforced N6 improved over 240% which is similar to the

achievement of 30wt% glass fibre/N6 composites. In addition to strength and modulus, sub-micro composite technology has been proved to be effective in improving fracture toughness and heat deflection temperature.

For multi-layered sub-micro graphite reinforced polypropylene, mechanical properties are dependent on the structure of graphite in the polymer. Only individual sheet-structured graphite reinforced composites showed significantly improved tensile modulus. Tensile strength of the composites, however, did not improve significantly, which may be partially caused by poor compatibility between the filler and matrix.

In addition to mechanical reinforcement, graphite/PP sub-micro composites exhibit much improved electrical conductivity. The enhancement of conductivity is dependent on the structure of sub-micro graphite in the polymer. The composites enhanced by the graphite containing interlinked structure are more conductive due to the easy formation of percolated conductive network.

Effects of sub-micro fillers on crystallisation behaviour of polymer composites are also studied. Sub-micro fillers do have significant influence on nucleation of the polymers. The nucleation effect increased with filler fraction and improvements of compatibility between filler and matrix. Crystallinity of all sub-micro composites studied was either the same or slight lower than the pure polymers. This may imply that the improvement in mechanical properties of sub-micro composites is primarily due to the contribution of sub-micro fillers.

The rheology study has shown that sub-micro composites can be processed in a similar way to the pristine polymers in a wide filler loading range. Although the viscosity of the sub-micro composites with high filler loading is higher than those of the non-filled polymers, they still exhibit good processability. In low filler loading, “lubrication effect” was observed for some composites with poor interfacial bonding between the filler and polymer. The ‘lubrication effect’ results in lower viscosity of a composite than that of the pure polymer.

In summary, the work conducted in this research has proved that the sub-micro composite approach is a competitive technology of improving polymer mechanical properties to nanocomposite technique at low filler loading and has potential to challenge fibre reinforced composites in higher filler loading. Further advance in this technology will lead to fill the gap between nano and micro reinforced materials.

7 Future work

For single-layer sub-micro fillers, breakage of silica flakes during extrusion processing is the main reason for the low reinforcement efficiency of silica flake/N6 composites at high filler loading. In order to avoid the breakage of silica flakes, new processing techniques need to be explored. In-situ polymerisation and rotational moulding are two such examples.

Layer agglomeration in composites is a key issue for multi-layered sub-micro graphite. Although graphite has been dispersed into the polymer in the sub-micro range via a multi-extrusion method, the thickness of graphite layers is still large when compared with the original layer thickness of expanded graphite. Therefore, to achieve finer dispersion of graphite in composites, new filler preparation and exfoliation techniques need to be investigated.

The compatibility between filler and matrix is a determining factor in the strength improvement of both single and multi-layered polypropylene composites. Although several compatibilisers were used to improve the compatibility of fillers with matrices, the results proved to be unsuccessful. For further mechanical property improvement of sub-micro composites, the synthesis and application of more efficient compatibilisers remains an important area for future research. In addition, filler functionalisation by means of plasma oxidation should also be considered [195]-[197].

In this research, only single-layered silica flakes and multi-layered graphite were investigated with N6 and polypropylene matrices. Applying sub-micro enhancement to

other polymers and fillers with different geometries, for example sub-micro fibres, particles and other layer-structured fillers have great interest for future work.

Finally, due to the smaller surface area of sub-micro fillers, sub-micro reinforcement did not exhibit any advantage over nanocomposites in improving dynamic thermal mechanical properties of polymers. This is an inherent limitation of sub-micro reinforcement. The combination of sub-micro and nano reinforcement is an efficient way to address this problem. Such a combination represents an interesting field of research and should be explored as part of future work.

References

- [1] Chung, D.D.L. 'Carbon fibre composites', *Butterworth-Heinemann*, London, 1994.
- [2] Gao, F. 'Clay/polymer composites: the story', *Materials Today*, 2004, November, 50-55.
- [3] Rand, B. and Turpin, M. 'Carbon fibres from pitch' in 'Handbook of polymer-fibre composites', Edited by Jones, F.R. *Longman Scientific and Technical*, UK, 1994.
- [4] Chang, J.S. and Cheng, C.H., 'Thermoplastic properties of short-coated fibre composites: effects of length and orientation distributions', *Composites Science and Technology*, 1995, 55, 329-341.
- [5] Hull, D. and Clyne, T.W. 'An introduction to composite materials', *Cambridge University Press*, New York, 1996.
- [6] Lambert, M. 'Focus on plastics', *Wayland*, England, 1987.
- [7] Morris, P.J.T. 'Polymer pioneers: a popular history of the science and technology of large molecules', *American Institute of Chemical Engineers*, USA, 1986.
- [8] Elias, H. 'New commercial polymers 1969-1975', *Gordon and Breach Science Publishers*, London, 1977.
- [9] Kaminsky, W. 'Polymerization catalysis', *Catalysis Today*, 2000, 62, 23-34.
- [10] Reboul, P. 'Britain and the bakelite revolution' in 'The development of plastics', Edited by Mossman S.T.I. and Morris, P.J.T. *The Royal Society of Chemistry*, UK, 1994.
- [11] Chandrasekhar, P. 'Conducting polymers, fundamentals and applications: a practical approach', *Kluwer Academic Publisher*, USA, 1999.
- [12] Waring, D.L. Kerpez, K.J. and Ungar, S.G. 'A newly emerging customer premises paradigm for delivery of network-based services', *Computer Networks*, 1999, 31, 411-424.
- [13] Zubia, J. and Arrue, J. 'Plastic optical fibres: an introduction to their technological processes and applications', *Optical Fibre Technology*, 2001, 7, 101-140.
- [14] Dumitriu, S. 'Polysaccharide as biomaterials' in 'Polymeric biomaterials', Edited by Dumitriu, S. *Marcel Dekker Inc.*, New York, 2002.

- [15] El-Zaim, H.S. and Hegggers, J.P. 'Silicones for pharmaceutical biomedical applications' in 'Polymeric biomaterials', Edited by Dumitriu, S. *Marcel Dekker Inc.*, New York, 2002.
- [16] Sharma, S.C. 'Composite materials', *Narosa Publishing House*, New Delhi, 2000.
- [17] Lyth, M. 'Science in action: man-made fibres', *Priory Press Limited*, England, 1975.
- [18] Rosato, D.V. 'Plastic design handbook', *Kluwer Academic Publishers*, Boston, 2000.
- [19] Matthews, F.L. and Rawlings, R.D. 'Composites materials: engineering and science', *Chapman and Hall*, London, 1994.
- [20] Parkyn, B. 'Fibre reinforced composites' in 'The development of plastics', Edited by Mossman S.T.I. and Morris, P.J.T. *The Royal Society of Chemistry*, UK, 1994.
- [21] Spencer, B.E. 'Composites in sporting goods' in 'Handbook of Composites', Edited by Peters, S.T. *Chapman and Hall*, London, 1998.
- [22] Einde, L.V.D. Zhao, L. and Seible, F. 'Use of FRP composites in civil structure applications', *Construction and Building Materials*, 2003, 17, 389-403.
- [23] Ye, L. Lu, Y. and Su, Z. 'Functionalized composite structures for new generation airframes: a review', *Composites Science and Technology*, 2005, 65, 1436-1446.
- [24] Mitschang, P. Blinzler, M. and Woginger, A. 'Processing technologies for continuous fibre reinforced thermoplastics with novel polymer blends', *Composites Science and Technology*, 2003, 63, 2099-2110.
- [25] Jacob, A. 'Car makers increase their use of composites', *Reinforced Plastic*, February, 2004, 20-21.
- [26] Kato, M. and Usuki, A. 'Polymer clay nanocomposites' in 'Polymer clay nanocomposites', Edited by Pinnavaia, T.J. and Beall, G.W. *Wiley & Sons Ltd*, New York, 2000.
- [27] Yasue, K. Katahira, S. and Yoshikawa, M. *et al.* 'In-situ polymerisation route to N6 clay nanocomposites' in 'Polymer clay nanocomposites', Edited by Pinnavaia, T.J. and Beall, G.W. *Wiley & Sons Ltd*, New York, 2000.
- [28] Gilman, J.W. and Kashiwagi, T. 'Polymer layered silicate nanocomposites with conventional flame retardants' in 'Polymer clay nanocomposites', Edited by Pinnavaia, T.J. and Beall, G.W. *Wiley & Sons Ltd*, New York, 2000.

- [29] Matayabas, J.C. and Turner, S.R. 'Nanocomposite technology for enhancing the gas barrier of polyethylene terephthalate' in 'Polymer clay nanocomposites', Edited by Pinnavaia, T.J. and Beall, G.W. *Wiley & Sons Ltd*, New York, 2000.
- [30] Thostenson, E.T. Ren, Z.F. and Chou, T.W. 'Advances in science and technology of carbon nanotubes and their composites: A review', *Composites Science and Technology*, 2001, 61, 1899-1912.
- [31] Andrews, R. and Weisenberger, M.C. 'Carbon nanotube polymer composites', *Current Opinion in Solid State and Materials Science*, 2004, 8, 31-37.
- [32] Thostenson, E.T. Li, C. and Chou, T. 'Nanocomposites in context', *Composites Science and Technology*, 2005, 65, 491-516.
- [33] Lafdi, K. and Wright, M.A. 'Carbon fibres' in 'Handbook of composites', Edited by Peters, S.T. *Chapman and Hall, London*, 1998.
- [34] Zweben, C. 'Composite materials' in 'Handbook of material selection', Edited by Kutz, M. *Myer Kutz Associates Inc*, New York, 2002.
- [35] Lowrie, R.S. and Ferguson, H.J.C. 'Chemistry an integrated approach', *Pergamon*, New York, 1975.
- [36] Vaughan, D.J. 'Fibreglass reinforcement' in 'Handbook of Composites', Edited by Peters, S.T. *Chapman and Hall*, London, 1998.
- [37] Wypych, G. 'Handbook of fillers', *ChemTec Publishing*, New York, 2000.
- [38] Velde, B. 'Clays and clay minerals in natural and synthetic systems', *Elsevier*, New York, 1997.
- [39] Ultracki, L.A. 'Clay-containing polymeric nanocomposites', *Rapra Technology*, UK, 2004.
- [40] Komori, Y. and Kuroda, K. 'Layered silicate-polymer intercalation compounds' in 'Polymer-clay nanocomposites' Edited by Pinnavaia, T.J. and Beall, G.W. *John Wiley & Sons Ltd*. New York, 2001.
- [41] Newman, A.C.D. and Brown, G. 'The chemical constitution of clays' in 'chemistry of clays and clay minerals', Edited by Newman, A.C.D. *Longman Scientific and Technical*, UK, 1987.
- [42] Pierson, H.O. 'Handbook of carbon, graphite, diamond and fullerenes properties, processing and applications', *William Andrew*, Noyes, 1993.
- [43] Hillert, M. and Lange, N. 'The structure of graphite filaments', *Zeitschr Kristall*, 1958, 111, 24-34.

- [44] Baker, R.T.K. and Harris P.S. 'The formation of filamentous carbon' in 'Chemistry and physics of carbon', Edited by Walker, P.L and Thrower, P.A. *Dekker*, New York, 1978.
- [45] Iijima, S. 'Helical microtubules of graphitic carbon', *Nature*, 1991, 354, 56-58.
- [46] Iijima, S and Ichihashi, T. 'Single-shell carbon nanotubes of 1-nm diameter', *Nature*, 1993, 363, 603-605.
- [47] Cox, B. Thamwattana, N. and Hill, J. 'Spherical and spheroidal fullerenes entering carbon nanotubes', *Current Applied Physics*, 2008, 8, 249-252.
- [48] Xu, Y. Wang, X. and Tian R. *et al.* 'Synthesis of carbon nanotubes and carbon onions by CVD using a Ni/Y catalyst supported on copper', *Materials Science and Engineering: A*, 2008, 475, 136-140.
- [49] Rivas, G.A. Rubianes, M.D. and Rodríguez, M.C. *et al.* 'Carbon nanotubes for electrochemical biosensing', *Talanta*, 2007, 74, 291-307.
- [50] Li, W.Z. Yan, X. and Kempa, K. *et al.* 'Structure of flattened carbon nanotubes', *Carbon*, 2007, 45, 2938-2945.
- [51] Thess, A. Lee, R. and Nikolaev, P. *et al.* 'Crystalline ropes of metallic carbon nanotubes', *Science*, 1996, 273, 483-487.
- [52] Liu, J. Zubiri, M.R. and Vigolo, B. *et al.* 'Efficient microwave-assisted radical functionalization of single-wall carbon nanotubes', *Carbon*, 2007, 45, 885-891.
- [53] Xu, Z. Wang, H. and Hwang, J.Y. 'Complex carbon nanotube superstructures synthesized with natural mineral catalysts', *Carbon*, 2007, 45, 873-879.
- [54] Sun, X. Li, R. and Standsfield, B. *et al.* 'Controlled synthesis of pointed carbon nanotube', *Carbon*, 2007, 45, 732-737.
- [55] Takemura, K. 'Development of wet chemical processing in nippon sheet glass', *Key Engineering Materials*, 1998, 150, 177-180.
- [56] Material news 'Corrosion resistant glass flakes', *Reinforced Plastics*, 1999, 20-21.
- [57] Material news 'Glass flakes move into composites', *Reinforced Plastics*, 2000, 44, 30-31.
- [58] Material news 'Flake glass products now have nano thicknesses', *Plastic Additives and Compounding*, 2005, 16-17.
- [59] Seymour, R.B. 'Reinforced plastics – property & applications', *ASM International*, USA, 1991.

- [60] Brooks, R. Mai-Ngam, B. and Hsu, C.Y. 'Strength prediction in short fibre reinforced thermoplastic', *Plastics, Rubber and Composites Processing and Applications*, 1998, 27, 172-178.
- [61] Andrew, R.M. and Flake, C.C. 'Autoclave processing' in 'Processing of Composites', Edited by Davé, R.S. and Loos, A.C. *Hanser Publisher*, Munich, 1999.
- [62] Åström, B.T. 'Pultrusion' in 'Processing of Composites', edited by Davé, R.S. and Loos, A.C. *Hanser Publisher*, Munich, 1999.
- [63] Moschiar, S.M. Reboredo, M.M and Vazquez, A. in 'Advanced polymer processing operations', Edited by Cheremisinoff, N.P. *Noyes Publications*, USA, 1998.
- [64] Mantell, S.C. and Cohen, D. 'Filament winding' in 'Processing of Composites', Edited by Davé, R.S. and Loos, A.C. *Hanser Publisher*, Munich, 1999.
- [65] Gibson, A.G. 'Injection moulding – thermosets' in 'Handbook of polymer-fibre composites' edited by John, F.R. *Longman Scientific and Technical*, England, 1994.
- [66] Béland, S. 'High performance thermoplastic resins and their composites', *Noyes Data Corporation*, USA, 1991.
- [67] Folkes, M.J. 'Injection moulding – thermoplastics' in 'Handbook of polymer-fibre composites' Edited by John, F.R. *Longman Scientific and Technical*, England, 1994.
- [68] Folkes, M.J. 'Short fibre reinforced thermoplastics', *John Wiley & Sons Ltd*, New York, 1982.
- [69] Berthelot, J.M. and Sefrani, Y. 'Longitudinal and transverse damping of unidirectional fibre composites', *Composite Structures*, 2007, 79, 423-431.
- [70] Iba, H. Chang, T. and Kagawa, Y. 'Optical transparent continuous glass fibre-reinforced epoxy matrix composite: fabrication, optical and mechanical properties', *Composites Science and Technology*, 2002, 62, 2043-2052.
- [71] Botelho, E.C. Figiel, L. and Rezende, M.C. 'Mechanical behaviour of carbon fibre reinforced polyamide composites', *Composites Science and Technology*, 2003, 63, 1843-1855.
- [72] Rijdsdijk, H.A. Contant, M. and Peijs, A.A.J.M. 'Continuous-glass-fibre-reinforced polypropylene composites: I. Influence of maleic-anhydride-modified polypropylene on mechanical properties', *Composites Science and Technology*, 1993, 48, 161-172.
- [73] Bureau, M.N. and Denault, J. 'Fatigue resistance of continuous glass fibre/polypropylene composites: consolidation dependence', *Composites Science and Technology*, 2004, 64, 1785-1794.

- [74] Jones, F.R. 'Moisture absorption – anomalous effects' in 'Handbook of polymer-fibre composites', Edited by Jones, F.R. *Longman Scientific and Technical*, UK, 1994.
- [75] Fung, K.L. and Li, R.K.Y. 'Mechanical properties of short glass fibre reinforced and functionalised rubber-toughened PET blends', *Polymer Testing*, 2000, 25, 923-931.
- [76] Ozkoc, G. Bayram, G. and Bayramli, E. 'Effects of polyamide incorporation to the short glass fibre reinforced ABS composites: an interfacial approach', *Polymer*, 2004, 45, 8957-8966.
- [77] Fu, S.Y. Lauke, B. and Li, R.K.Y. *et al.* 'Effects of PA66/PP ratio on the mechanical properties of short glass fibre reinforced and rubber-toughened polyamide6, 6/polypropylene blends', *Composites: Part B*, 2006, 37, 182-190.
- [78] Wand, W. Tand, L. and Qu, B. 'Mechanical properties and morphological structures of short glass fibre reinforced PP/EPDM composites', *European Polymer Journal*, 2003, 39, 2129-2134.
- [79] Sui, G. Wong, S.C. and Yue, C.Y. 'Effects of extrusion compounding on the mechanical properties of rubber-toughened polymer containing short glass fibres', *Journal of Materials Processing Technology*, 2001, 113, 167-171.
- [80] Tjong, S.C. Xu, S.A. and Mai, Y.W. 'Impact fracture toughness of short glass fibre-reinforced polyamide 6,6 hybrid composites containing elastomer particles using essential work of fracture concept', *Materials Science and Engineering: A*, 2003, 347, 338-345.
- [81] Güllü, A. Özdemir, A. and Özdemir, E. 'Experimental investigation of the effect of glass fibres on the mechanical properties of polypropylene (PP) and polyamide 6 (PA6) plastics', *Materials and Design*, 2006, 27, 316-323.
- [82] Noh, C.H. Yoon, B.S. and Suh, M.H. *et al.* 'Interfacial component of glass fibre in ternary composites of GF/PC/PP: effect of the preferential encapsulation of glass fibre', *Polymer*, 2001, 42, 2695-2700.
- [83] Moriwaki, T. 'Mechanical property enhancement of glass fibre reinforced polyamide composite made by direct injection moulding process', *Composites: Part A*, 1995, 27, 379-384.
- [84] García, M. Eguiazábal, J.I. and Nazábal, J. 'Two scale reinforcement in hybrid composites based on poly (ether sulfone), glass fibre and liquid crystalline polymer', *Composites Science and Technology*, 2003, 63, 2163-2170.
- [85] Xiao, Y. Hu, K.A. and Wu, R.J. 'Novel preparation of polyethylene oxide/LixMoO3 nanocomposite by direct melt intercalation', *Materials Research Bulletin*, 2000, 35, 1669-1675.

- [86] Terrones, M. Jorio, A. and Endo, M. *et al.* 'New direction in nanotube science', *Materials Today*, 2004, 30-45.
- [87] Hemmel, E. Tang, X. and Trampert, M. *et al.* 'Carbon nanofibres for composite applications', *Carbon*, 2004, 42, 1153-1158.
- [88] Kashiwagi, T. Harris Jr, R.H. and Zhang, X. *et al.* 'Flame retardant mechanism of polyamide 6-clay nanocomposites', *Polymer*, 2004, 45, 881-891.
- [89] Njugunna, B. and Pielichowski, K. 'Polymer nanocomposites for aerospace applications: properties', *Advanced Engineering Materials*, 2003, 5, 769-778.
- [90] Modesti, M. Besco, S. and Lorenzetti, A. 'Reinforcing effect of organo-modified layered silicates in high-density polyethylene', *Journal of Nanoscience and Nanotechnology*, 2005, 5, 958-963.
- [91] Ivankovic, H. Tkalcec, E. and Nass, R. *et al.* 'Correlation of the precursor type with densification behaviour and microstructure of sintered mullite ceramics', *Journal of the European Ceramic Society*, 2003, 23, 283-292.
- [92] Ozdilek, C. Kazimierzak, K. and Beek, D.V. *et al.* 'Preparation and properties of polyamide-6-boehmite nanocomposites', *Polymer*, 2004, 45, 5207-5214.
- [93] Wu, S.H. Wang, F.Y. and Ma, C.C.M. *et al.* 'Mechanical, thermal and morphology properties of glass fibre and carbon fibre reinforced polyamide 6 and polyamide 6 / clay nanocomposites', *Materials Letters*, 2001, 49, 327-333.
- [94] Cho, J.W. and Paul, D.R. 'N6 nanocomposites by melt compounding', *Polymer*, 2001, 42, 1083-1094.
- [95] Ray, S.S. and Okamoto, M. 'Polymer/layered silicate nanocomposites: a review from preparation to processing', *Progress Polymer Science*, 2003, 28, 1539-1641.
- [96] Burmistr, M.V. Sukhyy, K.M. and Shilov, V.V. *et al.* 'Synthesis, structure, thermal and mechanical properties of nanocomposites based on linear polymers and layered silicates modified by polymeric quaternary ammonium salts (ionens)', *Polymer*, 2005, 46, 12226-12232.
- [97] Zeng, H. Gao, C. and Wang, Y. *et al.* 'In suit polymerisation approach to multiwalled carbon nanotubes-reinforced nylon 1010 composites: Mechanical properties and crystallisation behaviour', *Polymer*, 2006, 47, 113-122.
- [98] Wang, Z. Massam, J. and Pinnavia, T.J. 'Epoxy-clay nanocomposites' in 'Polymer clay nanocomposites' edited by Pinnavaia, T.J. and Beall, G.W. *John Wiley & Sons*, England, 2000.

- [99] Wang, L. Wang, K. and Chen, L. *et al.* 'Preparation, morphology and thermal/mechanical properties of epoxy/nanoclay composite', *Composites: Part A*, 2006, 37, 1890-1896.
- [100] Wang, Y. Chen, F.B. and Li, Y.C. *et al.* 'Melt processing of polypropylene/clay nanocomposites modified with maleated polypropylene compatibilisers', *Composites: Part B*, 2004, 35, 111-124.
- [101] Wang, L. and Sheng, J. 'Preparation and properties of polypropylene/org-attapulgite nanocomposites', *Polymer*, 2005, 46, 6243-6249.
- [102] Cui, L. and Paul, D.R. 'Evaluation of amine functionalised polypropylenes as compatibilisers for polypropylene nanocomposites', *Polymer*, 2007, 48, 1632-1640.
- [103] Osman, M.A. Rupp, J.E.P. and Suter, U.W. 'Tensile properties of polyethylene-layered silicate nanocomposites', *Polymer*, 2005, 46, 1653-1660.
- [104] Araújo, E.M. Mélo, T.J.A. and Santana, G.A. *et al.* 'The influence of organo-bentonite clay on the processing and mechanical properties of N6 and polystyrene composites', *Materials Science and Engineering B*, 2004, 112, 175-178.
- [105] Jin S.H. Park, Y.B. and Yoon, K.H. 'Rheological and mechanical properties of surface modified multi-walled carbon nanotube-filled PET composite', *Composites Science and Technology*, 2007, doi:10.1016/j.compscitech. 2007. 03.013.
- [106] Gintert, M.J. Jana, S.C. and Miller, S.G. 'A Novel strategy for nanoclay exfoliation in thermoset polyimide nanocomposite systems', *Polymer*, 2007, doi:10.1016/j.polymer: 2007.05.053.
- [107] Yasmin, A. Luo, J.J. and Abot, J.L. *et al.* 'Mechanical and thermal behaviour of clay/epoxy nanocomposites', *Composites Science and Technology*, 2006, 66, 2415-2422.
- [108] Wang, J. and Qin, S. 'Study on the thermal and mechanical properties of epoxy-nanoclay composites: The effect of ultrasonic stirring time', *Materials Letters*, doi: 10.1016/j.matlet.2007.01.058.
- [109] Xiong, J. Zheng, Z. and Jiang, H. *et al.* 'Reinforcement of polyurethane composites with an organically modified montmorillonite', *Composites: Part A*, 2007, 38, 132-137.
- [110] Peeterbroeck, S. Alexandre, M. and Nagy, J.B. *et al.* 'Polymer-layered silicate-carbon nanotube nanocomposites: unique nanofiller synergistic effect', *Composites Science and Technology*, 2004, 64, 2317-2323.
- [111] Diagne, M. Gueye, M. and Vidal, L. *et al.* 'Thermostability and fire retardant performance of photo-oxidized nanocomposites of polypropylene-graft-maleic anhydride/clay', *Polymer Degradation and Stability*, 2005, 89, 418-426.

- [112] Jiang, T. Wang, Y. and Yeh, J. *et al.* 'Study on solvent permeation resistance properties of nylon/clay nanocomposite', *European Polymer Journal*, 2005, 41, 459-466.
- [113] Bourbigot, S. Devaux, E. and Flambard, X. 'Flammability of polyamide-6/clay hybrid nanocomposite textiles', *Polymer Degradation and Stability*, 2002, 75, 397-402.
- [114] Zhu, J. Morgan, A.B. Lamelas, F.J. 'Fire properties of polystyrene clay nanocomposites', *Chemical Materials*, 2001, 13, 3774-3780.
- [115] Ding, R. Hu, Y. and Gui, Z. *et al.* 'Preparation and characterization of polystyrene/graphite oxide nanocomposite by emulsion polymerisation', *Polymer Degradation and Stability*, 2003, 81, 473-476.
- [116] Zheng, W. Wong, S. and Sue, H. 'Transport behaviour of PMMA/expanded graphite nanocomposites', *Polymer*, 2002, 73, 6767-6773.
- [117] Zanetti, M. and Costa, L. 'Preparation and combustion behaviour of polymer/layered silicate nanocomposites based on PE and EVA', *Polymer*, 2004, 45, 4367-4372.
- [118] Zhang, B. Fu, R. and Zhang, M. *et al.* 'Preparation and characterization of gas-sensitive composites from multi-walled carbon nanotubes/polystyrene', *Sensors and Actuators B, Chemical*, 2005, 109, 323-328.
- [119] Preston, C.M.L. Amarasinghe, G. and Hopewell, J.L. *et al.* 'Evaluation of polar ethylene copolymers as fire retardant nanocomposite matrices', *Polymer Degradation and Stability*, 2004, 84, 533-544.
- [120] Gao, F. Chen, S. and Hull, J.B. 'Layer expansion of layered silicates in solid polymer matrices by compression', *Journal of Materials Science Letters*, 2001, 20, 1807-1810.
- [121] Brinker, C.J. and Scherer, G.W. 'The physics and chemistry of sol-gel processing', *Academic Press Inc*, New York, 1990.
- [122] Chen, Y. Zhou, S. and Yang, H. *et al.* 'Preparation and characterization of nanocomposite polyurethane', *Journal of Colloid and Interface Science*, 2004, 279, 370-378.
- [123] Yang, S. Castilleja, J.R. and Barrera, E.V. 'Thermal analysis of an acrylonitrile-butadiene-styrene/SWNT composite', *Polymer Degradation and Stability*, 2004, 83, 383-388.
- [124] Mammerra, F. Bourhis, E.L. and Rozesa, L. 'Elaboration and mechanical characterization of nanocomposites thin films part 1: determination of the mechanical properties of thin films prepared by in-situ polymerisation of

- tetraethoxysilane in poly (methyl methacrylate)', *Journal of the European Ceramic Society*, 2006, 26, 259-266.
- [125] Sadeghian, R. Gangireddy, S. and Minaie, B. *et al.* 'Manufacturing carbon nanofibres toughened polyester/glass fibre composites using vacuum assisted resin transfer moulding for enhancing the model-I delamination resistance', *Composites: Part A*, 2006, 37, 1787-1795.
- [126] Zhu, J. Imam, A. Crane, R. and Lozano, K. *et al.* 'Processing a glass reinforced vinyl ester composite with nanotube enhancement of interlaminar shear strength' *Composites Science and Technology*, 2007, 67, 1509-1517.
- [127] Vlasveld, D.P.N. Daud, W. Bersee, H.E.N. and Picken, S.J. 'Continuous fibre composites with a nanocomposite matrix: Improvement of flexural and compressive strength at elevated temperature', *Composites, Part A*, 2007, 38, 730-738.
- [128] Gilman, J.W. and Kashiwagi, T. 'A revolutionary new flame retardant approach', *42nd international SAMPE Symposium*, Anaheim, 1997, 1078-1089.
- [129] Chigwada, G. and Wilkie, C.A. 'Synergy between conventional phosphorus fire retardants and organically-modified clays can lead to fire retardancy of styrenics', *Polymer Degradation and Stability*, 2003, 80, 551-557.
- [130] Zhang, R. Hu, Y. and Xu, J. *et al.* 'Flammability and thermal stability studies of styrene butyl acrylate copolymer/graphite oxide nanocomposite', *Polymer Degradation and Stability*, 2004, 85, 583-588.
- [131] Gao, F. Li, Y. and Moloney, S. 'The structure of chars formed from clay/polymer nanocomposites', *5th World Congress in Nanocomposites*, San Francisco, 2005, 1120-1126.
- [132] Gao, F. Beyer, G. and Yuan, Q. *et al.* 'A mechanistic understanding of fire retardancy of carbon nanotube/EVA composites and their clay hybrids', *Polymer Degradation and Stability*, 2005, 89(3), 559-564.
- [133] Tasi, T.Y. 'Polyethylene terephthalate clay nanocomposites', Edited by Pinnavaia, T.J. and Beall, G.W. *John Wiley & Sons*, England, 2000.
- [134] Lu, J. Chen, X. and Lu, W. 'The piezoresistive behaviours of polyethylene/foiled graphite nanocomposites', *European Polymer Journal*, 2006, 42, 1015-1021.
- [135] Du, X.S. Xiao, M. and Meng, Y.Z. 'Facile synthesis of highly conductive polyaniline/graphite nanocomposites', *European Polymer Journal*, 2004, 40, 1489-1493.
- [136] Li, J. Kim, J.K. and Sham, M.L. 'Conductive graphite nanoplatelet/epoxy nanocomposites: Effects of exfoliation and UV/ozone treatment of graphite', *Scripta Materialia*, 2005, 53, 235-240.

- [137] Feller, J.F. Linossier, I. and Grohens, Y. 'Conductive polymer composites: comparative study of poly(ester)-short carbon fibres and poly(epoxy)-short carbon fibre mechanical and electrical properties', *Materials Letters*, 2002, 57, 64-71.
- [138] Celzard, A. Marêché, J.F. and Furdin, G. 'Modelling of exfoliated graphite', *Progress in Materials Science*, 2005, 50, 93-179.
- [139] Wycisk, R. Poźniak, R. and Pasternak, A. 'Conductive polymer materials with low filler content', *Journal of Electrostatics*, 2002, 56, 55-66.
- [140] Wang W.P. and Pan, C.Y. 'Preparation and characterisation of polystyrene/graphite composite prepared by cationic grafting polymerisation', *Polymer*, 2004, 45, 3987-3995.
- [141] Chen, G. Weng, W. and Wu, D. 'PMMA/graphite nanosheets composite and its conducting properties', *European Polymer Journal*, 2003, 39, 2329-2335.
- [142] Zheng, W. Wong, S.C. and Sue, H.J. 'Transport behaviour of PMMA/expanded graphite nanocomposites', *Polymer*, 2002, 73, 6767-6773.
- [143] Zheng, W. and Wong, S.C. 'Electrical conductivity and dielectric properties of PMMA/expanded graphite composites', *Composites Science and Technology*, 2003, 63, 225-235.
- [144] Xiao, P. Xiao, M. and Gong, K. 'Preparation of exfoliated graphite/polystyrene composite by polymerisation-filling technique', *Polymer*, 2001, 42, 4813-4816.
- [145] Chen, G. Wu, C. and Weng, W. *et al.* 'Preparation of polystyrene/graphite nanosheet composite', *Polymer*, 2003, 44, 1781-1784.
- [146] Pan, Y. Yu, Z.Z. and Ou, Y.C. *et al.* 'A new process of fabricating electrically conducting N6/graphite nanocomposites via intercalation polymerisation', *Journal of Polymer Science: Part B: Polymer Physics*, 2000, 38, 1626-1633.
- [147] Shen, J.W. Chen, X.M. and Huang, W.Y. 'Structure and electrical properties of grafted polypropylene/graphite nanocomposites prepared by solution intercalation', *Journal of Applied Polymer Science*, 2003, 88, 1864-1869.
- [148] Qu, S. and Wong, S.C. 'Piezoresistive behaviour of polymer reinforced by expanded graphite', *Composites Science and Technology*, 2007, 67, 231-237.
- [149] Chung, D.D.L. 'Composites get smart', *Materials Today*, 2002, January, 30-35.
- [150] Sandler, J.K.W. Kirk, J.E. and Shaffer, M.S.P. *et al.* 'Ultra-low electrical percolation threshold in carbon nanotube-epoxy composites', *Polymer*, 2003, 44, 5893-5899.

- [151] So, H.H. Cho, J.W. and Sahoo, N.G. 'Effect of carbon nanotubes on mechanical and electrical properties of polyimide/carbon nanotubes nanocomposites', *European Polymer Journal*, 2007, 43, 3750-3756.
- [152] Chen, L. Pang, X.J. and Yu, Z.L. 'Study on polycarbonate/multi-walled carbon nanotubes composites produced by melt processing', *Materials Science and Engineering A*, 2007, 457, 287-291.
- [153] Gojny, F.H. Wichmann, M.H.G. and Fiedler, B. *et al.* 'Evaluation and identification of electrical and thermal conduction mechanisms in carbon nanotube/epoxy composites', *Polymer*, 2006, 47, 2036-2045.
- [154] Pham, G.T. Park, Y.B. and Liang, Z. *et al.* 'Processing and modelling of conductive thermoplastic/carbon nanotube film for strain sensing', *Composites: Part B*, 2008, 39, 209-216.
- [155] Luo, X. and Chung, D.D.L. 'Carbon-fibre/polymer matrix composites as capacitors', *Composites Science and Technology*, 2001, 61, 885-888.
- [156] Rotheron, R.N. 'Particulate fillers for polymers', *Rapra Technology Ltd*, UK, 2002.
- [157] Vlasveld, D.P.N. Groenewold, J. and Bersee, H.E.N. *et al.* 'Analysis of the modulus polyamide-6 silicate nanocomposites using moisture controlled variation of the matrix properties', *Polymer*, 2005, 46, 1-12.
- [158] Sun, P.L. Yu, C.Y. and Kao, P.W. 'Influence of boundary of characters on the tensile behaviour of sub-micron-grained aluminium', *Scripta Materialia*, 2005, 52, 265-269.
- [159] Snoswell, D.R.E. Duan, J. and Fornasiero, D. 'The selective aggregation and separation of titania from a mixed suspension of silica and titania', *International Mineral process*, 2005, 78, 1-10.
- [160] Koizumi, Y. Ueyama, M. and Tsuji, N. *et al.* 'High damping capacity of ultra-fine grained aluminium produced by accumulative roll bonding', *Journal of Alloys and Compounds*, 2003, 355, 47-51.
- [161] Gan, C.L. Pey, K.L. and Chim, W.K. 'Effects of high current conduction in sub-micro Ti-silicided films', *Solid-State Electronics*, 2000, 44, 1837-1845.
- [162] Andreyev, D.S. and Arriaga, A.E. 'Fabrication of perforated sub-micron silica shells', *Scripta Materialia*, 2007, 57, 957-959.
- [163] Mortera, R. Onida, B. and Fiorilli, S. *et al.* 'Synthesis and characterization of MCM-41 spheres inside bioactive glass-ceramic scaffold', *Chemical Engineering Journal*, 2008, 137, 54-61.

- [164] Howard, A.G. and Khedary, N.H. 'Spray synthesis of monodisperse sub-micron spherical silica particles', *Materials Letters*, 2007, 61, 1951-1954.
- [165] Qutub, A.M. Allam, I.M. and Qureshi, T.W. 'Effect of sub-micro Al₂O₃ concentration on dry wear properties of 6061 aluminium based composite', *Journal of Materials Processing Technology*, 2006, 172, 327-331.
- [166] Chen, L. and Kny, E. 'Reaction hot-pressed sub-micro Al₂O₃ + TiC ceramic composites', *International Journal of Refractory Metals and Hard Materials*, 2000, 18, 163-167.
- [167] Kouzeli, M. and Dunand, D.C. 'Effect of reinforcement connectivity on the elastoplastic behaviour of aluminium composites containing sub-micron alumina particles', *Acta Materialia*, 2003, 51, 6105-6121.
- [168] Jiang, L. Zhao, M. and Wu, G. 'Aging behaviour of sub-micro Al₂O₃p/2024Al composites', *Materials Science and Engineering A*, 2005, 392, 366-372.
- [169] Wang, X. Wu, G. and Sun, D. *et al.* 'Micro-yield property of sub-micro Al₂O₃ particle reinforced 2024 aluminium matrix composite' *Materials Letters*, 2004, 58, 333-336.
- [170] Wilhelm, M. Werdenich, S. and Wruss, W. 'Influence of resin content and compaction pressure on the mechanical properties of SiC-Si composites with sub-micron SiC microstructures', *Journal of the European Ceramic Society*, 2001, 21, 981-990.
- [171] Boey, F.Y.C. Yuan, Z. and Khor, K.A. 'Mechanical alloying for the effective dispersion of sub-micro reinforcements in Al-Li alloy composite', *Materials Science and Engineering A*, 1998, 252, 276-287.
- [172] Beaudoin, J.J. Gu, P. and Myers, R.E. 'Flexural strength of cement past composites containing micron and sub-micron nickel particulates', *Cement and Concrete Research*, 1997, 27, 23-27.
- [173] Xing, X.S. and Li, R.K.Y. 'Wear behaviour of epoxy matrix composites filled with uniform sized sub-micron spherical silica particles', *Wear*, 2004, 256, 21-26.
- [174] Chang, L. Zhang, Z. and Ye, L. *et al.* 'Tribology properties of high temperature resistant polymer composites with fine particles', *Tribology International*, 2007, 40, 1170-1178.
- [175] Bugnicourt, E. Galy, J. and Gérard, J.F. *et al.* 'Effect of sub-micron silica fillers on the mechanical performances of epoxy-based composites', *Polymer*, 2007, 48, 1596-1605.
- [176] Williams, J.G. and Cawood, M.J. 'European group on fracture: K_c and G_c methods for polymers', *Polymer Testing*, 1990, 9, 15-26.

- [177] Malkin, A. Askadsky, A. and Chalykh, A. 'Experimental methods of polymer physics', *Prentice-Hall Inc*, New Jersey, 1983.
- [178] Jiang, T. Wang, Y. and Yang, J. *et al.* 'Study on solvent permeation resistance properties of N6/clay nanocomposites', *European Polymer Journal*, 2005, 42, 459-466.
- [179] Campoy, I. Gómez, M.A. and Marco, C. 'Structure and thermal properties of blends of N6 and a liquid crystal copolyester', *Polymer*, 1998, 39, 6279-6288.
- [180] Wunderlich, B. 'Macromolecular physics' Vol. 3, *Academic Press*, New York, 1983.
- [181] Wang, H. Tan, G. and Cen, S. *et al.* 'Numerical determination of effective properties of voided piezoelectric materials using BNM', *Engineering Analysis with Boundary Elements*, 2005, 29, 636-646.
- [182] Tucker, C.L. and Liang, E. 'Stiffness predictions for unidirectional short-fibre composites: review and evaluation', *Composites Science and Technology*, 1999, 59, 655-671.
- [183] Chang, J.S. and Cheng, C.H. 'Thermoplastic properties of short-coated fibre composites: effects of length and orientation distributions', *Composites Science and Technology*, 1995, 55, 329-341.
- [184] Lu, P. and Lee, K.H. 'A modified model for prediction of effective elastic moduli of composite materials', *International Journal of Solids and Structures*, 2002, 39, 649-657.
- [185] Hine, P.J. Lusti, H.R. and Gusev, A.A. 'Numerical simulation of the effects of volume fraction, aspect ratio and fibre length distribution on the elastic and thermoelastic properties of short fibre composites', *Composites Science and Technology*, 2002, 62, 1445-1453.
- [186] Fornes, T.D. and Paul, D.R. 'Modelling properties of N6/clay nanocomposites using composite theories', *Polymer*, 2003, 44, 4993-5013.
- [187] Fertig, R.S. and Garnich, M.R. 'Influence of constituent properties and microstructural parameters on the tensile modulus of a polymer/clay nanocomposite', *Composites Science and Technology*, 2004, 64, 2577-2588.
- [188] Villoria, R.G. and Miravete, A. 'Mechanical model to evaluate the effect of the dispersion in nanocomposites', *Acta Materialia*, 2007, 55, 3025-3031.
- [189] Nicholas, P. 'Handbook of chemical Engineering calculations', *McGran Hill*, New York, 2003.

- [190] Zhao, X.Y. and Wang, M.Z. 'Synthesis, characterisation and thermal history dependence of the polymorphic structure of N6/montmorillonite nanocomposites', *Journal of Material Science*, 2006, 41, 7225-7231.
- [191] Rem, H. 'Treatise of inorganic chemistry', vol. 1-2, *Elsevier*, New York, 1956.
- [192] Inagaki, M. Tashiro, R. and Washino, Y. *et al.* 'Exfoliation process of graphite via intercalation compounds with sulphuric acid', *Journal of Physics and Chemistry of Solids*, 2004, 65, 133-137.
- [193] Mercuri, R.A. *US Patent*, 5,985,452 (1999).
- [194] Sun, K. Lu, W. and Wu, F. *et al.* 'Preparation of expandable graphite with low sulphur content', *Journal of Inorganic Materials (Chinese)*, 1994, 46, 455-460.
- [195] Wong, M. Paramsothy, M. and Xu, X.J. *et al.* 'Physical interaction at carbon nanotube-polymer interface', *Polymer*, 2003, 44, 7757-7764.
- [196] Keszei, S. Matko, S.Z. and Bertalan, G.Y. *et al.* 'Progress in interface modifications: from compatibilization to adaptive and smart interphases', *European Polymer Journal*, 2005, 41, 697-705.
- [197] Chirila, V. Marginean, G. and Brandl, W. 'Effect of the oxygen plasma treatment parameters on the carbon nanotubes surface properties', *Surface and Coatings Technology*, 2005, 200, 548-551.

Appendix A: Definition of terminology

Bagley correction: a method used to correct the shear stress of a fluid in capillary extrusion rheology measurements, in which capillaries with different lengths, but equivalent diameter, are used. The actual shear stress (τ) is calculated according to the equation:

$$\tau = \frac{(\Delta P_1 - \Delta P_2)R}{2(L_1 - L_2)}, \text{ where } \Delta P_1 \text{ and } \Delta P_2 \text{ represent pressure drops along dies of length } L_1 \text{ and } L_2.$$

Congswell convergent flow model: a flow model in which the entry pressure drop over an area of converging flow, from a circular barrel into a capillary die, is made up of two components, one related to shear flow and the other related to extensional flow, i.e. $\Delta P = \Delta P_S + \Delta P_E$, ΔP , ΔP_S , ΔP_E represent entry pressure drop and pressure drops contributed by shear flow and extensional flow respectively.

Complex modulus: E^* , the ratio of oscillatory stress to strain, is comprised of elastic modulus and viscous modulus and expressed in complex number form:

$$E^* = E' + iE'' = \frac{\sigma^*}{\gamma} \cos \delta + i \frac{\sigma^*}{\gamma} \sin \delta$$

where σ^* , γ , E' and E'' denote oscillatory stress, strain, storage modulus and loss modulus, respectively. δ is the phase angle. For a perfect elastic material, $\delta = 0$ and for an ideal viscous fluid $\delta = \pi/2$.

Critical stress intensity: the stress intensity at fracture ignition used to evaluate impact toughness of materials.

Crystallization enthalpy of polymer: the heat released to crystallize a unit polymer with 100 % crystalline.

Dynamic thermal mechanical analysis: also known as dynamic mechanical analysis. In general, a method used to measure the viscoelastic properties of polymers, for example the dynamic changes of complex modulus, storage modulus and loss modulus over time or under temperature.

Elastic modulus: the slope of the linear-elastic part of the stress & strain curve.

Flexural modulus: Young's modulus under flexural load.

Longitudinal modulus: elastic modulus in the fibre/filler aligned direction.

Loss modulus: unrecoverable portion of complex modulus, i.e. viscous modulus, $E'' = E^* \sin \delta$

Melting enthalpy of polymer: the heat consumed to melt a unit of polymer.

Notched Izod strength: strength measured using the standard Notched Izod impact method where specimens are notched using a saw or razor blade before the test.

Poisson ratio: the negative of the ratio of the lateral strain to the axial strain in axial loading.

Residence time: duration of time that materials stay in an extruder. In this research, residence time was measured by adding five grams of coloured additive during polypropylene extrusion. The period time from addition to removal of the additive from the extruder was taken as the residence time.

Shear modulus: elastic modulus under shear loading.

Specific modulus/strength: the ratio of modulus/strength to density, commonly used for evaluation of mechanical properties of fibre composites.

Storage modulus: the recoverable portion of complex modulus, i.e. elastic modulus obtained from dynamic thermal mechanical analysis and expressed as:

$$E' = E * \cos \delta$$

Strain: includes normal strain, shear strain and true strain.

- Normal strain: the change in length per unit length of a line segment in the direction under consideration, i.e. $\frac{L_f - L}{L}$

Where $\varepsilon \Delta L_f$, L represent final length and original length, respectively.

- Shear strain: the tangent of angle change under the material deformation when a shear force applied.
- True strain (ε_t): the change in length divided by the instantaneous value of the length

$$(\ell), \text{ i.e. } \varepsilon_t = \int_L^{L_f} \frac{d\ell}{\ell} = \ln \frac{L_f}{L}$$

For a small strain, for which the linear elasticity is valid, the value of true strain is the same as normal strain.

Strain magnification: A phenomenon that fibre composites possess, in which a magnified matrix deformation happens in the local area around the fibre when a transverse stress is applied. Strain magnification is caused by the difference of stiffness between fibre and matrix.

Stress: the force load per unit area, i.e. $\frac{F}{A}$ where F and A represent the force and area of force bearing respectively. Stress can be applied in tensile stress or shear stress.

Tensile modulus: Young's modulus under tension.

Young's modulus: elastic modulus under tension or compression.

Appendix B: List of symbols

Parameters

d	diameter
E	elastic modulus, Young's modulus or tensile modulus
f	flake volume fraction
P	general expression of mechanical properties
s	aspect ratio
T	temperature
t	thickness
η	ratio of $\frac{P_f}{P_m} - 1$ to $\frac{P_f}{P_m} + \zeta$, flake orientation efficiency factor or aspect ratio efficiency factor, depended on the subscript
ζ	geometric factor
ν	Poisson's ratio
ε	normal strain
σ	tensile stress or strength
τ	shear stress

Subscripts

1	longitudinal direction
2	transverse
c	crystallization temperature of polymers
f	fibre
l	flake length
m	matrix
m	melting temperature
o	orientation
s	aspect ratio
u	ultimate tensile

Appendix C: List of abbreviations

DMA	dynamic mechanical analysis or dynamic thermal mechanical analysis
DSC	differential scanning calorimetry
EG	expanded graphite
EVA	ethylene vinyl acetate copolymer
HDT	heat deflection temperature or heat distortion temperature
HRR	heat release rate
MLR	mass loss rate
MWNTs	multi-walled carbon nanotubes
N6	nylon 6 or polyamide 6
PET	poly (ethylene terephthalate)
PHRR	peak heat release rate
PP	polypropylene
SEM	scanning electron microscopy
SF	silica flakes
SWNTs	single-walled carbon nanotubes
TEM	transmission electron microscopy
XRD	X-ray diffraction